EXPERIMENTAL & NUMERICAL INVESTIGATIONS OF OXY-FUEL COMBUSTION USING POROUS PLATE REACTOR

BY

FURQAN TAHIR

A Thesis Presented to the

DEANSHIP OF GRADUATE STUDIES

KING FAHD UNIVERSITY OF PETROLEUM & MINERALS

DHAHRAN, SAUDI ARABIA

In Partial Fulfillment of the
Requirements for the Degree of

MASTER OF SCIENCE

In

MECHANICAL ENGINEERING DEPARTMENT

MAY, 2014

KING FAHD UNIVERSITY OF PETROLEUM & MINERALS

DHAHRAN- 31261, SAUDI ARABIA

DEANSHIP OF GRADUATE STUDIES

This thesis, written by Furqan Tahir under the direction his thesis advisor and approved by his thesis committee, has been presented and accepted by the Dean of Graduate Studies, in partial fulfillment of the requirements for the degree of

MASTER OF SCIENCE IN MECHANICAL ENGINEERING

Thesis Committee

Dr Mohamed A. Habib. (Advisor)

Dr Hassan M. Badr. (Member)

Dr. Wael H. Ahmed (Member)

Dr. Zuhair Gasem

Department Chairman

Dr. Salam A. Zummo
Dean of Graduate Studies

27/8/14

Date

To my Father and Mother, without their prayers and support I may not be able to come this far

To my younger brother ‘Hammad Tahir’ for his continuous encouragement

To Emma & Aimen, the Happiness & Charm in my life

To my Teachers for their guidance and tutelage

To my beloved country ‘Pakistan’

ACKNOWLEDGEMENTS

"In the name of Allah, The Most Gracious and The Most Merciful"

All praise belongs to Almighty Allah (s.w.t.) for bestowing me with courage and perseverance to carry out this work sincerely. I thank Almighty Allah for giving me chance to do my M.S. successfully at King Fahd University of Petroleum and Minerals, Dhahran.

My great thanks to King Fahd University of Petroleum and Minerals for providing me good academic platform and financial support during my M.S., thanks is also due to the KACST TIC-CCS at KFUPM.

My deep gratitude and appreciation goes to my thesis advisor and mentor Dr. M.A. Habib for his constant guidance, motivation and support during the course of my studies. His valuable suggestions broadened my horizon in the field of combustion, made this work interesting and challenging for me. I also wish to express my deep appreciation to Dr. Hassan M. Badr and Dr. Wael H. Ahmed for their help, guidance, and constant encouragement during my M.S.

Many thanks to Mr. Karam, supervisor of heat engines lab at kfupm for his support and technical assistance during experimental work. I would also like to thank Dr. Medhat A. Nemitallah and Mr. Pervez Ahmed for their encouragement and guidance.

I am very grateful to Yasir Jamil, Binash Imtiyaz, Ahmer Ali and Maimoon Atif for their help and encouragement during my Masters. Also special thanks to Danish Sattar, Haider Ali and Waqas Ahmed for their support. I would also like to acknowledge all the Mechanical Engineering faculty members with whom I took courses during my M.S., who helped me a lot during my coursework. I also owe thanks to all the students and faculty with whom I interacted during my Masters program.

TABLE OF CONTENTS

LIST OF TABLES

LIST OF FIGURES

LIST OF ABBREVIATIONS

CCS	:	Carbon Capture and Sequestration
CFD	:	Computational Fluid Dynamics
IPCC	:	Inter-governmental Panel on Climate Change
IGCC	:	Integrated Gasification Combined Cycle
ITM	:	Ion Transport Membranes
MOFs	:	Metal Organic Frame works
OTR	:	Oxygen Transport Reactor
OR	:	Oxidizer ratio
TCD	:	Thermal Conductivity Detector
FID	:	Flame Ionization Detector
DO	:	Discrete Ordinate
O/N	:	Oxygen to Nitrogen ratio
O/F	:	Oxygen to Fuel ratio
ppm	:	Parts per million
MEA	:	Mono Ethanol Amine
DAQ	:	Data Acquisition System
ARR	:	Arhenius Reaction Rate
WSGGM	:	Weighted Sum of Gray Gas Model

ABSTRACT

FULL NAME : FURQAN TAHIR

THESIS TITLE : EXPERIMENTAL AND NUMERICAL INVESTIGATIONS OF OXY-FUEL COMBUSTION USING POROUS PLATE REACTOR

MAJOR FIELD : MECHANICAL ENGINEERING

DATE OF DEGREE : MAY, 2014

Fossil fuels are in abundant use to meet growing global energy demand. Burning of these fossil fuels produces CO_2 which is considered a greenhouse gas. The carbon dioxide (CO_2), resulting after the combustion of fossil fuels, is disturbing the CO_2 cycle and consequently posing serious climate change which is a threat as global warming. Many studies are being undertaken for Carbon Capture and Sequestration (CCS) technologies which include pre-combustion, oxy-fuel combustion and post combustion. Oxy-fuel combustion provides a novel mean of capturing carbon since fuel is burnt in the presence of pure Oxygen only producing CO_2 and water as combustion products. CO_2 can be captured easily after condensation of water and there are no emissions at all.

The present study focuses on experimentation and modeling of oxy-fuel combustion reaction in a specially designed combustion reactor using porous plates. The porous plates are used for the permeation of oxygen; the advantages of using porous plates include parallel flow configuration, controlled permeation of oxygen and stability at higher temperatures. Initially non-reactive flow experiments are performed to analyze the permeation rate of Oxygen in order to obtain desired stoichiometric ratios. Both axial and

vertical concentration profiles of species were measured. Numerical model has been validated against the experimental results for non reactive flows. Simulations employing one step reaction and two step reaction kinetics models for methane combustion are performed and parametric study is carried out to analyze the effect of equivalence ratio, oxidizer ratio, permeability, and Reynolds number on the performance of the reactor. It was found that the maximum temperature in the reactor increases by increasing oxidizer ratio, equivalence ratio (up to 1) and Reynolds number and the outlet temperature increases by increasing the sweep flow rate, equivalence ratio and Reynolds number. The one step model over-predicts the temperature and reaction rates as compared to two step model. It was found that the reaction zone can be adjusted to desired region within the reaction chamber by varying inlet conditions.

ملخص الرسالة

الاسم الكامل: فرقان طاهر

عنوان الرسالة: دراسة معملية ورقمية لإختبار احتراق وقود الأوكسي باستخدام مفاعل ذو لوحة مسامية

التخصص: هندسة ميكانيكية

تاريخ الدرجة العلمية: مايو 2014

يعتبر الوقود الاحفوري من أكثر الوسائل المستخدمة في تلبية تنامي الطلب العالمي للطاقة. واحتراق هذا الوقود ينتج غاز ثاني أكسيد الكربون والذي يعتبر أحد غازات الاحتباس الحراري. وثاني أكسيد الكربون الاصطناعي الناتج بعد احتراق الوقود الاحفوري يشكل تهديدات خطيرة تؤدي الى تغيير المناخ مثل ظاهرة الاحتباس الحراري. تجرى العديد من الدراسات لتتنفيذ تقنيات احتجاز وتخزين الكربون والتي تشمل ما قبل الاحتراق، واحتراق أوكسي الوقود وبعد الاحتراق. احتراق اوكسي الوقود يعتبر وسيلة مهمة لحجز الكربون. تتم عملية احتراق وقود الاوكسي في وجود الأكسجين النقي وينتج عن ذلك غاز ثاني أكسيد الكربون والماء كنواتج احتراق. وبعد ان يتم تكثيف الماء يمكن بسهولة احتجاز ثاني أكسيد الكربون وبالتالي لن يكون هنالك اي انبعاثات على الاطلاق.

تم في هذه الدراسة التركيز على نموذج احتراق وقود الأوكسي في مفاعل احتراق مصمم باستخدام لوحات مسامية. في البداية يتم اجراء تجارب للتدفق بدون تفاعل لتحليل معدل مرور الأكسجين بغرض الحصول على نسب التكافؤ المطلوبة (قوة المزيج). تم قياس كل من التركيز المحوري والعمودي لمكونات غازات الاحتراق ثم تم عمل نموذج عددي باستخدام برنامج ديناميكا الموائع (CFD_FLUENT 6.3) التجاري ورسم النموذج باستخدام (Gambit 2.4) وتعريف الشروط الحدية للنموذج. بعد ذلك تم التأكد من صحة النموذج بعمل مطابقة مع النتائج المعملية وتم تنفيذ نموذج الخطوة الواحدة لتفاعل احتراق الميثان ثم اجريت دراسة لتحليل أثر نسبة التكافؤ، نسبة المؤكسد، النفاذية ورقم رينولدز. ووجد ان اقصى درجة حرارة في المفاعل تزيد بزيادة نسبة المؤكسد، نسبة التكافؤ (تصل الى1) ورقم رينولدز بنما تزيد درجة الحرارة الخارجة بزيادة معدل التدفق، نسبة التكافؤ و رقم رينولدز. أيضا فان نموذج الخطوة الواحدة يمكنه توقع درجة الحرارة ومعدل التفاعل اذا ما قورنت مع النموذج ذو الخطوتين والذي

هو اكثر واقعية. أخيرا وجد ايضا ان منطقة التفاعل يمكن ضبطها للموقع المناسب في غرفة الاحتراق وذلك بتغيير حالات الدخول.

CHAPTER 1

INTRODUCTION

1.1 Global Warming and CO_2 emissions

As the world's population is growing and the standard of living is improving day by day, the global energy requirements are increasing and to overcome this substantial need of energy; more power plants have to be established. Currently around 80% of the energy demand is met by fossils fuels and among fossils fuels 40% is coal and rest includes furnace oil, natural gas, diesel etc [1]. The fossil fuels power plants are smooth in operation; take less time to commission and efficient but the disadvantages are severe in terms of global impact. These plants are producing tons of CO_2 every second making the earth warmer by global warming. The two green house gases i.e. carbon dioxide and water vapor are the main gases responsible for the global warming. The carbon dioxide resides in the atmosphere for more than one century. Global warming is damaging the earth atmosphere for the present and next generations by climate change, water scarcity, ice caps depletion, air pollution etc. The maximum temperature rise of the world in 2090 is 8 ^{0}C starting from 1990 [2] as shown in Figure 1. Therefore, the CO_2 emissions must be controlled by developing alternative technologies for energy needs and capturing the mechanism.

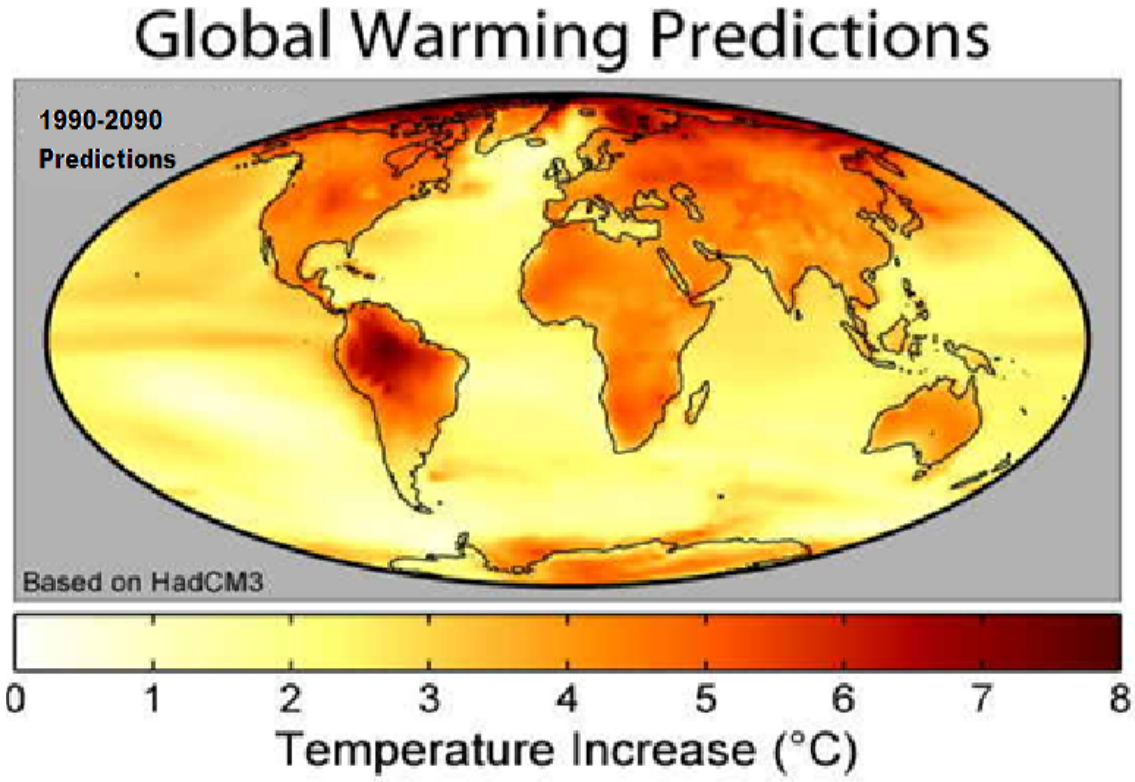

Figure 1: Predictions of temperature rise from 1990-2990 around the globe [2]

In the assessment report by the Inter-governmental Panel on Climate Change (IPCC) published in 2007 [3] reported some important observations that include the rise in the average temperature of the Earth's surface is +1 ^{0}C since 1910, the average sea level rise for past 100 years is 16 cm and the snow cover reduction in the Northern hemisphere is 9 % within the past 50 years. These phenomena are speeding up and the predicted temperature rise till 2030 is 0.2 ^{o}C and if the fossils fuels are being used continuously then the sea level rise would be 59 cm from 18 cm by 2099. In order to avoid catastrophic consequences of the global warming, the carbon dioxide concentration should not cross 450 ppm by 2050. Therefore the CO_2 emissions must be reduced by developing alternative technologies for energy needs and capturing the mechanism.

1.2 Carbon Capture technologies

In order to reduce the CO_2 emissions, several approaches have been proposed in the literature; one way is the forestation, according to Pacala and Socolow [4]; if the rate of forestation is doubled and the stopping deforestation can result in the decrement of CO_2 emissions by 3.70 Giga tons by 2050. They have shown the prediction of CO_2 emissions in 'Billions of tons per annum' till 2054 which will be 14 Giga tons per annum as shown in Figure 2, so it is important to limit CO_2 emissions from the primary source i.e. thermal power plants.

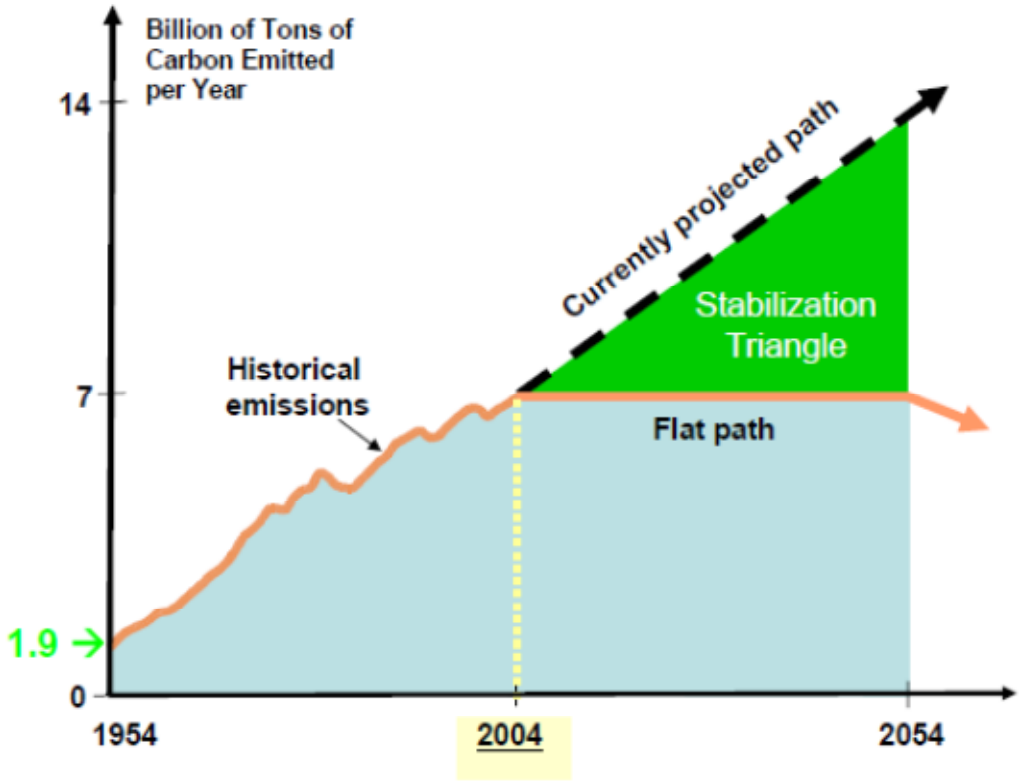

Figure 2: Projection of CO_2 emissions in billions of tons of year till 2054 [4]

The approaches related directly to power plants are termed as 'Carbon Capture and Storage' (CCS) These technologies are namely, pre combustion, post combustion and oxy-fuel combustion as reported by Habib et al [5] as shown in Figure 3. In pre combustion, the fuel is treated such that the carbon contents are removed at the initial stage and there will be no CO_2 in the exhaust. The fuel is first converted in to carbon monoxide (CO) and hydrogen gas (H_2), the mixture is called syngas which is produced by the steam reforming process. Then, the syngas is converted in CO_2 and H_2 gas by means of shift reaction, the CO_2 is removed and sent for compression and then to storage or enhanced oil recovery. The remainder that is hydrogen gas is burnt to produce power. In post combustion, the flue gases are treated to remove the CO_2 contents. The flue gases are passed through solvents and packed beds that only absorb CO_2 and then absorbed gases are removed by lowering the pressure or increasing temperatures. The removed CO_2 is then compressed and sent for storage. For absorption, most commonly solvents are amine solvents and for the adsorption Metal Organic Frame works (MOFs) or Zeolite. In the oxy fuel combustion, instead of air, oxygen reacts with the fuel. Therefore there will no NO_x in the emissions and only CO_2 and H_2O will be present at the outlet, CO_2 then easily be separated by means of condensation. The CO_2 can be re circulated as a carrier gas to reduce the maximum temperature in the combustor. The oxygen from air can be separated by cryogenics techniques or by incorporating ion transport membranes (ITM).

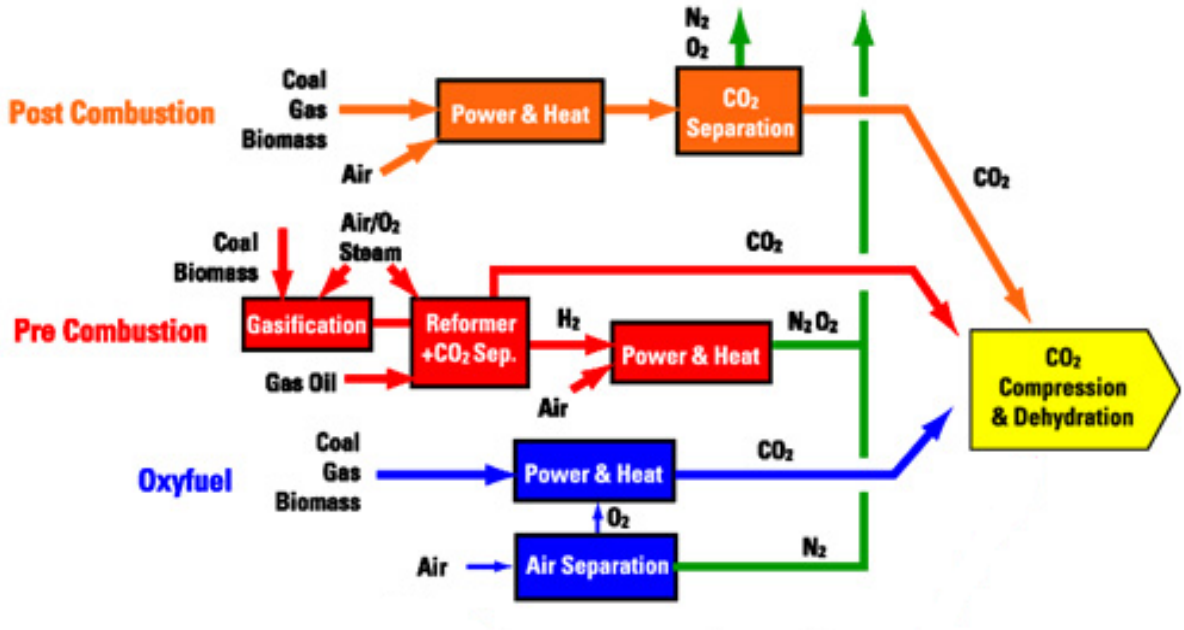

Figure 3: Proposed Carbon capture technologies [1]

1.3 Sequestration and Storage

After solving the issue of separating CO_2 contents from flue gases of power plants, the next task is to store CO_2, so that it cannot be the part of environment. It has been already established in IPCC report [3] that the CO_2 can be stored in the deep aquifers, coal mines, depleted oil and gas fields, limestone, sandstones as shown in Figure 4. The CO_2 can also be used for enhanced oil recovery. The carbon dioxide must be stored at the depths of more than 800 m to obtain temperature and pressure at which the volume is minimum (super critical state i.e. 74 bar and 31 ^{0}C) [2]. From the study three types of the storage were found feasible, they are:

- Deep aquifers
- Depleted Oil and Gas fields
- Coal mines.

Among different kinds of storage, aquifers can store CO_2 more than ten times than the depleted oil and gas reservoirs.

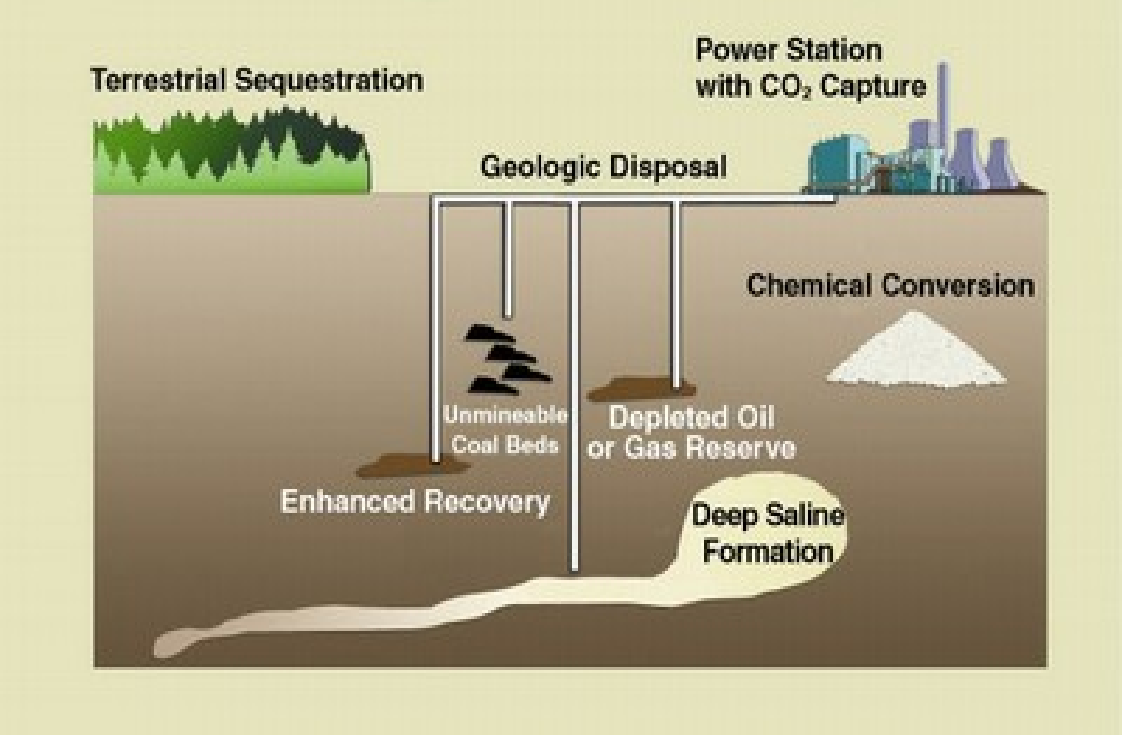

Figure 4: CO_2 sequestration options [3]

1.4 Oxy-fuel Combustion for Power plants

The oxy-fuel combustion is one of the promising carbon capture technologies that can be used in the new plants and existing plants with some modifications [6]. The combustion between pure oxygen and fuel results in very high temperatures which most of the materials cannot withstand, in order to reduce temperature CO_2 is re-circulated to and reduce the overall temperature. The main advantage is that we can control the flue gas in order to optimize the combustion process. Kunze and Spliethoff [7] assessed carbon capture technologies for Integrated Gasification Combined Cycle (IGCC) Plants. They studied all three techniques i.e. pre combustion, post combustion and oxy-fuel combustion for IGCC plants. In their study, IGCC concept based for oxy-fuel combustion showed a substantial improvement in efficiency reaching 45.74% but this concept also needs certain modifications and new equipments. The use of CO_2 as a carrier gas in the oxy-fuel combustion process will reduce the flame speed as compared to the nitrogen as reported by Law et al [8]. This resulted in the poor performance and temperature and species were different for nitrogen and for carbon dioxide cases. Anderson and Jonhsson [9] conducted experiments on combustion in environment of O_2/CO_2. The experiments showed that the flame temperature is reduced when the fuel is burnt with the ratio of O_2/CO_2=21/79 as compared to the burning of fuel in air. He found that the combustion is delayed for ratio of oxygen to carbon dioxide on volumetric basis O_2/CO_2=21/79, the results for ratio O_2/CO_2=27/73 were better than the previous case. Figure 5 shows the schematic of oxy-fuel combustion coal based power plant in which oxygen is separated and then burns the fuel in the boiler, the fly ash and the sulfur are

removed that are left over of combustion then the water vapor are separated by condensation and only CO_2 is left which is compressed and transported for sequestration.

Oxygen can be separated from air at very low temperatures (cryogenics), but it needs a lot of power for the air compression [10]. The cryogenics plants available at the market have low second law efficiency in the range of 15-24% [11] and these plants can substantially reduce the overall efficiency of the power plants [12], so the incorporation of cryogenic plants would be costly, inefficient and require more space. Recent investigations have been going on in developing ion transport membranes (ITMs), they are mixed ionic and conducting ceramic membranes. The membranes that are being focused for are lanthanum cobalite perovskite type ceramics [13]. Different kinds of membranes have been developed which are semi permeable for oxygen and provides high oxygen flux at high temperature when it is exposed to air and a hydrocarbon. These membranes are efficient as compared to the cryogenics process.

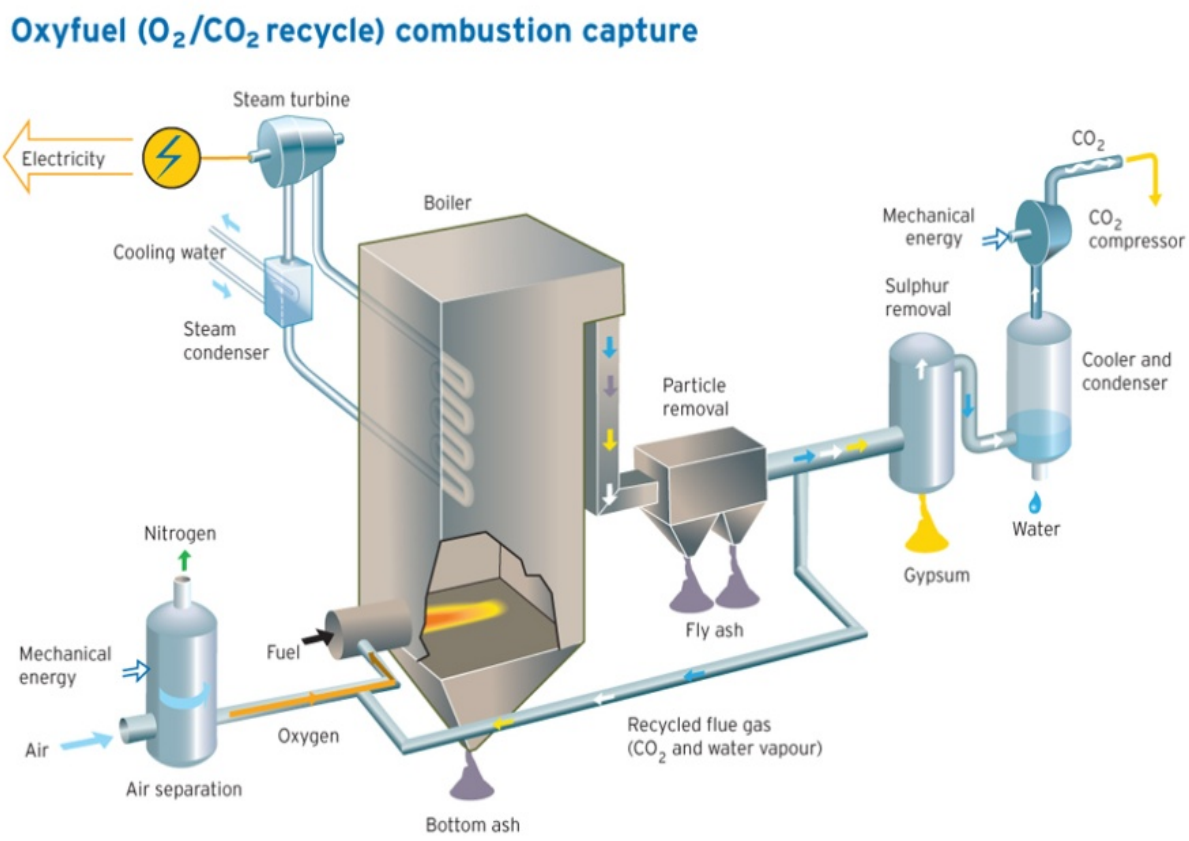

Figure 5: Schematic of oxy-fuel combustion coal based power plants [14]

1.5 Ion Transport Membranes (ITMs)

Ion Transport Membranes are used to separate oxygen from air by means of conduction and diffusion as shown in Figure 6. There are three main types of ITMs perovskite, fluorite and mixed. Mixed membranes are simply membranes made of a mixture of different types of ITMs in order to combine advantages of both. Air products (USA); has developed the commercial units for oxygen separation based on ITMs. They have developed ITMs stacks which can separate oxygen with the rate of one ton per day. Different configurations have been proposed by the Air products for efficient separation and utilization of ITMs [15]. The most important parameter in the oxygen separation is the oxygen partial pressures across the membrane, the partial pressure ratio is the driving force [16]–[18]. Usually, the permeate side is operated under vacuum. Diethelm et al [19] compared different membranes and normalized the results for 1 mm thickness, he found that the thicker membrane have less oxygen flux than the thinner membranes. Wang et al [20] studied the oxygen permeation by changing the feed side conditions; they observed that the flux is increased for the flow rate up to 0.15 L/min. Patridge et al [21] studied four different types of polypyrole conductive membranes, they demonstrated that the incorporation of different dopant ions changes the physical characteristics of membranes; they also showed that increasing the concentration of feed solution resulted in higher flux.

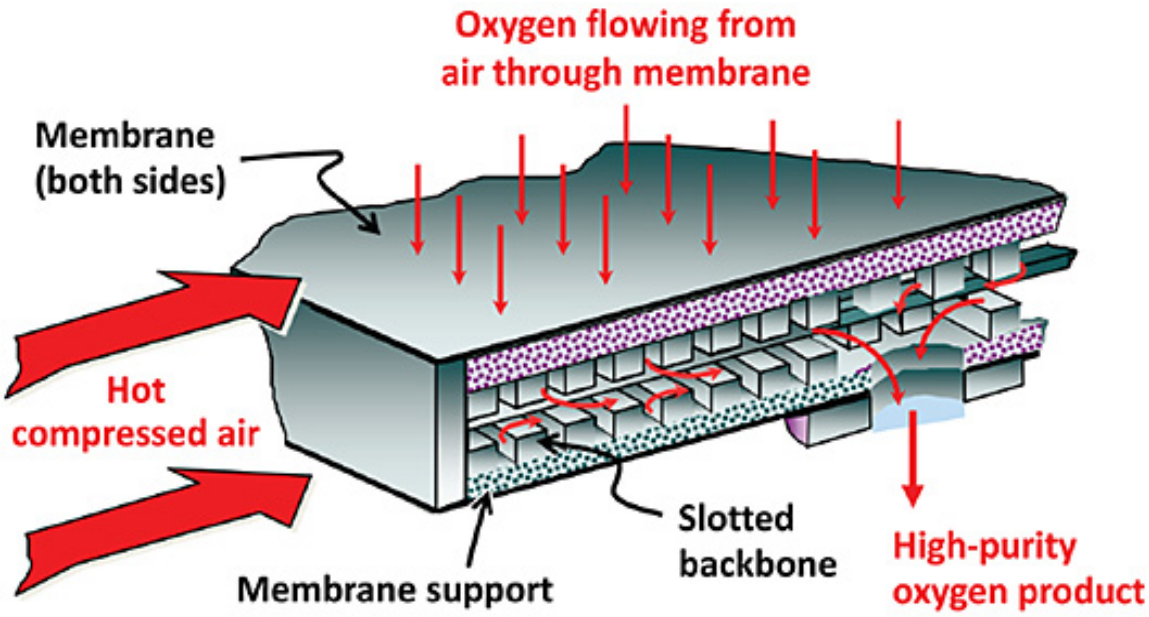

Figure 6: Separation of oxygen from high pressure and temperature air by means of ITMs [22]

1.6 Problem Statement

This study is focused in finding possible solutions to decrease CO_2 by means of oxy-fuel combustion process. In this study, a porous plate reactor has been developed in which methane is burnt in the presence of oxygen and carbon dioxide. The carbon dioxide serves as a carrier gas. Oxygen supply will be made possible by means of cylinders. Both experimental and numerical work has to be carried out in order to study the combustion process and to optimize the performance of the reactor by means of numerical work. A reactor has been modeled that contains three chambers all of 30 mm in height as shown in Figure 7. The top and bottom chambers are for oxygen inlet and center chamber is for fuel (methane)/nitrogen and carries gas (CO_2). The oxygen passes through the porous plates to get into middle section where it reacts with the fuel and the flue gases will pass out from the exit on the right. The porous plate dimensions are; length 'L'=150mm, width 'w'=50 mm and thickness 't'=1.13 mm. The experimental results will be used to validate numerical model. The parametric study and optimization of the porous plate reactor is to be carried out in terms of permeability of porous plates, oxidizer ratio, equivalence ratio, Reynolds number, maximum temperature and reaction zone.

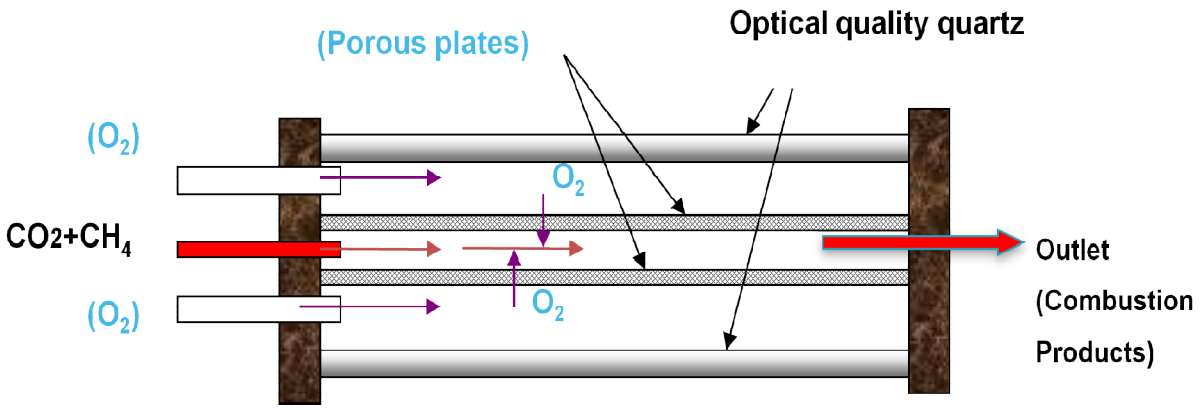

Figure 7: Porous plate reactor for oxy-fuel combustion

1.7 Research Objectives

The research objectives of this study are as follow:

- To investigate experimentally concentrations of species and study the effect of different variables on oxygen to nitrogen ratio at different locations of the porous plate reactor.
- To develop a 2D CFD model for non reactive and reactive (combustion) cases.
- To validate numerical results against experimental data.
- To conduct sensitivity analysis of all parameters affecting performance of the reactor and the identification of the parameters those have strong impact on the performance.
- To optimize the porous plate reactor in terms of oxygen permeation, reaction zone, fuel to carrier gas ratio, minimum oxidizer etc.

1.8 Thesis Outline

The thesis is comprised of eight chapters.

Chapter 1 introduces the challenges to address global warming issues; need and availability of carbon capture technologies, Ion Transport Membranes for oxygen separation, problem statement of thesis and the research objectives set to accomplish in this work.

Chapter 2 focuses on literature review mainly related to carbon capture technologies, advancements in oxy-fuel combustion technologies, development and applications of porous media.

Chapter 3 gives the details related to the development of experimental setup, equipments that are used in operation, accuracies and error analysis of Gas chromatograph, gas purity, mass flow controllers and misc. equipments.

Chapter 4 describes the methodologies related to both experimental and numerical work, computer packages that are used to descritized and solve the domain of the problem, governing equations and laws that are required to solve for numerical modeling.

Chapter 5 focuses on numerical study that includes validation of porous media flows. It presents the validation of numerical models by means of experimental results for non reactive flow in order to ensure reliability of numerical results for reactive cases. Numerical results for both non reactive and reactive flows using 1 step model and 2 step modified model for combustion. Parametric study has been conducted at end to find optimum conditions for the reactor design.

In chapter 6 the conclusion of this study is presented and the possible future recommendations are proposed for continuation of this study in order to further improve the performance of the oxy-fuel combustion processes.

CHAPTER 2

LITERATURE REVIEW

2.1 Carbon Capture Technologies

As stated before, around 40% of energy demands are met by coal and it is the largest contributor in the production CO_2 emissions followed by liquid fuels (furnace oil and diesel) and then natural gas as shown in Figure 8. The actual usage of each type of fuel is presented for up to 2008 and projections were made for the next 42 years in which the coal utilization in energy sector increases drastically. The CO_2 emissions may rise up to 42 Giga tons per annum by 2035 [23]. Carbon Capture and Sequestration (CCS) is a promising technology to limit the CO_2 emissions. CCS is applicable to all types of combustion processes and is considered viable to commercial power plants. Three approaches have been developed under the umbrella of CCS; namely pre combustion, post combustion and oxy-fuel combustion. The main goal of all these approaches is to capture CO_2. After separating CO_2 from the flue gases, it is compressed and transported for sequestration.

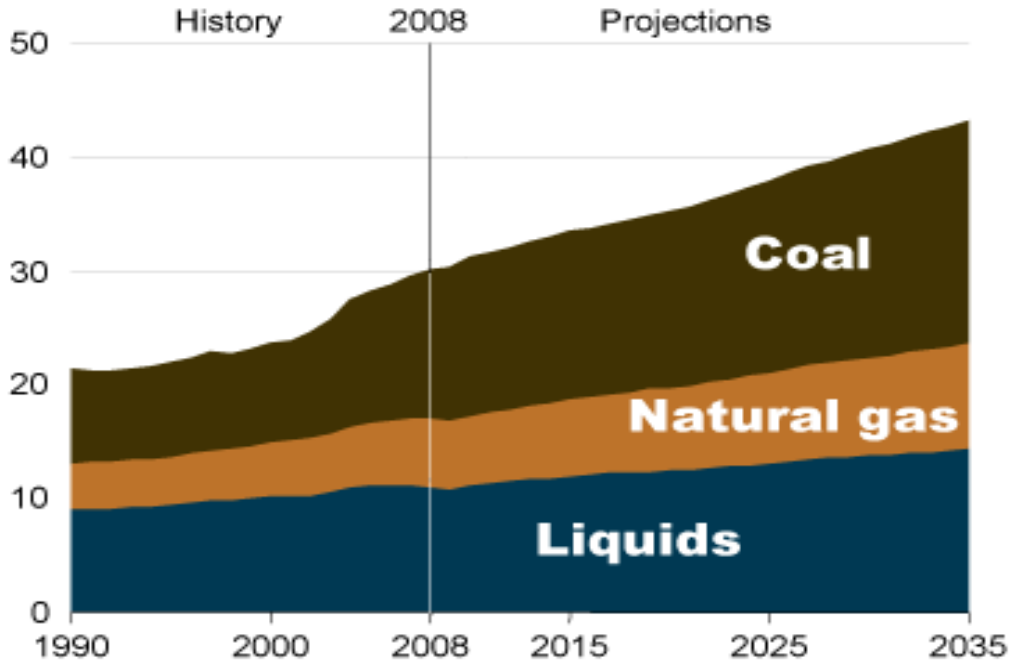

Figure 8: History and predictions of CO_2 emissions in Giga tons per annum by the usage of different fuels [24]

In pre-combustion approach, the fuel is decarbonized and all the carbon contents are removed before combustion. In refining, fertilizer and petrochemical plants, this process is used for the production of hydrogen for more than half century [25]. In this method, fuel is converted in to syngas in the presence of steam and air. Syngas is the mixture of carbon monoxide and hydrogen then carbon monoxide is converted into hydrogen and CO_2 by second shift reaction. The CO_2, can, then be removed and carbon free fuel i.e. hydrogen is combusted in the reactor. One example of the power plant incorporating pre-combustion approach is shown in Figure 9, in which fuel and steam produces syngas which is then cooled and particulates and hazardous gases like H_2S are removed then CO_2 is removed and compressed and the clean syngas is utilized in the combined cycle power plant.

The post-combustion technique can be easily incorporated in the existing plants as compared to other approaches. In this approach, flue gases are passed through solvents or beds of MOFs where the CO_2 is separated by absorption or adsorption. Liquid solvents are usually amine based solvents such as MEA: Mono Ethanol Amine are used, MEA is used in different industries in CO_2 separation processes [26]. Few years back, Metal Organic Frameworks (MOFs) were developed which are porous in nature and have high surface area to volume ratio for adsorption. MOFs are superior than liquid solvents in terms of energy consumption and ease of operation [27]. One example of the power plant incorporating post combustion approach is shown in Figure 10; in which fuel is burnt in the furnace (without any modifications), the flue gases are treated such that NO_x and

particulates are removed in the first stages and then the flue gas is desulphurised in the SO_x removal chamber and then CO_2 is removed and compressed for transportation.

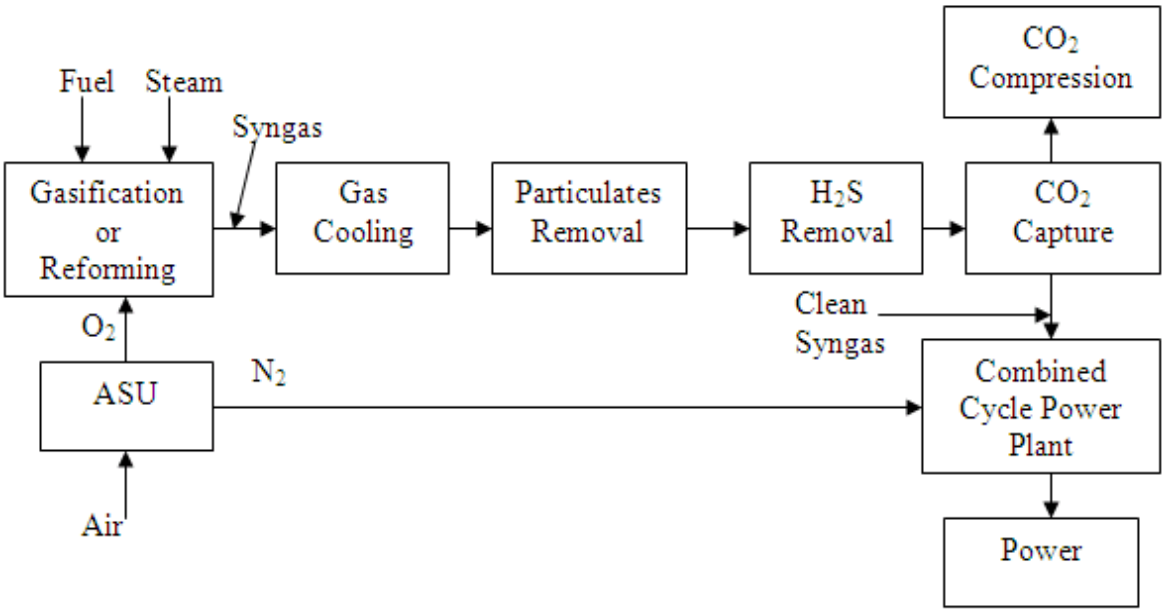

Figure 9: Layout of Pre-combustion approach for power plant. [1]

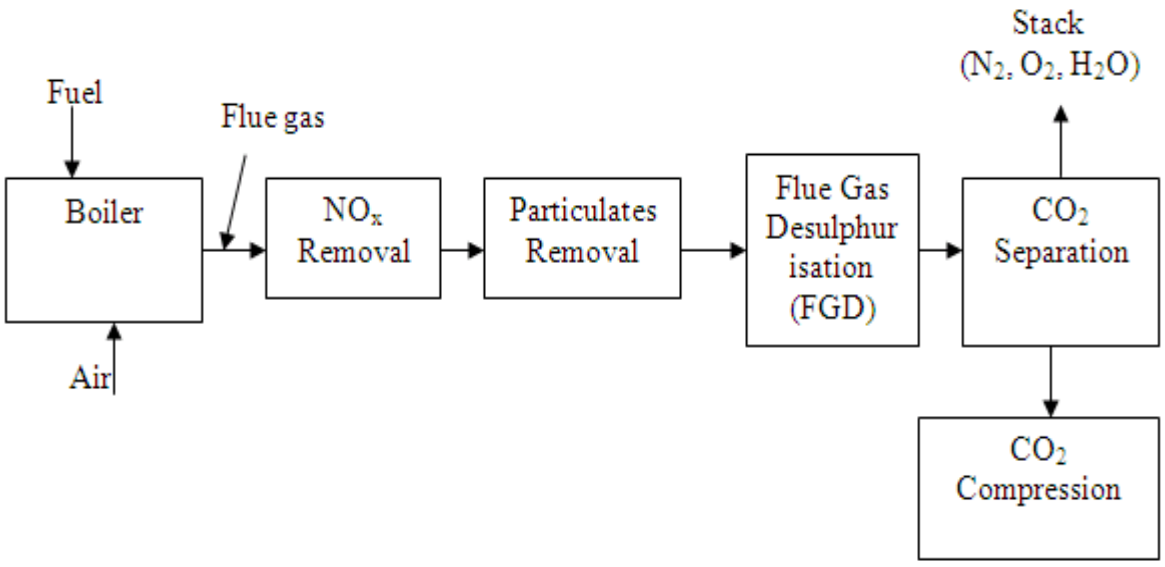

Figure 10: Layout of Post-combustion approach for power plant. [1]

In oxy-fuel combustion, fuel is combusted in oxygen environment instead of air which eliminates the possibility of NO_x formation. However, the oxygen availability is the drawback of this approach; oxygen is to be made available from air by separation processes which are costly. Reaction between fuel and pure oxygen gas will result in very high temperatures which most of the materials cannot withstand, so CO_2 has to be recycled as a carrier gas to reduce overall temperatures. The flue gases only contain water vapor and CO_2 ideally out of which water vapor can be easily removed by condensation. The high concentration of CO_2 in the exhaust makes it more economical for downstream process as compared to other approaches. Removal of up to 98% of CO_2 is possible by oxy-fuel combustion [28]. This approach has also been studied for gas turbine applications but still it is in research phase and it is important to integrate oxy-fuel combustion with the thermodynamic cycle of the plant in order to enhance carbon capture and efficiency [29]. One example of the power plant incorporating oxy combustion approach is shown in Figure 11; in which air is separated in the air separation unit to generate pure oxygen for combustion, the fuel is burnt in the mixture of oxygen and carbon dioxide and then CO_2 is removed from flue gases, some portion of the CO_2 are recirculated in the combustion chamber.

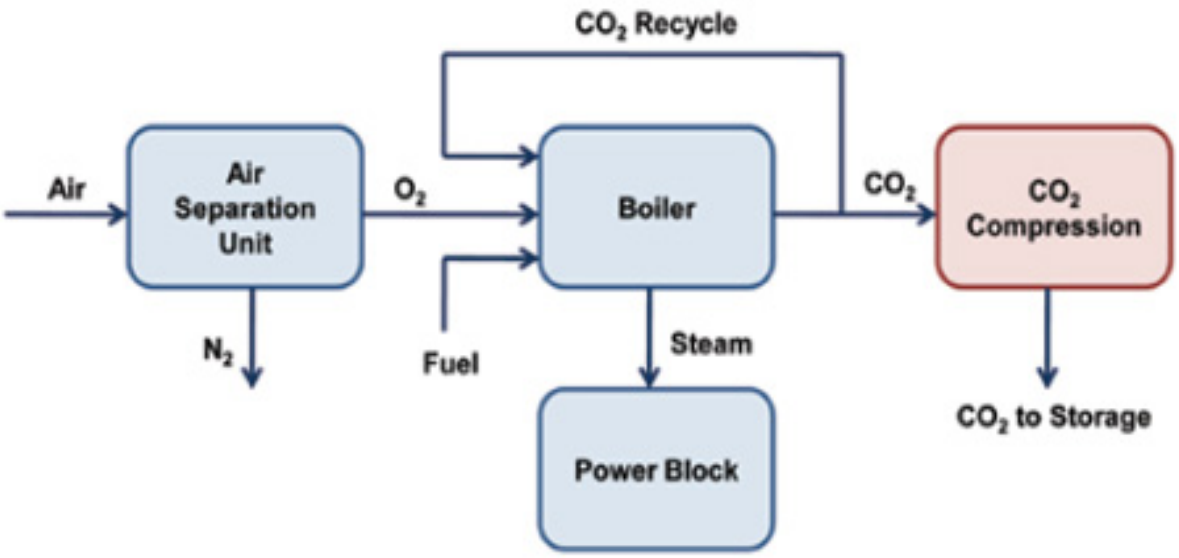

Figure 11: Layout of Oxy combustion approach for power plant. [1]

These three approaches are summarized based on their merits and demerits in Table 1.

Table 1: Comparison between CCS approaches [2], [3], [24], [30]

S.No.	Technique	Advantages	Disadvantages
1.	Post combustion	➢ Can be retrofitted to existing plants ➢ Immediate solution	➢ Due to low conc. in exhaust, the separation is very costly. ➢ Net power decreases by 30%
2.	Pre combustion	➢ Carbon contents are removed before combustion ➢ Water gas shift reaction commercially practiced	➢ Hydrogen fired gas turbine are not commercially available. ➢ Net power decreases by 20% ➢ Dilution of H_2 is needed.
3.	Oxy-fuel combustion	➢ Removal of CO_2 up to 98% ➢ Combustion can be controlled by varying O_2/CO_2 ➢ No emissions at all.	➢ Modification and replacement of some equipment is needed ➢ Air separation is needed ➢ Net power decreases by 25%. (cryogenic separation)

2.2 Oxy-fuel Combustion

Oxy-fuel combustion has more oxygen rich environment than the normal air combustion so flue gases from oxy-fuel combustion will be relatively clean; oxy-fuel combustion has been used in the metal and glass manufacturing industries. Oxy-fuel approach can be implemented to the existing coal based power plants and new one by building reactors for oxy-fuel [6]. Oxy-combustion has not yet fully matured for application in large scale power production units. Many researchers show large potential to implement the membrane integration technology for oxygen separation with oxy-fuel combustion [9], [31]–[33]. The main objective is to investigate several features of oxy-fuel process for power plants, e.g. boiler design, combustion kinetics, sealing issues in oxygen separation equipments to make this technology more applicable [34]-[35]. This idea can be extended to combustion of natural gas with oxygen separation membrane integration in combustion reactor. Efforts has to be made for efficient combustion process such as ignition in case of coal-fired, reaction kinetics, flame stability, sealing of membrane and the activation energy required [36]–[39]. Many researchers used numerical techniques in order to evaluate the performance of oxy fired power plants. Boilers, burners, reactors, and furnaces etc have been modeled using the CFD approach and detailed investigations were made in order to enhance the performance [40]-[41].

Heil et al [42] tested different types of swirl burner for coal combustion. His study shows that when the oxygen concentration in the O_2/CO_2 mixture was set to 21%, poor combustion and unstable dark flame was observed but when the oxygen concentration

was increased to 27%-34%, the stable flame and full burnout were obtained. Hong et al [43] reported that the detailed kinetics of oxy-fuel combustion for methane reduces from 1000+ reactions to 217 reaction and 316 species, so the analysis with detailed chemistry become easier than that of qir combustion. Andersen et al [44] studied the combustion process for the oxy-fuel conditions. They studied the Westbrook two step model and Jones four step model for combustion and compared with the Detailed Kinetics model and it was concluded that the two models had to be modified in order to predict acceptable results when they are to be used in CFD of oxy-fuel combustion. Andersen modified and refined the Westbrook and Jones models for oxy-fuel conditions. Bibrzycki and Poinsot [45] studied the detailed chemical kinetics involved in the air combustion and oxy-fuel combustion. They concluded that the kinetics for oxy-fuel combustion are reduced and Jones four step model with refinement give better results as well as the GRI Mech.

Oxygen available by air separation unit for oxy-fuel combustion is more than 95% pure and the rest is being nitrogen [46]. In coal based combustion, excess oxygen has to be supplied to ensure stoichiometric and homogenous combustion. In the flue gas, CO_2 and water vapor with small portions of NO_X, SO_X, etc. are present. The flue gases are sent to remove acidic gases and solid particulates. Although, oxy-fuel combustion is a very promising technique in CCS, lower adiabatic flame temperature, delayed ignition and lower burning rate in O_2-CO_2 environment are some of its major challenges to be dealt with [47]–[50]. An attempt to increase the thermal efficiency often comes at the cost of increased NO_x emissions. Moderate or Intense Low-oxygen Dilution (MILD) combustion

technique offers great advantage of achieving higher thermal efficiency in oxy-combustion with reduced pollutant formation [47], [51]. Blasiak et al. [52] investigated the MILD oxy-combustion of natural gas in the thermal treatment processes of wastes and the recovery of zinc bearing feed on a rotary kiln and found that it reduces the fuel consumption as well as NO_x emissions in addition to increasing the productivity of the rotary kiln. Krishnamurthy et al [53] found that the MILD oxy-combustion also reduces the soot formation significantly than the conventional oxy-combustion. The flue gases are treated for the removal of NO_x, which is known as deNO_x treatment. NO_x is present in the exhaust due to the leakage in boiler which is around 8%-15% [46]. After NO_x removal, SO_x (Sulfur contents) are removed, this process is known as DeSO_X treatment [54]. After dehumidification of the flue gas, it is estimated by the researchers that purity of CO2 ranges from 85%-95% ready for compression and sequestration [26]-[55]. In natural gas combustion with the assistance of OTR then DeNO_X and DeSO_X treatments can be avoided since with membranes we have very high purity of oxygen and the leakage is also negligible. Oxygen flames give higher temperatures which have to be controlled, because of the material melting temperature constraints, around 2/3 of the flue gas needs to be recycled [30]. Nitrogen is replaced by carbon dioxide which will carry away heat and will increase the concentration of CO_2 which is needed to separate it from the flue gas [54]. Chen et al [32] compared the CO_2, NO_x and SO_x emissions for air combustion and for different O_2/CO_2 ratios for oxy-fuel combustion. Their work shows that flue gases can have CO_2 concentration up to 90% and 34% in oxy-fuel combustion and air combustion respectively, so it is easier to separate CO_2 from oxy-fuel combustion power plant due to high concentration of carbon dioxide.

Habib et al [56] modeled combined ITMs-Porous reactor in which isothermal conditions were achieved by incorporating porous plates of different permeability. This is done by achieving constant Oxygen to fuel ratio in the middle chamber with the help of carrier gas i.e. CO_2. It was also observed that the oxygen permeation increases with the increase in fuel to carrier gas ratio and it was showed that the proposed reactor has the flexibility of controlled reaction zone. Nemitallah et al [57] investigated the oxy-fuel combustion in an ITM reactor using two step reaction kinetics model. The model has been validated against the experimental data available. It was found that the factors that are important to operation of ITM reactor are Inlet species temperature, fuel percentage and the reactor geometry. Nemitallah and Habib [58] studied the oxy-fuel combustion in a gas turbine combustor. The experiments were conducted and validated by means of numerical model. The modified two step reaction kinetics model was implemented and found in better agreement with the experimental results. After validation parametric study has been carried out. The combustion was improved with the increment of oxygen in the inlet but this improvement is limited due to temperature limitations.

Abdul-Sater and Krishnamoorthy [59] studied the various radiation modelling strategies in simulations of oxy-methane diffusion flames. They confirmed the numerical results with the experimental data that the flame length increases with the increase in fuel-inlet Reynolds number but decreases increase in O_2 composition in the oxidizer stream. They used gray and non-gray formulations of weighted-sum-of gray-gas-model (WSGGM) to compute the radiation. They found that the radiant fraction was increasing with decrease in Reynolds number which was attributed to shorter flames and steeper temperature

gradient. WSGG models are popular for the calculations of radiation with the combustion model because of lower computational cost, better accuracies and ease of implementation. The accuracies of WSGG models were assessed and compared against the standard solutions in prototypical geometries [60]–[63]. Yin [64] and Krishnamoorthy [60], in their respective studies on numerical investigation of oxy-combustion of natural gas, found that the non-gray gas models are more accurate in predicting the wall fluxes than temperatures. Though, the importance of this model was diminished if the particles are present in the flame. In a numerical study on oxy-combustion of coal in small scale furnaces by Nakod et al. [65], it was concluded that the difference between gray-gas and non-gray gas model was minimal as the particle radiation was prominent than the gas radiation. While in large scale furnaces, where the effect of gas radiation was dominant over the particle radiation, non-gay gas model gives better accuracies [66]. Hjartstam et al. [67] concluded from their numerical investigations on oxy-propane flames in a lab-scale furnace that the accurate soot models are of much more importance than the non-gray radiation models in predicting the radiation field and temperature. Turbulence Radiation Interaction (TRI) was found to be important in oxy-combustion of coal [68] and natural gas [69] due to the presence of large concentrations of radiatively participating gases. However, Krishnamoorthy [60] has found that the introduction of TRI was of not much significance for highly swirling flames.

Habib et al [70] modeled the oxygen permeation through LSCF ITM and the effect of combustion on the permeate side was studied. It was found that increasing the air pressure on the feed side will affect the oxygen permeation. It was also noted that the higher concentration of CO_2 on the permeate side will reduce the partial pressure of oxygen on the permeate side; therefore there will be more oxygen flux. Nemitallah et al [57] used the two step modified model to predict the performance of an ITM reactor based on methane combustion. A 2D symmetric model was developed using CFD approach. It was found that the combustion has a strong effect on oxygen permeation and permeation is enhanced. Jongsup et al [43], [71] simulate the ITM reactor and studied oxygen permeation and fuel conversion in 2013 they extended their study and observed the interactions between the oxygen permeation and fuel conversion on the sweep side of membrane. The oxygen permeation was influenced by the fuel conversion; fuel conversion enhances the oxygen permeation.

2.3 Porous Media flows

Experimental studies have demonstrated the physical laws related to flow through porous media, revealing that darcy regime can predict the flow behavior properly when the flow velocity is sufficiently small, while Forchheimer regime, considering the inertial effects, is able to describe the flow pattern when the flow velocity becomes adequately large [72]–[75]. Zhong et al [76] analyzed the effect of differential pressure from the charged air into an isothermal chamber to determine the permeability coefficient and the inertia coefficient, and represent the flow rate regime in terms of darcy equation and Forchheimer equation. They verified the effectiveness of the proposed method experimentally. Zhong et al measured the pressure drop and the mass flow rates for different sintered metal porous materials by using charged air method, the inertial resistance and viscous resistance were calculated with an error of 3%.

Mancin et al [77] conducted experiments of Aluminum foams (porous) and measured the pressure drops, the experimental data was tabulated and regression was applied to calculate inertial resistance and permeability. Mancin et al [78] conducted experiments for Copper and Aluminum foams, in this study Pressure drop was calculated for isothermal and then Heat transfer coefficients were calculated. Figure 12 shows the variation of mass flux with pressure drop through various metallic foams. The modeling was carried out with the help of experimental results.

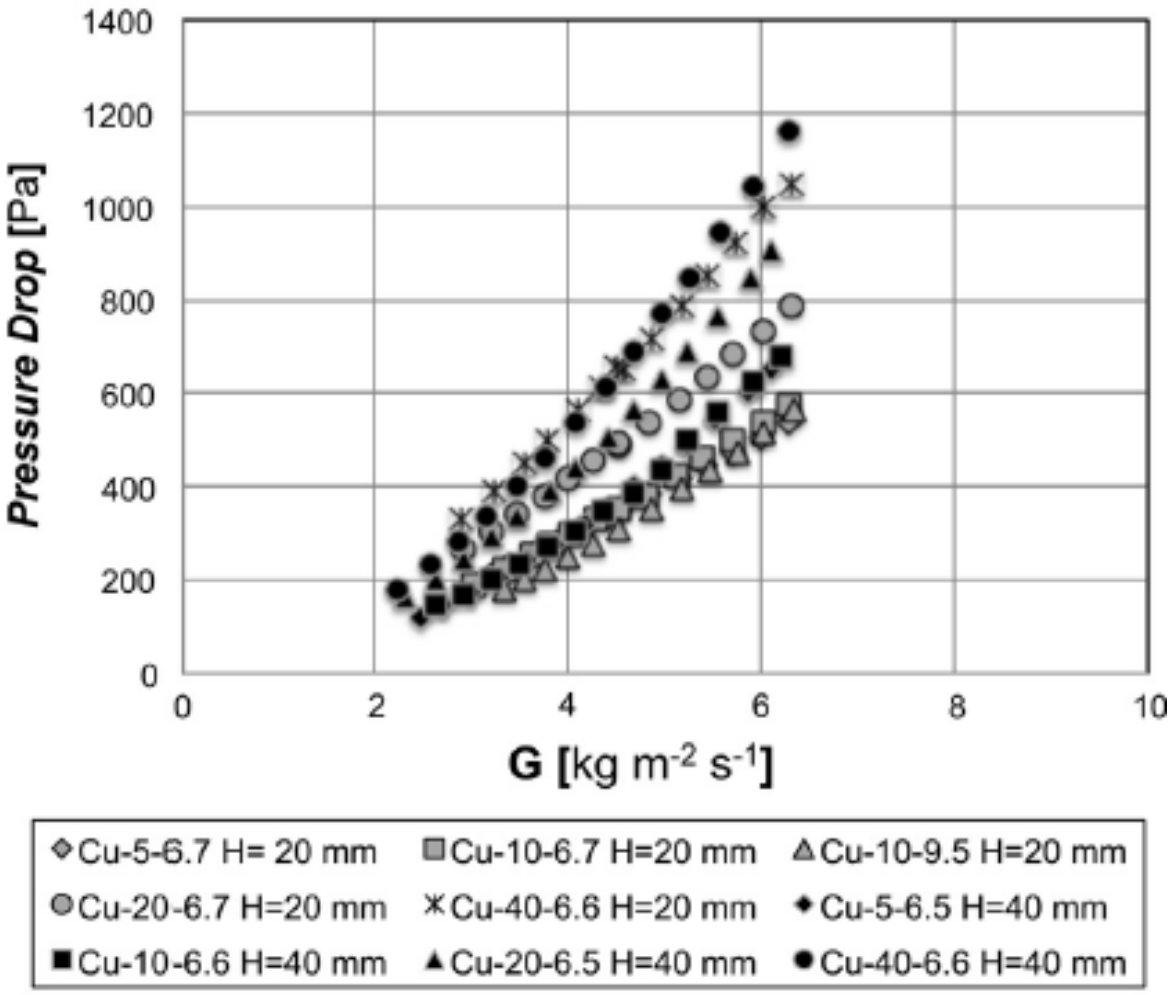

Figure 12: Pressure Vs Mass flux for various foams materials[78]

Under steady state operation, effect of small pressure drop on the flow rate is approximately proportional to the pressure difference across the porous material, indicating the application of darcy regime. In porous materials, it is examined that Poiseulle flow is predominant only when Knudsen number (the ratio of gas mean free path to pore diameter) is less than 0.01. When the Knudsen number is greater than 10, Knudsen diffusion is predominant in porous regime [79].

Shelekhin et al [80]-[81] examined the gas permeability properties of different gases like helium, hydrogen, carbon dioxide, oxygen, nitrogen, and methane in micro porous membranes made of silica as a function of pressure and temperature. They showed that the permeation rate of helium and other gases in porous membranes was comparable to that of industrially produced polymeric membranes. Sawley et al [82] proposed a numerical method porous flow simulations, the approach was proved to provide acceptable results for both saturated and unsaturated porous media flow. From his results the Darcy law was confirmed for low drift velocities in a saturated medium, while non-linear behavior was observed for higher velocities.

CHAPTER 3

EXPERIMENTAL SETUP FOR NON REACTIVE FLOWS

An experimental set up has been established at the heat engines lab in KFUPM to conduct experiments related to oxy-fuel combustion. The reactor consists of three chambers; the top and bottom are for oxidizer supply, pure oxygen is made available by means of gas cylinders. The central chamber is the reaction zone, where the fuel (methane) along with the carrier gas (carbon dioxide) enter and mix with the oxidizer that is coming through the porous plate from top and bottom chambers. The top and bottom chambers are closed so that all the oxygen supply is led to central chamber. The reaction begins when the oxygen to fuel ratios lie in combustible range and the flue gases leave from the outlet section. The reactor is equipped with quartz plates to visualize the combustion process. The height of each chamber is 30 mm, length of the reactor along with extension is 500 mm. width of the reactor is 55mm. Two alumina porous plates are used and each of them has 150 mm length and thickness of 1mm.

3.1 Set up for non reactive flow

The schematic of the experimental setup is shown in Figure 13. Three gas cylinders having purities of 99.5% are available for fuel (i.e. nitrogen), oxidizer (i.e. oxygen) and carrier gas (i.e. carbon dioxide) which are connected to the mass flow controllers that control the flow rate of each species entering in the reactor. The fuel is represented by nitrogen for non reactive case. To improve the mixing of fuel and carrier gases, a mixing chamber is provided before the reactor that contains honey comb structure to maintain laminar flow. Fuel along with the carrier gas enters the mixing chamber before entering the reactor. The length of the mixing chamber is 800 mm and the length of the reactor cover is 440 mm with an extension of 100 mm. For sample collection, a 1/8" probe has been placed inside the reaction chamber that can move horizontally and vertically by means of gear mechanism to cover whole chamber. The probe is connected to data acquisition system (DAQ) i.e. gas chromatograph through the compressor. The pressure ratio across compressor is low so that it won't disturb the flow field inside the chamber. Compressor is provided with dehumidifier to avoid moisture content entering to gas chromatograph. Gas chromatograph measures the species concentration on molar basis. For data logging and processing, data acquisition system is provided.

Figure 14 shows the 3D model of reactor along with the mixing chamber that was built in 'solid works' for manufacturing. The reactor is made of stainless steel and the quartz plates are sealed by means of high temperature resistant sealant. The experimental set up was made and set up in Heat engines lab situated in Building 26 of King Fahd University of Petroleum and Minerals. The built in set up is shown in Figure 14 which comprises of reactor, mixing chamber, gas chromatograph, gas cylinders, mass flow controllers and miscellaneous fittings.

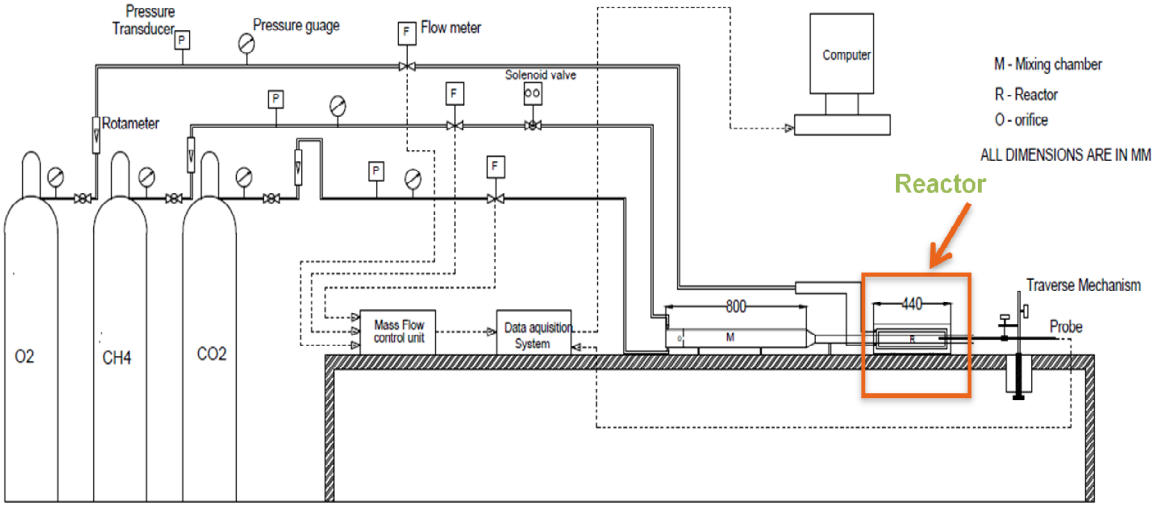

Figure 13: Schematic of Experimental set up

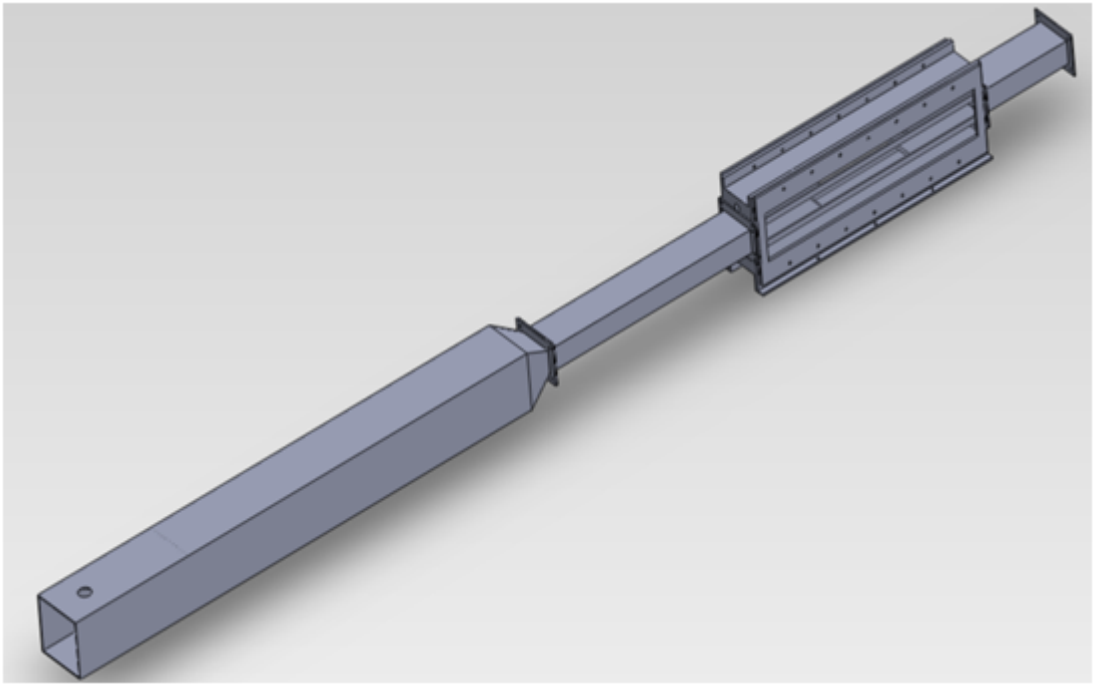

Figure 14: 3D model of porous plate reactor

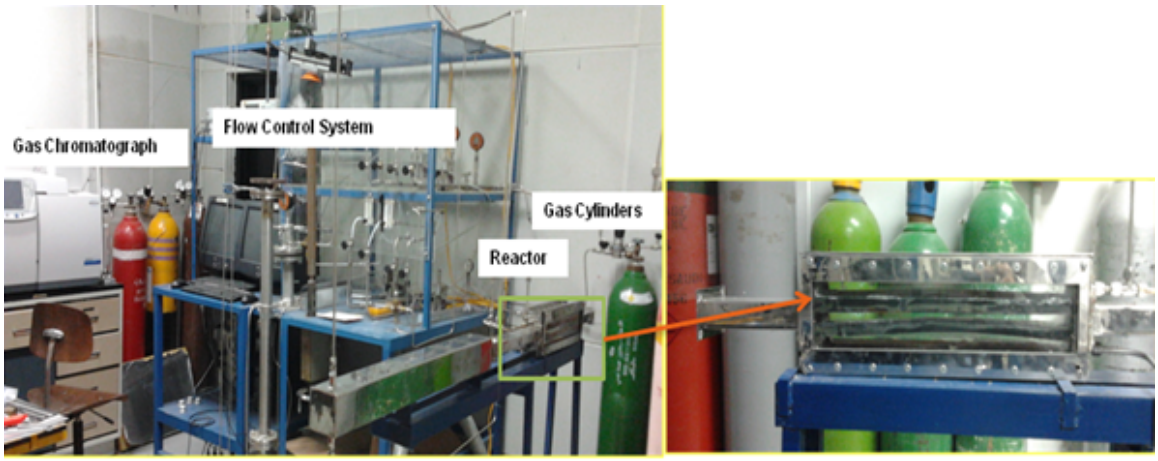

Figure 15: Experimental setup showing reactor, mixing chamber, cylinders, gas chromatograph

3.2 Equipments

To control the flow rate of gases, Bronkhorst high-tech D-type controllers have been used, the accuracy of the controllers is $\pm$ 0.5% of full scale. For manual measurement of flow rates in Liters per minute, Rota meters have been added to each gas line. Bruker 450-GC Gas chromatograph has been used for species concentration measurement. The Flame Ionization detector (FID) is used to measure total hydrocarbon measurement as methane equivalents. The Thermal Conductivity Detector (TCD) is the most commonly used detector to quantify the concentrations of CO, CO_2, N_2 and O_2. The standard deviation in the concentration measurement of the Gas chromatograph is less than 1% for three samples of same composition.

3.2.1 Gas chromatograph 450-GC

For measurement of species concentration consisting of O_2, N_2 and CO_2, Gas chromatograph '450-GC' of Bruker is used, which is fully automated and easy to operate. It gives very accurate results with standard deviation less than 1% if three sample of same concentration are processed, however the variation of mass flow rates should be small. It uses three carrier gases for processing. Hydrogen, helium and zero air are used in non reactive flow experiments. Before intake, the sample is passed through various filters to enhance the life of chromatograph such as moisture, oxygen and hydrocarbons filters.

After the sample is processed, the gas is exhausted to water bath. For processing gases contained in the sample, 450-GC uses two kinds of detectors are used namely; Thermal Conductivity Detector (TCD) and Flame Ionization Detector (FID). The TCD and FID are generally used in petroleum and petroleum industries, FID is most commonly used for hydrocarbons, naphtha, petroleum and BTX, whereas TCD is commonly used for air (O_2 and N_2) and fuel gases (like CO, CO_2 etc) [83]. For non reactive flow study, TCD is enough for sample measurements.

3.2.2 Vacuum pump

A vacuum pump is provided to suck and deliver the sample from the reactor to the gas chromatograph. The suction pressure is very low so that it wouldn't affect the velocity field inside the reactor.

3.2.3 Mass flow controllers

To control the species mass flow rates, Bronkhorst 'D' type flow controllers 'In-flow' with an uncertainty of $\pm$0.5%are used. The capacity of the flow controllers is ranging from 10 L/min to 70 L/min. The flow controllers are connected to data acquisition system from where the mass flow rate can be controlled.

3.2.4 Data acquisition system

.The mass flow controllers and Gas chromatograph are attached to data acquisition for data logging and processing. There are two scales in the control panel of flow controllers, one is the set point and the other is the measured against the set point. The scale ranges from 0 to 100%; showing how much the valve is open for particular flow. The flow controllers can be calibrated for different gases based on the method given in brochure. Gas chromatograph is also connected to a PC, from where one can upload the method and make necessary settings for the measurements.

3.2.5 Rotameters

The species flow rate can be controlled either from controllers or manually. For manual operation, flow rate can be set by opening or closing of the valve and the flow rate can be measured by means of rotameters that are installed in lines of different species.

3.2.6 Pressure gauges and regulators

To measure the oxygen supply pressure, Keller Leo 1 type digital pressure gauges are equipped having an uncertainty of $\pm$ 0.2% [84]. All the gas cylinders are equipped with pressure gauges and regulators for supply pressure control.

3.2.7 Sampling

For sample collection, probe of 1/8" is inserted inside the reactor and can be moved horizontally and vertically by a gear mechanism so that sample can be collected from desired location.

3.3 Uncertainty Analysis

In order to ensure the credibility of experimental results, uncertainty analysis has to be carried out for experimental set up. The final results may be affected by instrument selection, instrument calibration and environment. The uncertainty analysis has been carried out according to the method described by the Holman et al. [85]. The uncertainties related to the instruments have already been addressed above. The cumulative uncertainty in the species concentration measurement can be found by:

$$z = (z_{gc}^{2} + \sum z_{gp}^{2} + \sum z_{fc}^{2})^{0.5} \quad (1)$$

Where z is the final uncertainty in the concentration measurement, z_{gc} is the uncertainty related to gas chromatograph, z_{gp} is the uncertainty related to gas purity (summation implies the number of species) and z_{fc} is the uncertainty related to flow controllers. After incorporating all the values the final uncertainty can be found. The summary of uncertainty analysis is shown in Table 2.

Table 2: Summary of uncertainty analysis

S. No.	Equipment	Uncertainty
1.	Pressure gauge	$\pm$ 0.2%
2.	Gas purity	$\pm$ 0.25%
3.	Mass flow controllers	$\pm$ 0.5%
4.	Gas chromatograph	S.D. < 1%
5.	Species concentration	$\pm$ 1.4%

CHAPTER 4

METHODOLOGY

4.1 Experimental work

The results reported in this study are for non reactive flows in which the fuel is replaced by the nitrogen for safety precautions since there is no combustion. These results will serve as the validation part of the numerical model and will help us in understanding the flow behavior. Both horizontal and vertical concentration profiles were measured for different cases. For horizontal profile, concentrations were measured at the centerline of the reactor. The concentrations were measured with the interval of 1mm in the porous region and with the interval of 2 mm outside the porous region. For vertical profiles, four sections were selected where the porous plate lies and concentrations were measured at these sections; the points are shown in Figure 16. At each section five readings were taken with the interval of 5mm.

Figure 16: Sections within the porous reactor for vertical concentration profiles

Five sets of experiments were conducted by varying the O_2 from 1 l/min to 8 l/min flow rate that changes inlet O/N ratio from 1 to 8; while the flow rates of N_2 and CO_2 were remain fixed as 1 l/min and 7.52 l/min respectively. The cases are listed in Table 3. These flow rates were set from the well known methane combustion reaction in air environment.

i.e. $CH_4 + 2O_2 + 7.52N_2$ ======> $CO_2 + 2H_2O + 7.52N_2$

For stoichiometric combustion of methane, one mole of methane requires 2 moles of oxygen and with every 2 moles of oxygen 7.52 moles of nitrogen are present in the air. For non reactive experiments, nitrogen is being used as the fuel so with one mole of nitrogen, 2 moles of oxygen and 7.52 moles of carbon dioxide (for oxy-fuel conditions) is provided. All the species enter the reactor at 25 ^{0}C (298K). All the sets of experiments were conducted twice and average results have been reported.

Table 3: Sets of experiments for non reactive flow

Case#	Q_{N2} (l/min)	Q_{O2} (l/min)	Q_{CO2} (l/min)	Inlet O/N
1.	1	8	7.52	8
2.	1	6	7.52	6
3.	1	4	7.52	4
4.	1	2	7.52	2
5.	1	1	7.52	1

4.2 Numerical Modeling

4.2.1 Calculation

The geometry is made as a 2D domain as shown in Figure 17 using commercial software GAMBIT 2.4 which is widely used for geometry and mesh generation. The porous plates are formulated as 2D rectangle having dimensions of 150 mm x 1mm. The x direction is along the length and y direction is along the height of the reactor. The domain of the reactor is meshed into 24,000 rectangular elements. The grid is made finer near to the wall, porous plates, and at the start and end of the porous plates where the gradients are expected to be high.

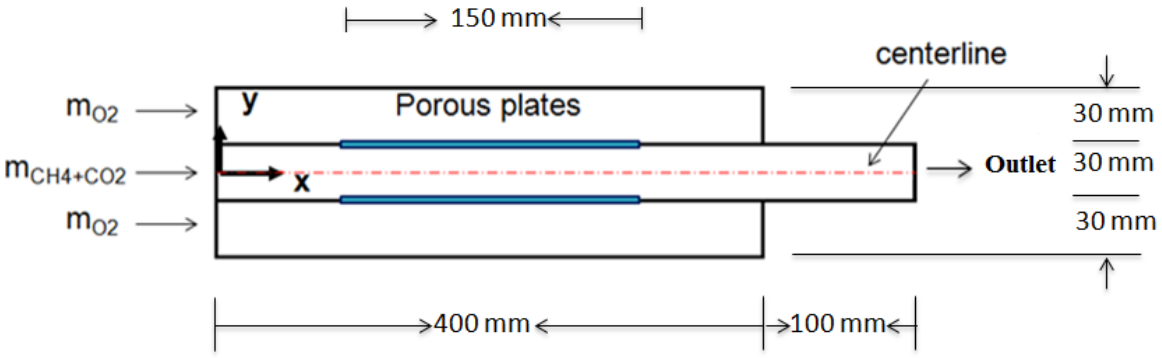

Figure 17: 2D representation of porous plate reactor

4.2.2 Governing Equations

The governing equations to calculate pressure, velocity, temperature, species concentrations are continuity, momentum conservation, energy, species transport equations and Darcy law which can be mathematically represented as:

$$\nabla.(\rho U) = 0 \quad (2)$$

$$\nabla.(\rho UU) = -\nabla P + \mu\nabla^2 U \quad (3)$$

$$(\rho C_p)U.\nabla T = \nabla.(k\nabla T) \quad (4)$$

$$\nabla.(\rho UY_i) - \nabla.(\rho D_{i,m}\nabla Y_i) = 0 \quad (5)$$

These equations are solved simultaneously in the FLUENT. The energy equation is not needed for non-reactive flow.

4.2.3 Radiation model

Radiative heat transfer is considered as an important heat transfer mode in combustion processes occurring in reactors and combustion chamber of gas turbines, boilers etc due to the presence of high temperatures more than 2000 K involved in combustion processes. The solution of the radiative heat transfer equation requires the knowledge of the temperature distribution, as well as the concentration of the different species present in the medium. Radiative heat transfer implementation has been accomplished by Discrete Ordinate (DO) model that is built in FLUENT. The mathematical representation of the radiation equation is:

$$\frac{dI(r,s)}{ds} = KI_b - (K+\sigma_s)I(r,s) \qquad (6)$$

The radiation stabilizes the flame and lowers the maximum temperatures by means of radiative heat transfer. The incorporation of radiation model gives more realistic results. The solution method for the DO model is similar to that of fluid flow and energy equations. Absorption coefficient of the fluid is calculated by domain based weighted sum-of-gray-gas model. The internal emissivity is taken as 0.8.

4.2.4 Reactions Kinetics model

Two different reaction kinetics models for methane combustion have been incorporated in this study. The flow is laminar everywhere inside the reactor; first a well known laminar finite rate single step reaction is used for the oxidation of Methane. The reaction is:

$$CH_4 + 2O_2 \text{ ======>} \quad CO_2 + 2H_2O$$

The rate of this reaction k_r can be determined by Arhenius equation

$$k_r = AT^{\beta} \exp(\frac{-E_a}{RT}) \qquad (7)$$

Where 'A (Pre exponential factor)', 'E_a (activation energy)' and 'β (Temperature exponent)' are determined experimentally. For the above reactions the values are:

$$A=2.119\text{x}10^{11},\ E_a=2.027\text{x}10^{8},\ \beta=0$$

In the second phase modified two step reaction kinetics model that incorporates the production of carbon monoxide (CO) is used, as proposed in [44]. This model was modified for the increased percentage of carbon dioxide under oxy-fuel combustion.

The reactions are:

$$CH_4 + 1.5O_2 \quad ======> \quad CO + 2H_2O \qquad (R1)$$

$$CO + 0.5O_2 \quad ======> \quad CO_2 \qquad (R2)$$

$$CO_2 \quad ======> \quad CO + 0.5O_2 \qquad (R3)$$

The particulars for modified two step model are stated in Table 4.

Table 4: Particulars for modified two step reaction model under oxy-fuel conditions

Reaction #	A	β	E_a (J/kmol)	Reaction orders
R1	1.59×10^{13}	0	1.998×10^{8}	$[CH_4]^{0.7}[O_2]^{0.8}$
R2	3.98×10^{8}	0	4.18×10^{7}	$[CO][O_2]^{0.25}[H_2O]^{0.5}$
R3	6.16×10^{13}	-0.97	3.277×10^{8}	$[CO_2][H_2O]^{0.5}[O_2]^{-0.25}$

4.2.5 CFD approach

The numerical simulations are based on the CFD approach in which finite volume method is used to discretize the governing equations. The finite volume is a conservative method, for discretization of the governing equations presented before; commercial software Fluent 6.3.26 is used. The domain is divided by the rectangular elements each presenting a finite volume and discretized governing equations will be solved for each element. Solving momentum equation along with the other equations is difficult because the pressure term is present in terms of gradient in the momentum equation so therefore staggered grid (new grid that is offset to original grid by half of the cell dimension) is used for the simulations as recommended by Versteeg and Malalasekera Iin [86]. All the scalars are calculated at the grid point expect the velocities which are computed at the center of the cell.

4.2.6 Boundary conditions

The inlet is equipped with the 'mass flow inlet' boundary condition, at outlet 'Pressure outlet' boundary condition is used. The viscous resistance and inertial resistance of the porous zone are 2.44×10^{13} /m^2 and 100/m respectively. The fluid porosity of the porous plate is 0.55; effective thermal conductivity is 3.85 W/m-K. The species enter at 298 K for non reactive flow and at 1173 K (higher than self ignition temperature of methane) for reactive flow. The species density is calculated by Ideal gas law; viscosity and thermal conductivity are measured from kinetic theory and specific heat is calculated from

piecewise functions for each species. The bulk properties are calculated by using Ideal gas mixing law.

The reactor is modeled as 2D and it is assumed that the width is 1m. The mass flow rates are normalized with 1m width such that the mass flux remains constant. For numerical investigations, the oxygen mass flow rate is taken as $2x10^{-3}$ kg/s, methane as $5x10^{-4}$ kg/s and carbon dioxide as $8x10^{-3}$ kg/s for the reactive flow and non reactive flow. However the mass flow rates have been varied for the parametric study. For oxidizer ratio 'OR', carbon dioxide flow rate was varied such that OR=0.2, 0.25, 0.30, 0.35 and 0.40 were achieved. For equivalence ratio, oxidizer ratio was kept constant as 0.25 and mass flow rate of methane is held constant as 5x10-4 kg/s and oxygen flow rate was varied such that equivalence ratios φ=1.0, 0.9, 0.8 and 0.7 were achieved. In the end, the mass flow rates were multiplied by factor 1, 2 and 3 to investigate the effect of Reynolds number by keeping OR=0.25 and φ=0.8 as constants.

4.2.7 Solver settings

The viscous resistance and inertial resistance of the porous zone are $2.44x10^{13}$ $/m^2$ and 100/m respectively. The fluid porosity of porous plate is 0.55; effective thermal conductivity is 3.85 W/m-K. The species enter at 298 K for non reactive flow and at 1173 K (higher than self ignition temperature of methane) for reactive flow. The species density is calculated by Ideal gas law; viscosity and thermal conductivity are measured from kinetic theory and specific heat is calculated from piecewise functions for each species. The bulk properties are calculated by using Ideal gas mixing law.

4.3 Performance parameters

The factors which were varied to investigate different parameters like maximum and outlet temperatures, reaction rates, diffusion, incident radiation and different modes of heat transfer are described as:

4.3.1 Oxidizer ratio (OR)

The oxidizer ratio is defined as ratio of oxidizer mass flow rate to the sum of oxidizer and carrier gas mass flow rates. It represents the percentage of oxygen in the mixture of oxygen and carbon dioxide. The mathematical representation is:

$$OR = \frac{m_{o2}}{m_{co2} + m_{o2}} \qquad (8)$$

Where:

m_{o2} = mass flow rate of oxygen

m_{co2} = mass flow rate of carbon dioxide

4.3.2 Oxy-fuel ratio (O/F)

The oxy-fuel ratio is the ratio between oxidizer mass flow rate and fuel mass flow rate. The mathematical representation is:

$$O/F = \frac{m_{o2}}{m_{CH4}} \qquad (9)$$

Where:

m_{CH4} = mass flow rate of methane (fuel)

4.3.3 Equivalence ratio (φ)

Equivalence ratio defines whether the mixture has more oxidizer than stoichiometric for complete combustion (lean) or less than stoichiometric (rich). The mathematical representation is:

$$\varphi = \frac{(O/F)_s}{(O/F)_a} \qquad (10)$$

Where subscripts are for:

s = stoichiometric

a = actual

4.3.4 Reynolds Number (Re)

Reynolds number is a dimensionless number that represents the ratio between inertial forces to the viscous forces. It defines whether the flow is laminar or turbulent. If 'Re' is less than or equal to 2100, then the flow in pipe is laminar. If the 'Re' is greater than 4000, then the flow in pipe is turbulent. If neither condition exists, then flow is transient.

The mathematical representation is:

$$\mathrm{Re} = \frac{\rho V d_h}{\mu} \qquad (11)$$

Where ρ is the density in 'kg/m^3', V is the velocity in 'm/s', d_h is the hydraulic diameter 'm' and μ is the absolute viscosity in 'kg/m-s'.

CHAPTER 5

RESULTS AND DISCUSSION

This chapter focuses on the numerical study that includes calibration of porous media flows using the experimental data available in the literature and grid independency check for accurate results and to save computational time. It presents the validation of numerical models by means of experimental results for non reactive flow in order to ensure reliability of numerical results for reactive cases. Moreover results and discussion are shown in which first experimental results are discussed and critically analyzed. The horizontal and vertical profiles of species are presented. This is followed by discussion of numerical results for both non reactive and reactive flows using 1 step model and 2 step modified model for combustion. Parametric study has been conducted using different variables like, oxidizer ratio (OR), equivalence ratio (φ), viscous resistance and Reynolds number, at the end to find optimum conditions for the reactor design.

5.1 Calibration for porous media flow

A CFD model has been developed for the calculation of porous media flows in order to assure the accuracy of the developed model presented in this study. The experimental data presented by Mancin et al [78] for porous media flows were compared with the present numerical model. In their work, effect of pressure drop on air mass flow rates have been observed for various metallic foams made of Aluminum and Copper. Experimental data of two Copper foams 'Cu: 10-6.6' and 'Cu: 20-6.5' have been extracted for calibration and the properties of these two samples are given in Table 1.

Table 5: Properties of copper foams for validation

	Sample	Permeability 'k' (m^2)	Inertial resistance 'C_2' (/m)	Thickness 't' (mm)	Height 'h' (mm)
Case I	Cu: 10-6.6	2.58×10^{-7}	405.6	0.432	40
Case II	Cu: 20-6.5	1.7×10^{-7}	584.7	0.320	40

A two dimensional CFD model is developed and the porous plate is modeled as one dimensional for simplicity of the problem solution. The 2D domain is shown in Figure 18. Experimental results were compared with the numerical model and were found in good agreement as shown in Figure 19. The symbols represent the experimental data while the solid lines represent numerical results. Results show that increase in pressure drop enhances the mass flux.

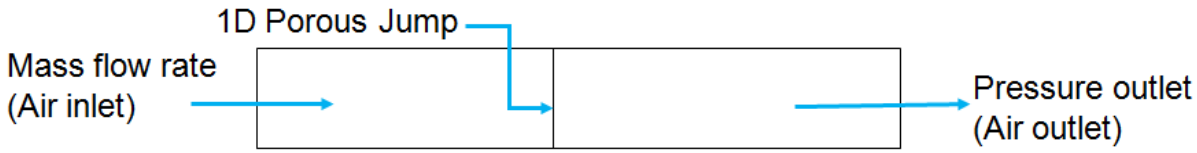

Figure 18: 2D domain of problem

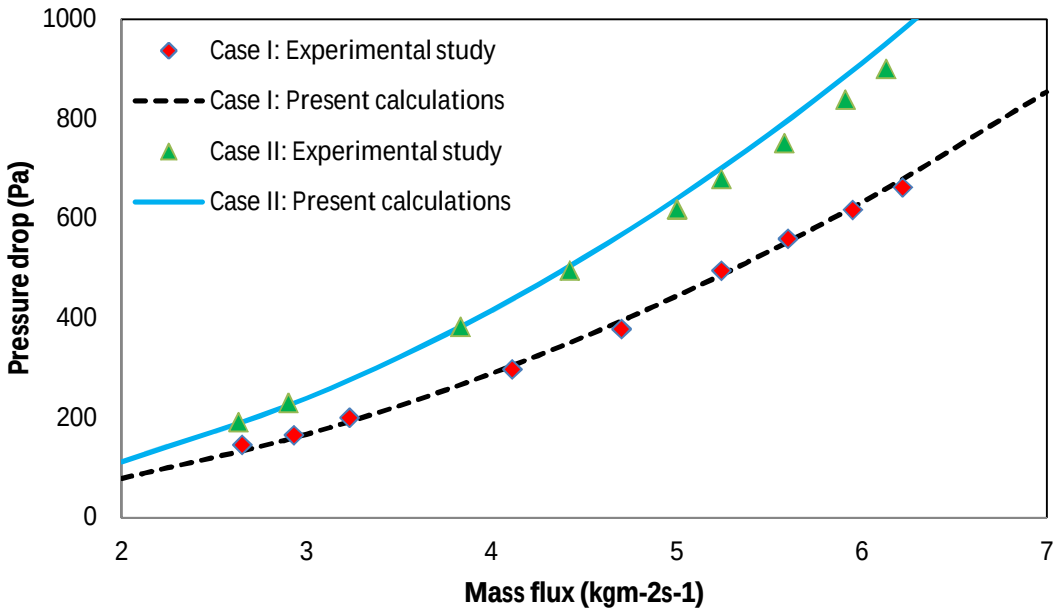

Figure 19: Comparison of experimental data from literature with present calculation for effect of pressure drop on mass flux [78]

5.2 Porous plates data

To measure the viscous resistance and inertial resistances of the porous plates used in the experimentation for the input in numerical study, experiments have been performed using the sample of porous plate and air is passed through for different pressure drop. Velocity, density and mass flux were measured as shown in Figure 20 and Figure 21. The figures show that increase in pressure raises the mass flow rate and density of air.

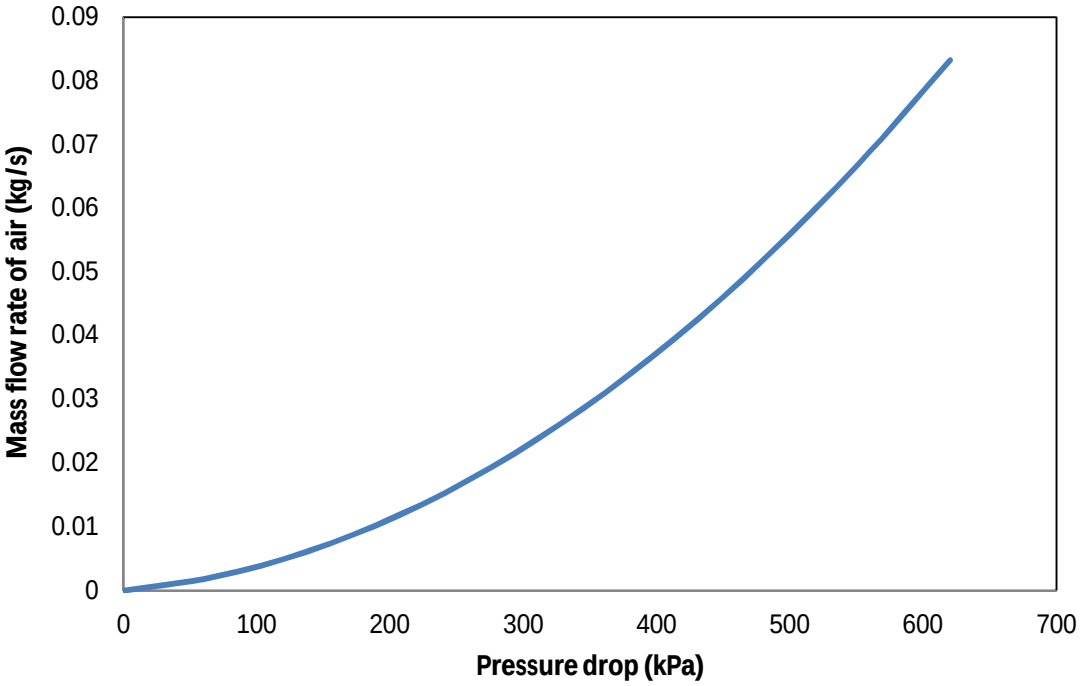

Figure 20: Pressure drop (kPa) Vs Mass flow rate (kg/s)

Using these data, viscous resistance 'α' and inertial resistance 'C_2' (α and C_2 are the representations of these resistances) can be calculated using Darcy law as shown in Eqn. (8)

$$\Delta P = -(\frac{\mu V}{\alpha} + \frac{1}{2} C_2 \rho V^2).\Delta x \qquad (12)$$

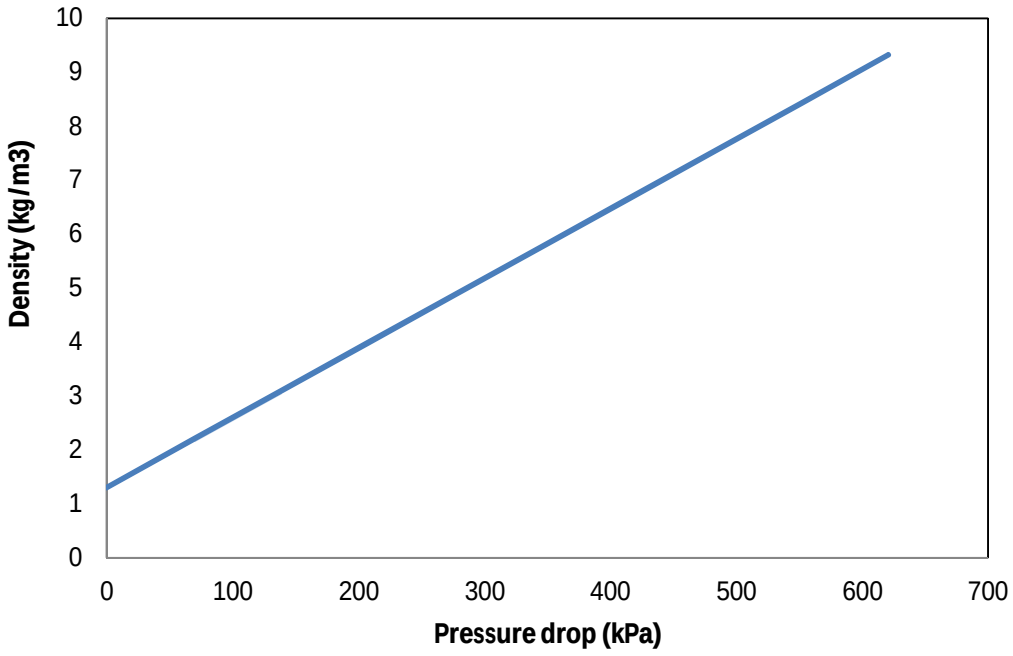

Figure 21: Pressure drop (kPa) Vs Density (kg/m^3) for porous plates

The computed resistances are:

$1/\alpha$ = 2.44×10^{13} ($/m^2$)

C_2 = 100 (/m)

Note: The inertial resistance is very small as compared to the viscous resistance and can be neglected.

5.3 Grid independency tests

Three meshes were generated and include 16,000, 24,000 and 30,000 rectangular elements in order to perform mesh independency check. The non reactive case for OR=0.20 was solved using these meshes. Oxygen permeation and oxy-fuel ratio along the centerline were matched for three meshes as shown in Figure 22 and Figure 23. The oxygen permeation and oxy-fuel ratio for 16,000 elements slightly deviates from 24,000 and 30,000 elements. However the difference in predicted results for 24,000 and 30,000 elements are calculated to be less than 0.02%.

The 16,000 elements grid has convergence issues for reactive cases, so, for accurate results and less computational time; grid of 24,000 elements was selected. The grid is refined in the regions where high gradients are expected like near porous plate regions, wall, entry and exit of porous plate as shown in Figure 24.

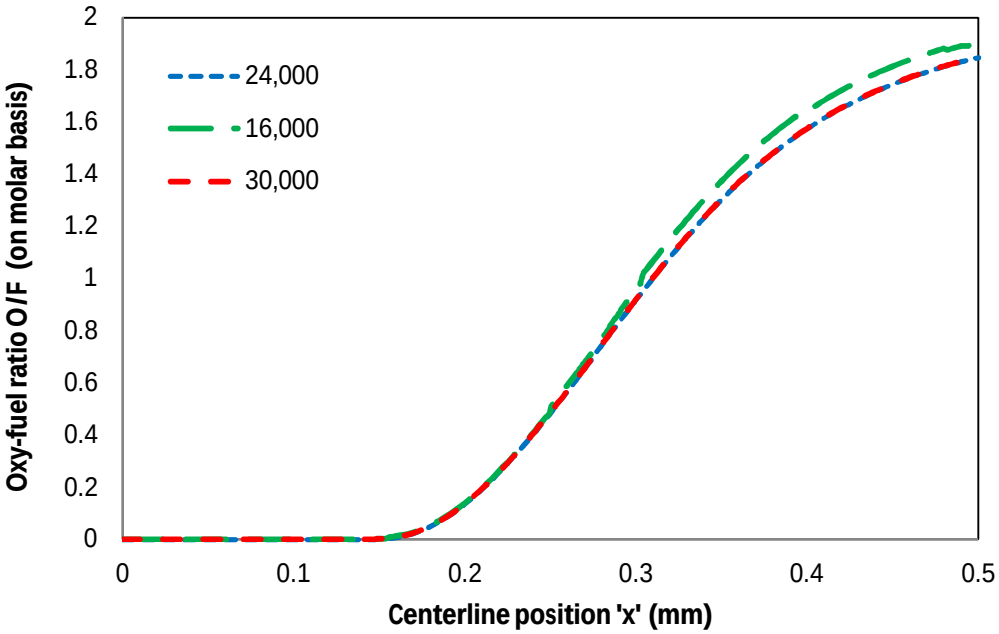

Figure 22: Variation of oxy-fuel ratio along centerline for OR=0.2

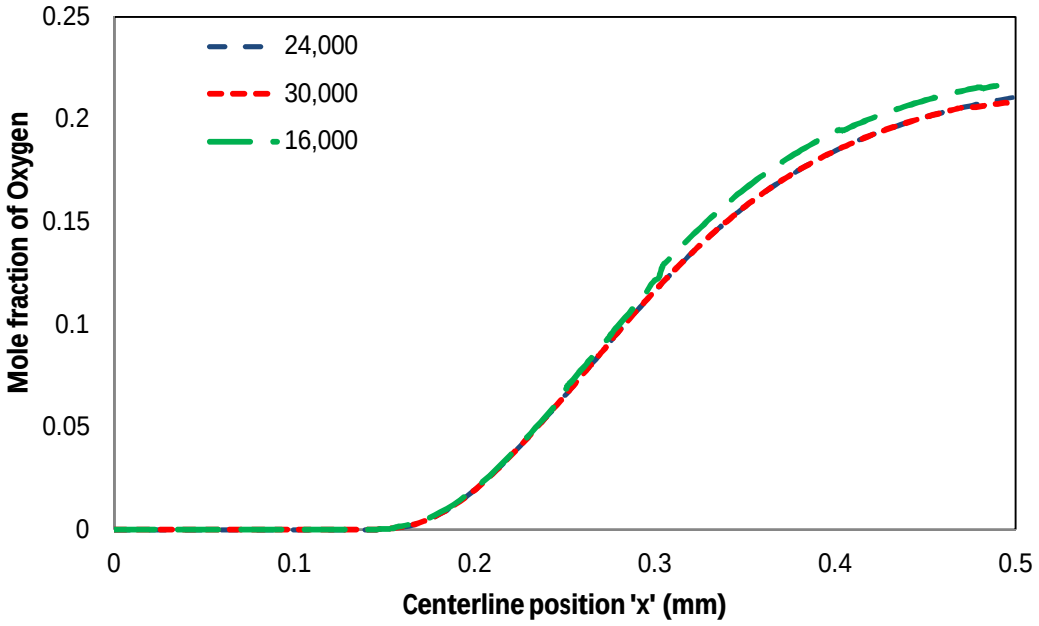

Figure 23: Variation of oxygen mole fraction along centerline for OR=0.2

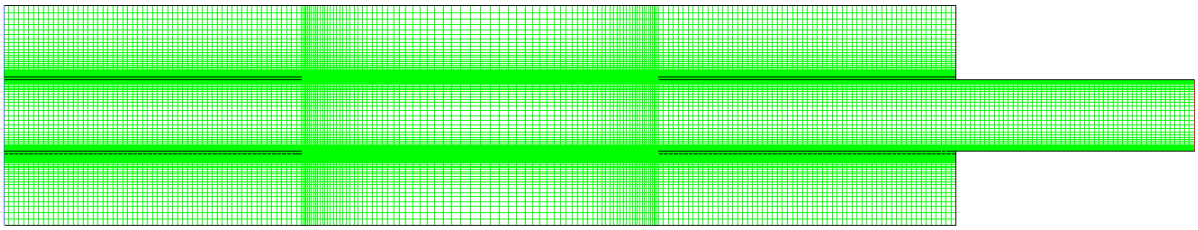

Figure 24: 24,000 elements grid for computational study

5.4 Experimental results

The non reactive flow experiments were performed and the species concentrations were measured along the horizontal and vertical directions. The centerline variation of oxygen permeation in terms of mole fraction and oxygen to nitrogen ratio was measured for different inlet O/N conditions for experiments as shown in Figure 25 and Figure 26.The oxygen molar fraction starts to increase slightly from almost zero at x=60 mm however, significant increase in the mole fraction is indicated at the start of porous plate and continues to rise as more oxygen is inducted through the plates. The trend is similar to that of O_2/N_2 ratio. The O_2/N_2 ratio increases slightly starting from zero as the flow moves in 'x' direction, the O_2/N_2 ratio increases significantly starting from x=125mm where the porous plates start, this is due to the permeation of oxygen through the porous plates and incorporation of permeated oxygen in the mainstream flow. The O_2/N_2 ratio keeps on increasing after the porous plates. This is attributed to the fact that oxygen concentration near walls is higher than the center, so as the flow moves the higher concentration of oxygen near wall mixes with the mainstream flow hence increasing the O_2/N_2 ratio in the center. The trends for oxygen molar fraction and local O_2/N_2 ratio do not become straight line and continue to increase after x=340 mm and near the walls, oxygen concentration is expected higher near the walls than the center and the oxygen is not fully mixed until x=340 mm. The reason behind that is the fact that the flow is laminar and there is less mixing of species as compared to turbulent flows.

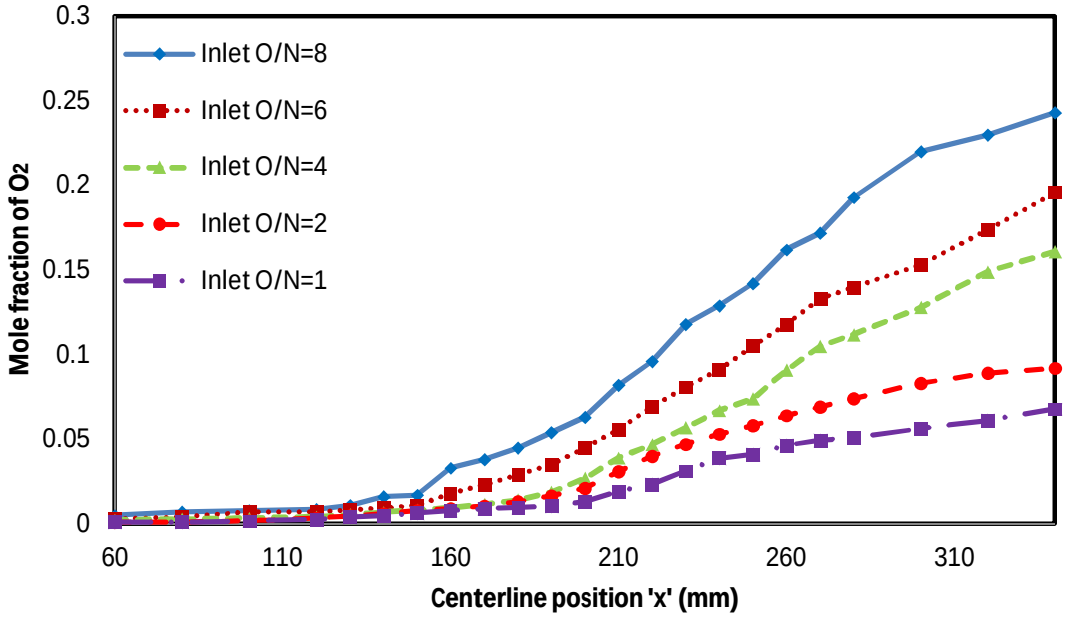

Figure 25: Variation oxygen mole fraction along x direction (centerline) for different inlet O/N conditions

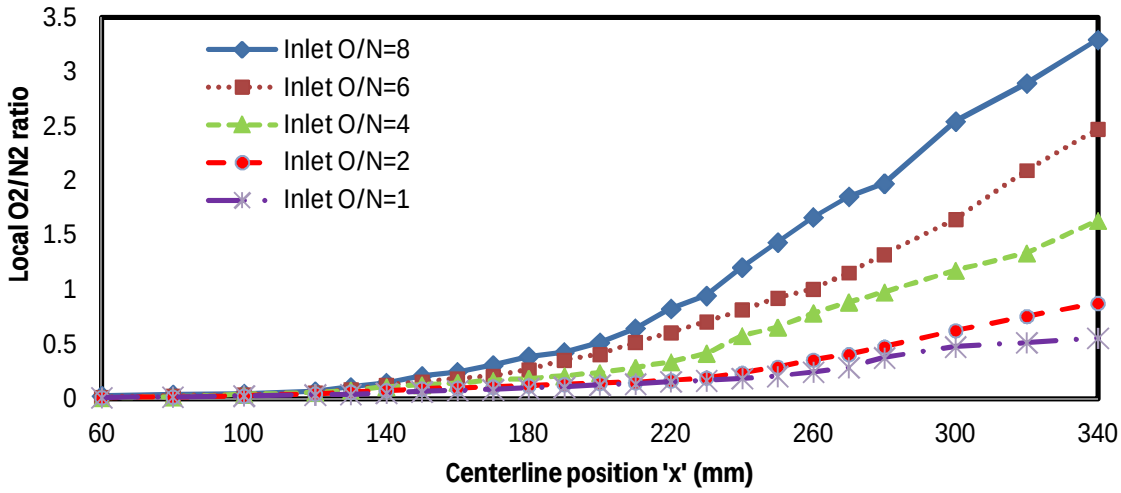

Figure 26: Variation of molar oxygen to nitrogen ratio along x direction (centerline) for different sets of inlet O/N ratio

As shown in Figure 26, the maximum local O_2/N_2 ratio for O/N=8 experiments is around 3.2, however the bulk ratio is 8 so it will continue to increase. Same can be said about other sets of experiment O/N=6, O/N=4, O/N=2 and O/N=1. The variations of O_2/N_2 ratio in y-direction for O/N=8, O/N=6 and O/N=4 are shown in Figure 27 (a), (b) and (c). The variation of O_2/N_2 ratio in the y-direction increases as the 'x' increases. The local O_2/N_2 ratio at the centerline reaches around 2 at x=270mm but the O_2/N_2 ratio at y=$\pm$ 10mm it ranges from 16-33 for O/N=8 experiment. The variations of local O_2/N_2 ratio in the y-direction increases as the 'x' increases, the local O_2/N_2 ratio at the centerline reaches around 1.2 at x=270mm but the local O_2/N_2 ratio at y=$\pm$ 10mm it ranges from 11-20 for O/N=6 experiment. The variations of local O_2/N_2 ratio in the y-direction increases as the 'x' increases, the O_2/N_2 ratio at the centerline reaches around 0.95 at x=270mm but the local O_2/N_2 ratio at y=$\pm$ 10mm it ranges from 7-12 for O/N=4 experiment. The ratio is lower at y=-10mm (below centerline) is due to the buoyancy effects; the carbon dioxide is heavier than the other gases so it tends to move in bottom making local O_2/N_2 ratio lower in the lower part than the upper part of reaction chamber.

The trends for O_2/CH_4 (in cases of reactivity if nitrogen is replaced with methane) are expected to be similar. So we can predict that for higher O_2/CH_4 inlet ratios, there will be lean mixture above and below the centerline and stoichiometric ratios are expected in some parts of central region and for lower O_2/CH_4 inlet ratios, there will be slightly lean and stoichiometric mixture above and below the centerline and rich O_2/CH_4 mixture are expected in central region of the reaction chamber.

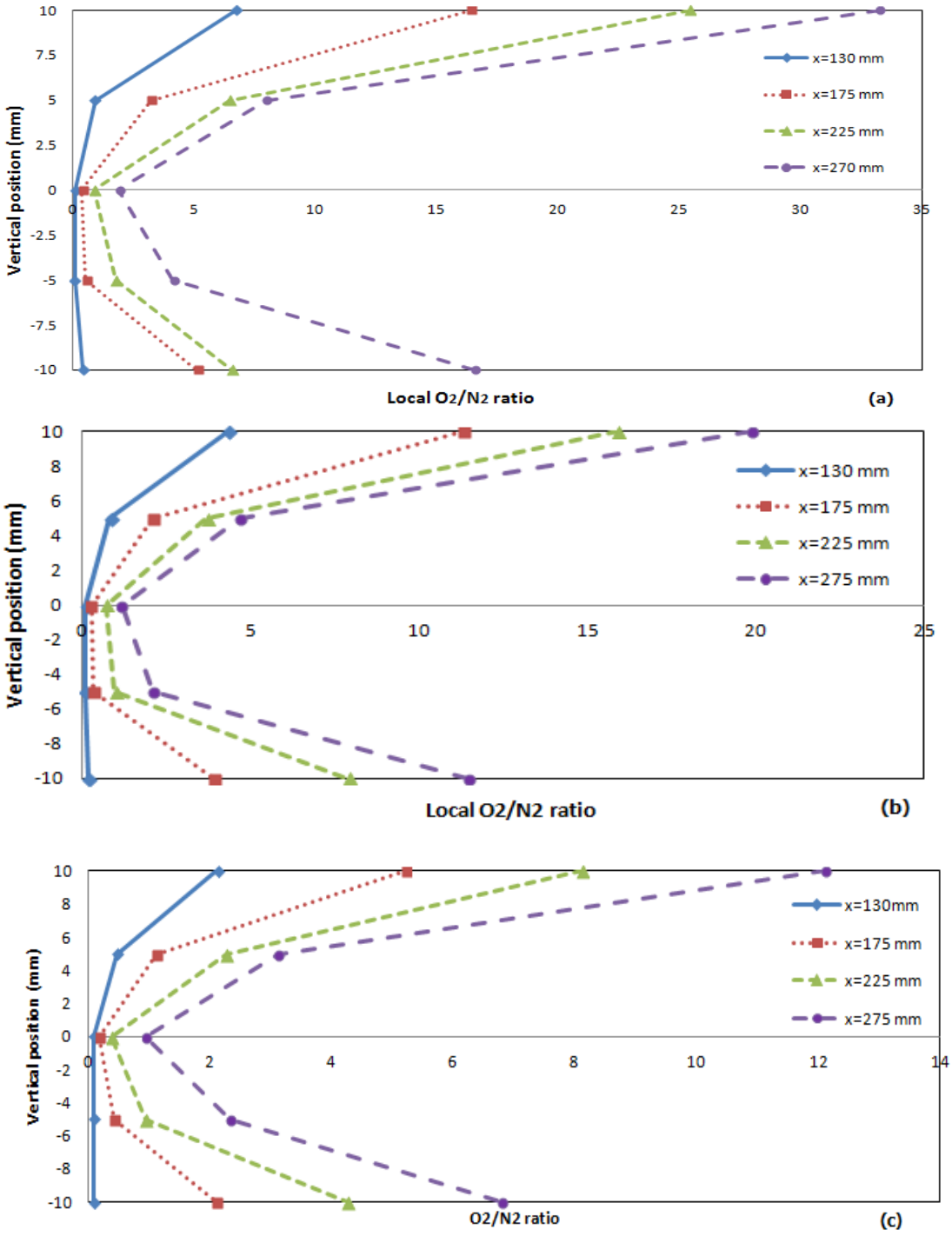

Figure 27: Vertical variation of local O_2/N_2 ratio at different section of the reactor for different inlet conditions (a) O/N=8, (b) O/N=6 and (c) O/N=4 experiments

5.5 Comparison of present experimental and numerical results

The numerical results from Fluent of local O_2/N_2 ratio and local mole fraction of oxygen were extracted and compared with the experimental data as shown in Figure 28, Figure 29 and Figure 30. Figure 28 represents comparison of numerical results with experimental results for oxygen molar fraction variation along centerline for different set of experiment. Figure 29 shows comparison of numerical results with experimental results for O_2/N_2 variation along centerline for different sets of experiment. Figure 30 shows comparison of numerical results with experimental results for O_2/N_2 variation in 'y' direction for different inlet conditions (a) O/N=8, (b) O/N=6 and (c) O/N=4. The symbols show the experimental data while the solid lines are from numerical results. The numerical results are in good agreement with the experimental data making the numerical model worthy for numerical predictions. However, there is some deviation at lower flow rates i.e. O/N=2 and O/N=1 at y=$\pm$ 10 mm. There can be several reasons like numerical errors, errors from simplified 2D model, turbulence and diffusion of species in other chambers. Ideally the top and bottom chamber should be completely filled with Oxygen but as the flow rates are decreased for e.g. O/N=4 and O/N=2, there is diffusion of nitrogen and carbon dioxide in the top and bottom chamber as shown in Figure 31 (a), (b), (c) and (d) creating recirculation of these species and making it difficult to measure accurate concentrations experimentally. The favorable ratio for combustion (i.e. 1-3 if N_2 is considered methane) can be predicted in the reaction chamber. But exact region can be estimated when methane is used instead of nitrogen.

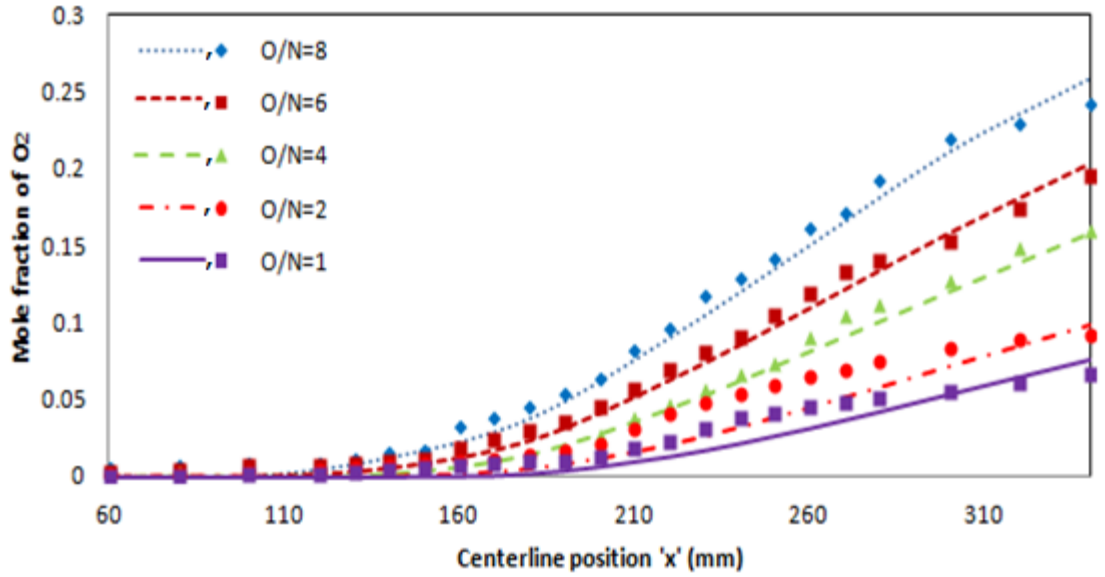

Figure 28: Comparison of numerical results with present experimental results for oxygen molar fraction variation along centerline, symbols represents experimental data and lines represent numerical results

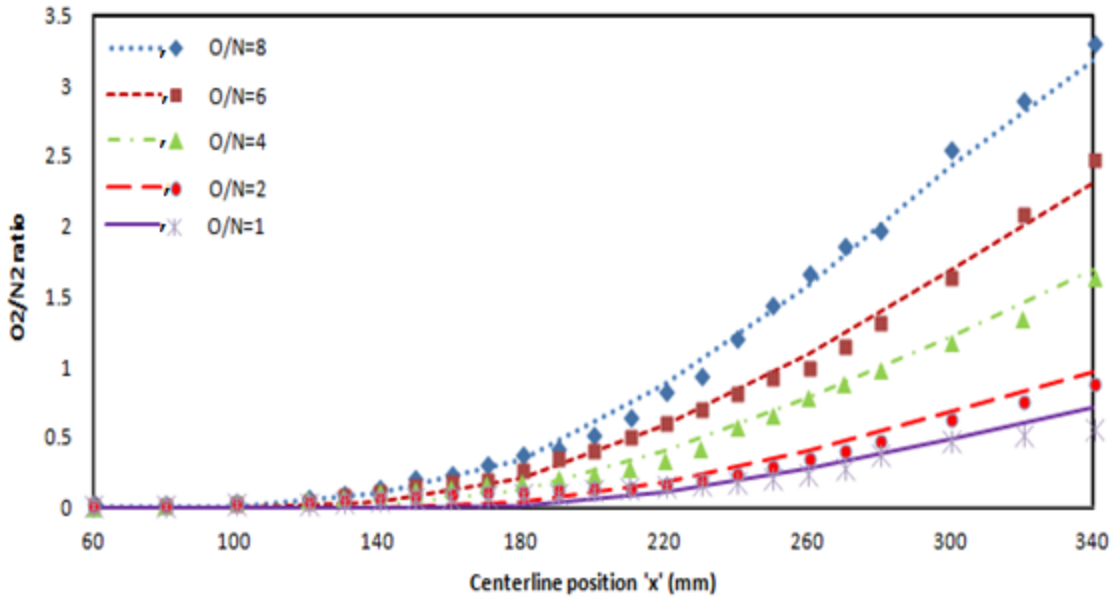

Figure 29: Comparison of numerical results with experimental results for local O_2/N_2 variation along centerline for different inlet conditions, symbols represent experimental data and lines represent numerical results

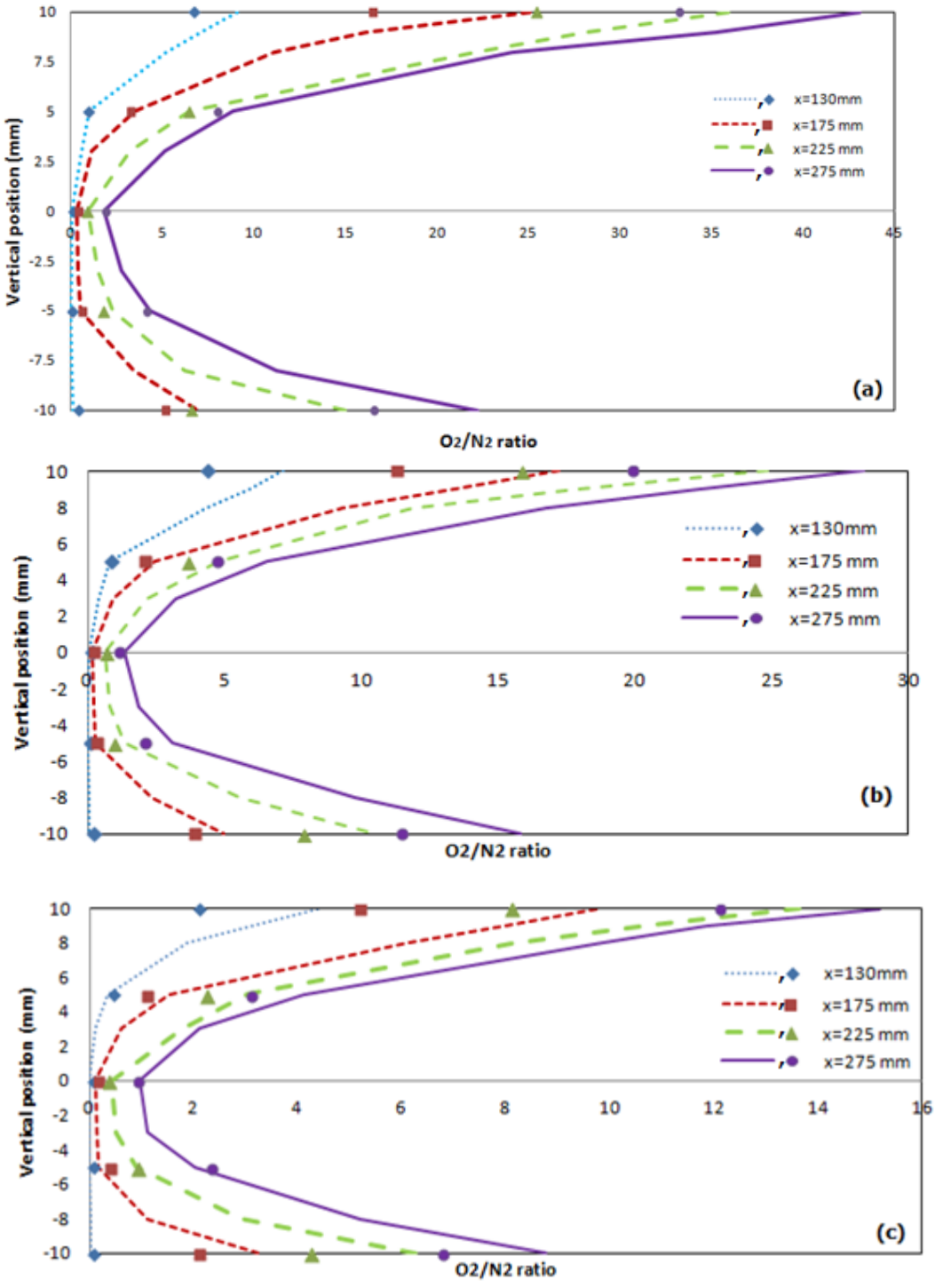

Figure 30: Comparison of present experimental with numerical results of local O_2/N_2 variation in 'y' direction for different inlet conditions (a) O/N=8, (b) O/N=6 and (c) O/N=4, symbols represents experimental data and lines represent numerical results

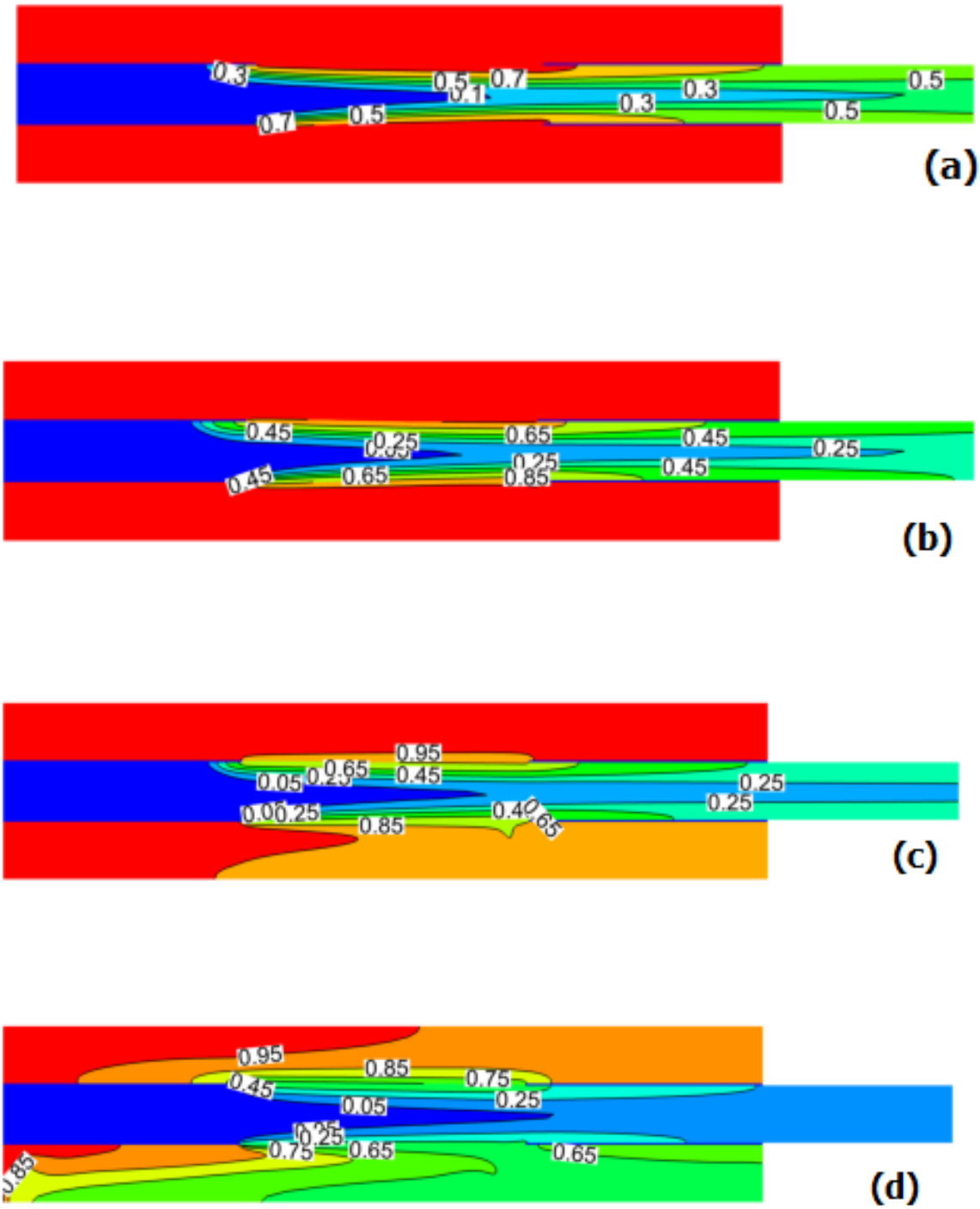

Figure 31: Contours of mass fraction of oxygen for different sets of experiments (a) O/N=8, (b) O/N=6, (c) O/N=4 and O/N=2

5.6 Non reactive flow

Before examining the numerical results for the combustion cases, it is important to analyze non reactive flow behavior in the reactor. One case for oxidizer ratio OR=0.20 is presented for non reactive and reactive study. The velocity contours are shown in Figure 32. The velocities in the top and bottom chamber are low due to low mass flow rate of oxygen as compared to reaction chamber (middle). The velocity in the middle chamber increases as the oxygen is added, thus increasing the total mass flow rate causing the velocity to increase in order to conserve continuity. At this state the Reynolds number at the outlet section is around 364. The contours of oxy-fuel ratio (on molar basis) are shown in Figure 33. The stoichiometric ratio for methane is 2 and the favorable region for combustion is near stoichiometric ratio, so the black and white region showing the ratio from 1 to 3, that starts near the porous plates and tend to move in the center; so combustion will most likely to occur in this region.

The contours for mass fraction of oxygen, carbon dioxide and methane are shown in Figure 34, Figure 35 and Figure 36. Oxygen concentration is maximum in the top and bottom inlet and zero at the fuel inlet, as the oxygen passes the porous plates and mixes with the mainstream flow, concentration of oxygen increases in the positive ‘x’ direction reaction chamber. Diffusion of carbon dioxide and methane occurs in the top and bottom sides of the chambers as shown in the contours. The contours of carbon dioxide and methane concentrations are highest at the fuel inlet and decreases in the flow direction as the mainstream flow mixes with oxygen.

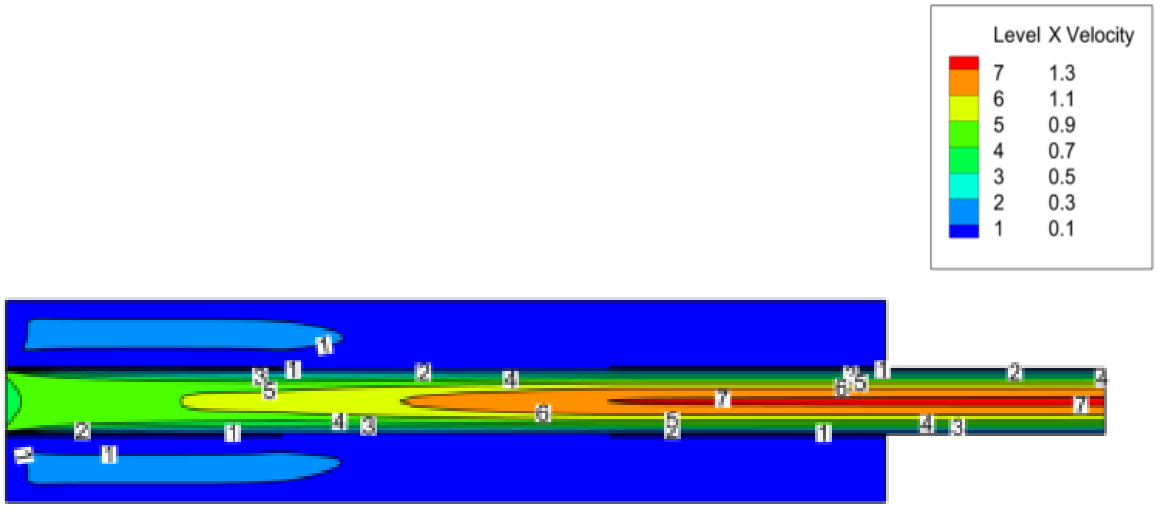

Figure 32: velocity (m/s) contours for non reactive flow OR=0.2

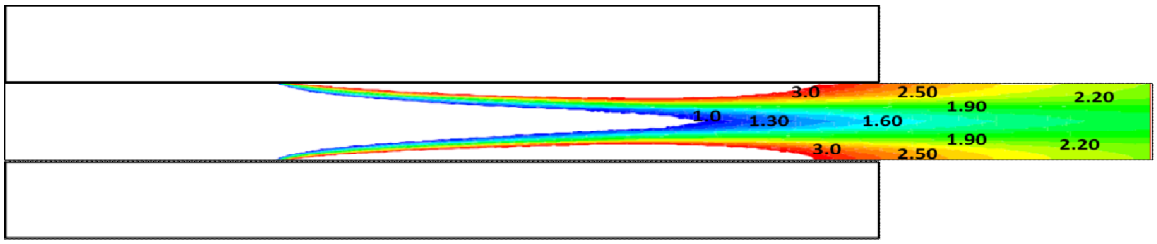

Figure 33: Combustible region showing oxy-fuel ratio (on molar basis) in the reaction chamber for OR=0.20 (Non reactive flow)

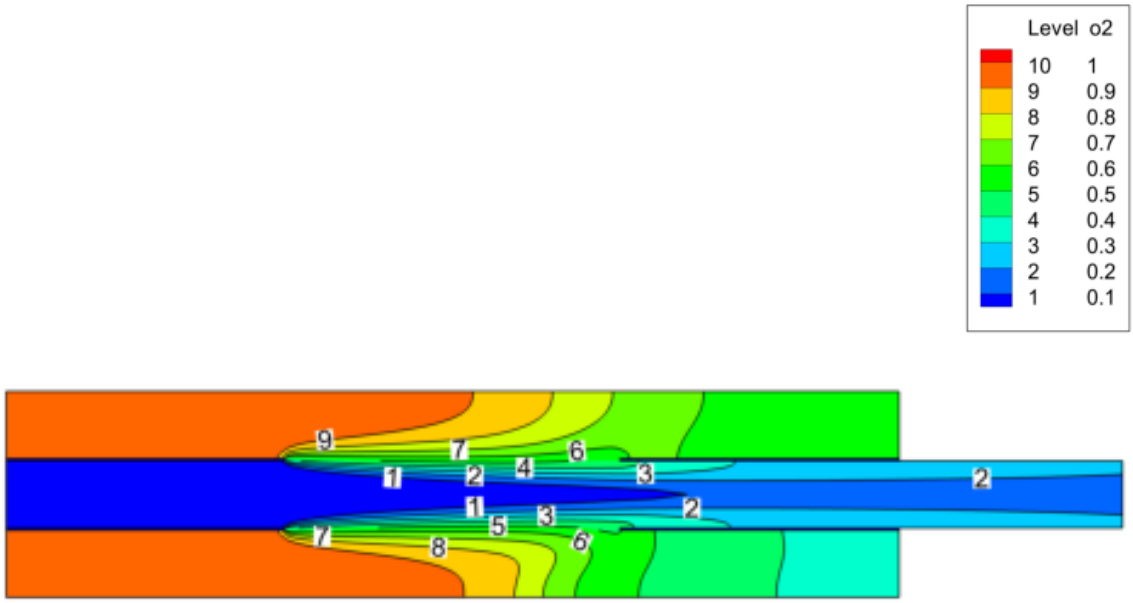

Figure 34: Contours of oxygen mass fraction for non reactive flow OR=0.2

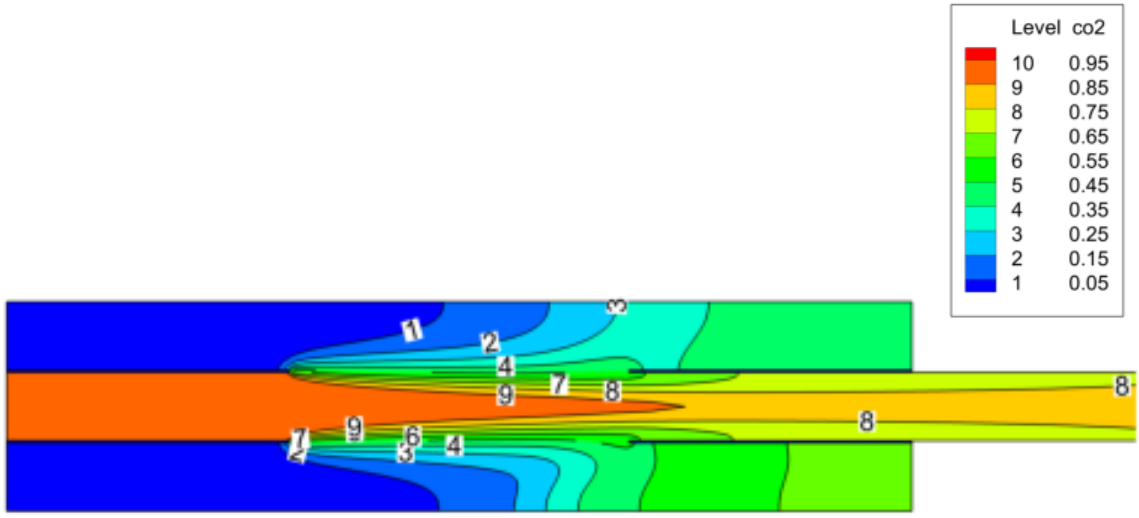

Figure 35: Contours of carbon dioxide mass fraction for non reactive flow OR=0.2

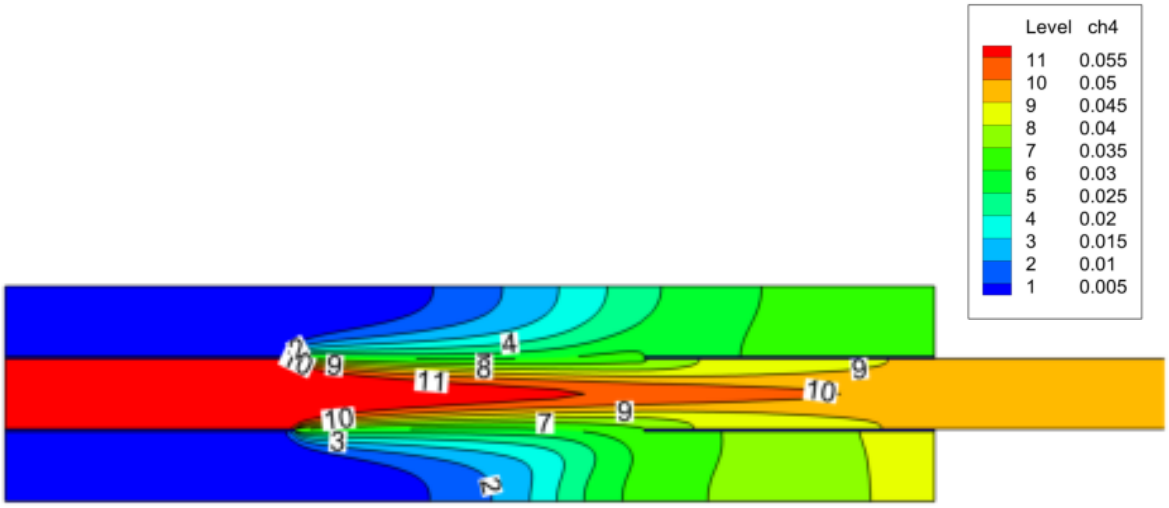

Figure 36: Contours of methane mass fraction for non reactive flow OR=0.2

The effect of sweep flow rate that contains mainly CO_2 on oxygen to fuel ratio (molar basis) at the centerline has been investigated by changing the oxidizer ratio from 0.2 to 0.4. The oxidizer ratio is changed by varying carbon dioxide mass flow rate while methane mass flow rate was kept constant. The inlet CO_2/CH_4 ratio has been set to 16, 9.33 and 6 (sweep flow rate is decreased) corresponding the OR=0.2, 0.3 and 0.4. The variation of oxy-fuel ratio at the centerline for different inlet CO_2/CH_4 ratio is shown in Figure 37. In this figure, as the sweep flow rate is decreased the oxy-fuel (O/F) ratio increases due to decrease in local pressure at the sweep side allowing more oxygen to induct in the reaction chamber. The effect of sweep flow rate on oxygen to fuel ratio (molar basis) at the centerline has been investigated by changing the equivalence ratio (phi=φ) from 1 to 0.8 with 0.1 interval. The equivalence ratio is decreased by increasing the oxygen mass flow rate. The variation of oxy-fuel ratio at the centerline for different equivalence ratios is shown in Figure 38. In this figure, as the equivalence ratio is decreased from 1.0 to 0.8 the oxy-fuel (O/F) ratio increases due to increase in local pressure at the top and bottom chambers side due to more oxygen available at the supply.

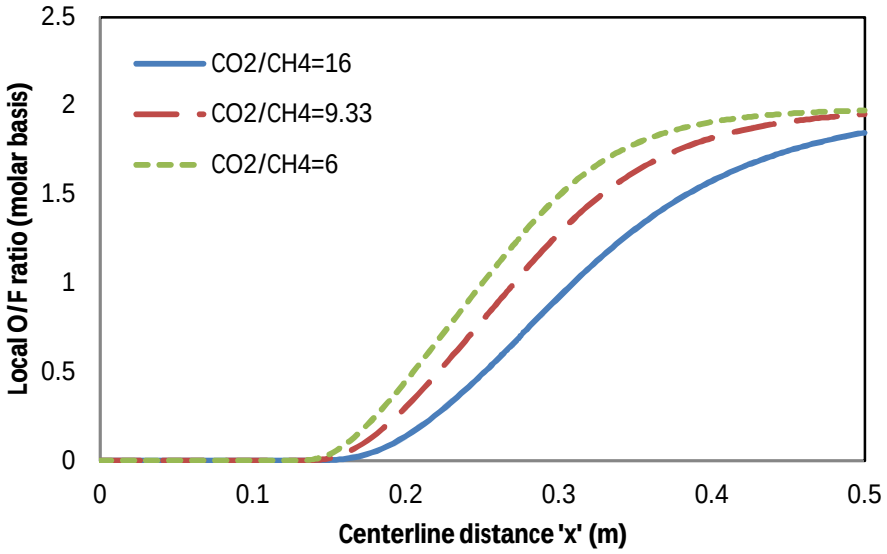

Figure 37: Variation of oxy-fuel ratio along centerline for different inlet CO_2/CH_4 ratios

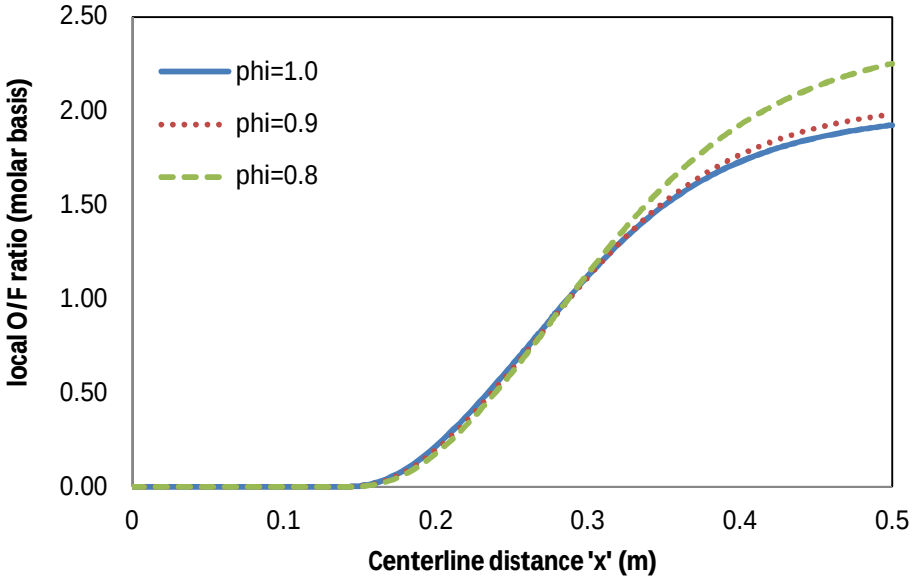

Figure 38: Variation of oxy-fuel ratio along centerline for different inlet equivalence ratios

5.7 Reactive flow (one step model)

The results for reactive cases using one step reaction model are as follows:

5.7.1 Effect of Radiation

In order to investigate the influence of radiative heat transfer on the combustion process inside the reactor, two cases were examined with and without the radiation model having oxidizer ratio OR=0.25. The temperature contours of both cases are shown in Figure 39 (a) and (b). In combustion without radiation model, the maximum temperature is too high i.e.4237 K, the outlet temperature is around 2975 K, the flame shape is not well defined and also combustion has no effect on upstream flow that is unrealistic. On the other hand the incorporation of radiation model affects the flame shape, maximum and outlet temperatures and on upstream flow. The radiation heat transfer cools down the flame and maximum temperature reduces to 3020 K and outlet temperature becomes 2028 K. The incident radiation contours are shown in Figure 40, in which the maximum incident radiation is near the outlet i.e. 3.81 MW/m^2 and is minimum near the inlet i.e. around 1.14 MW/m^2, so the radiation heat transfer has more effect near the outlet than at the inlet. Comparison of temperature distribution is made in Figure 41, the mass weighted average temperature with radiation model is higher than the temperature without radiation model but after x=150mm temperature with radiation model is much lower than the temperature without radiation model due to factors discussed above. Methane depletion for cases is analyzed in Figure 42, the trend is similar for both the models at the beginning but methane depletes faster with the radiation model activated.

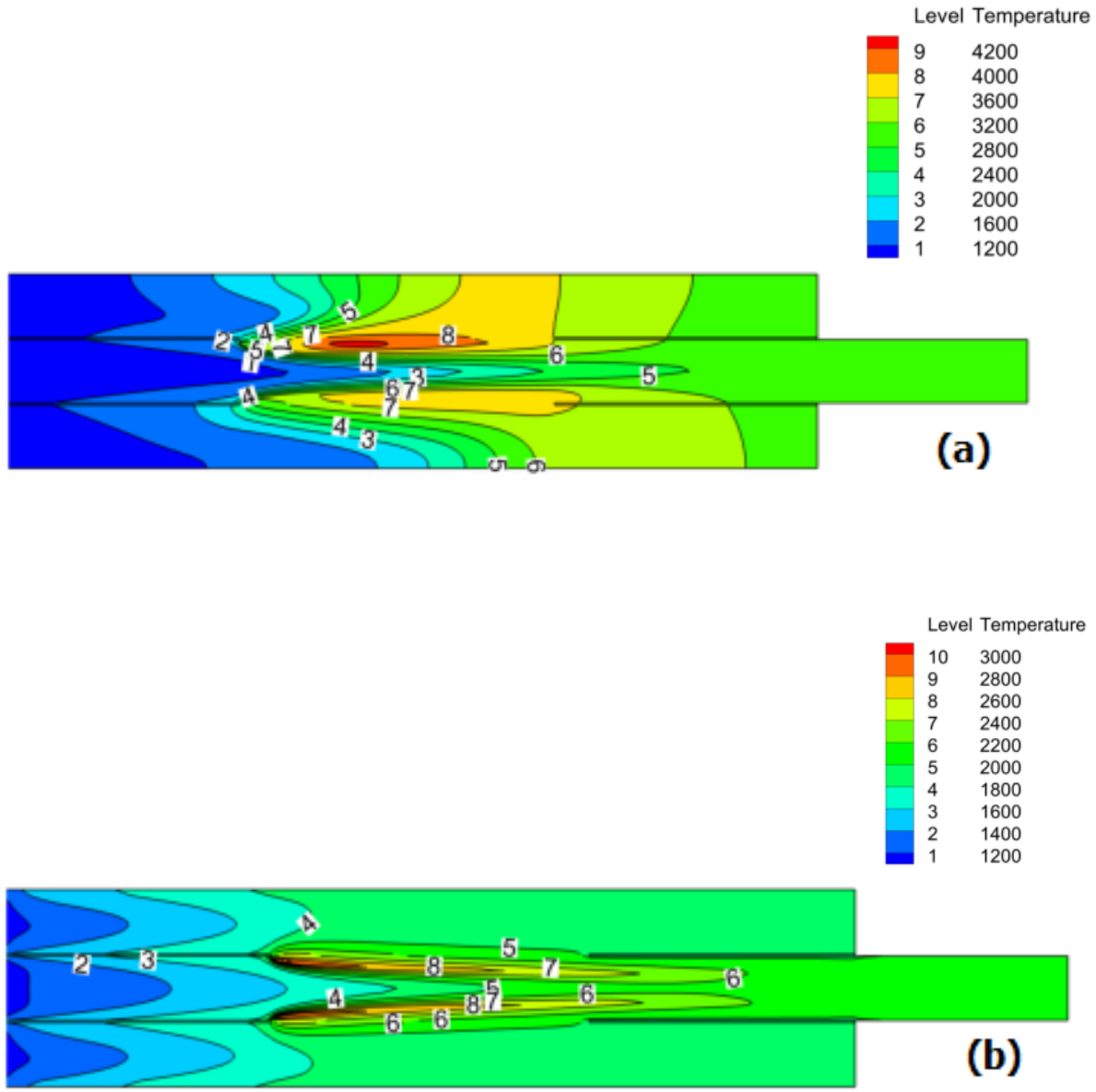

Figure 39: Contours of Temperature in 'K' inside the reactor for OR=0.25 (a) without radiation model and (b) with radiation model

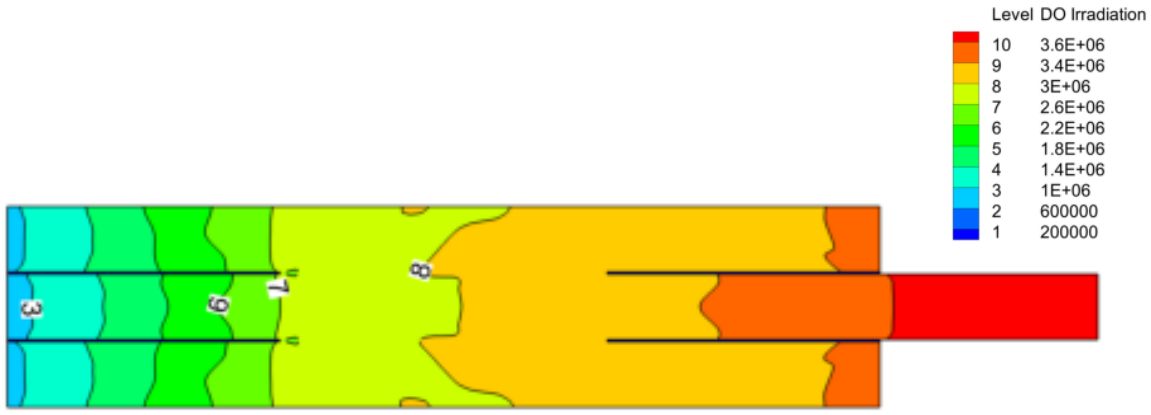

Figure 40: Contours of incident radiation in 'W/m^2'for OR=0.25

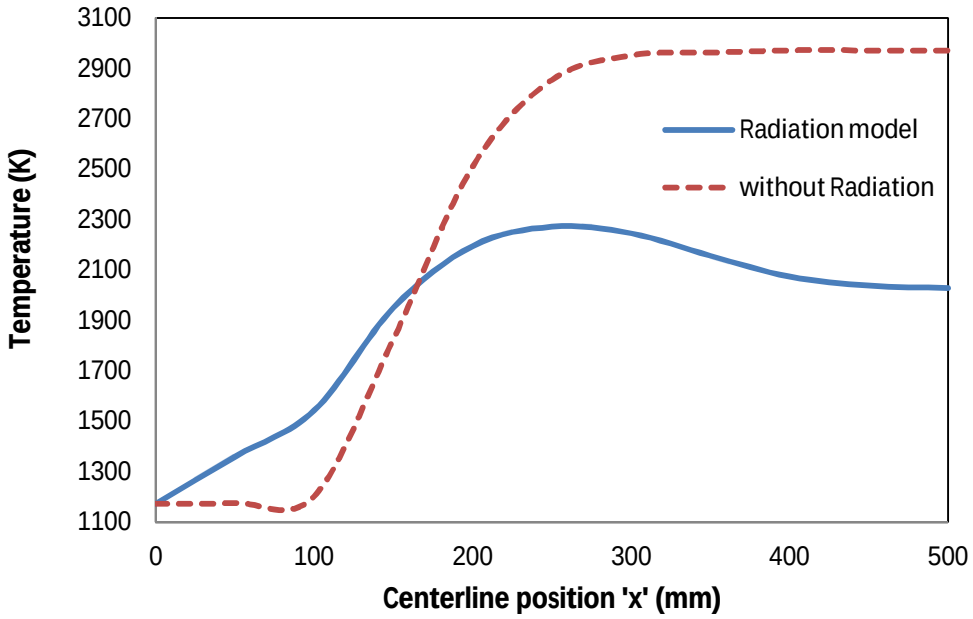

Figure 41: Comparison of Temperature profile in the reaction chamber for the cases of Radiation and without radiation

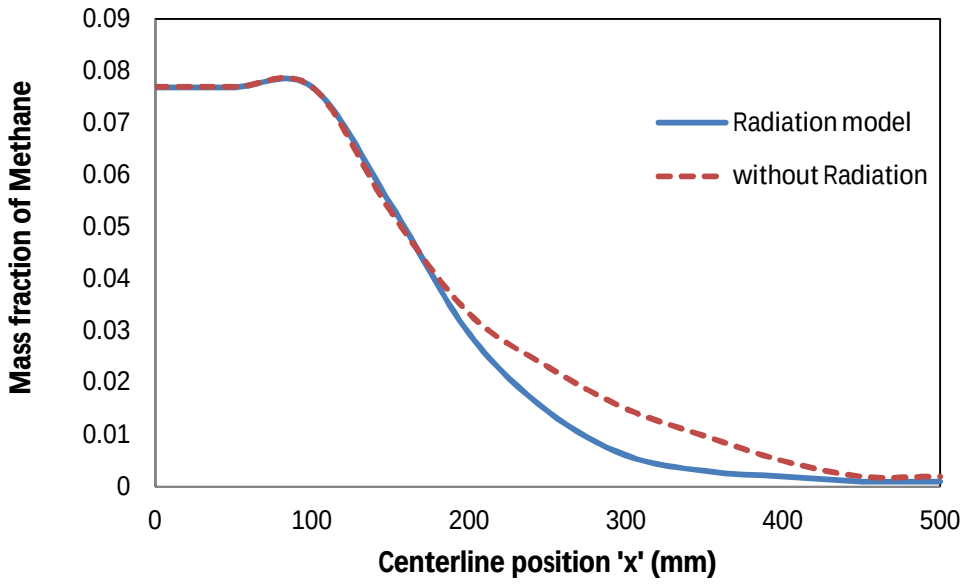

Figure 42: Comparison of methane depletion in the reaction chamber for OR =0.25 with radiation and without radiation model

5.7.2 Combustion characteristics

As the combustion starts, methane starts to deplete near the porous plate region and it continues to deplete till the end of combustion as shown in Figure 43 (a). All the oxygen that enters in the reaction is used to oxidize methane and there is no oxygen left at the outlet as shown in Figure 43 (b). Carbon dioxide and water vapor are produced due to combustion; some of these quantities diffuses to top and bottom chambers and then come back to reaction chamber as shown in Figure 44 (a) and (b). The velocity for the reactive case is much higher than the non reactive case as shown in Figure 45, in which centerline velocities are compared. The difference is due to increase in density of gases by temperature increase after combustion so the velocities need to be increased in order to maintain the same mass flow rates.

Figure 46 represents the variation of species in terms of mass fractions along the reaction chamber. Methane starts to deplete after x=100mm as the reaction begins, water vapor forms as the reaction product, the amount of carbon dioxide increases but the mass fraction decreases as the water vapor are formed. As the combustion is complete the mass fraction of carbon dioxide increases. By the end of combustion the species mass fraction remains constant. The flame shape and temperature distribution in the reactor is presented in Figure 47, in which two flames are shown, they start with the beginning of the porous plate with the maximum temperature of 2848 K. The flames are directed towards the center due to the upstream flow and the flow through the porous plates that pushes the flame towards the centerline. The outlet temperature is around 2035 K, the

temperature of the top and bottom chamber rises more than 1900 K mostly due to radiation heat transfer and diffusion of species from reaction chamber to top and bottom chamber. The temperature of upstream flow also increases due to radiation heat transfer.

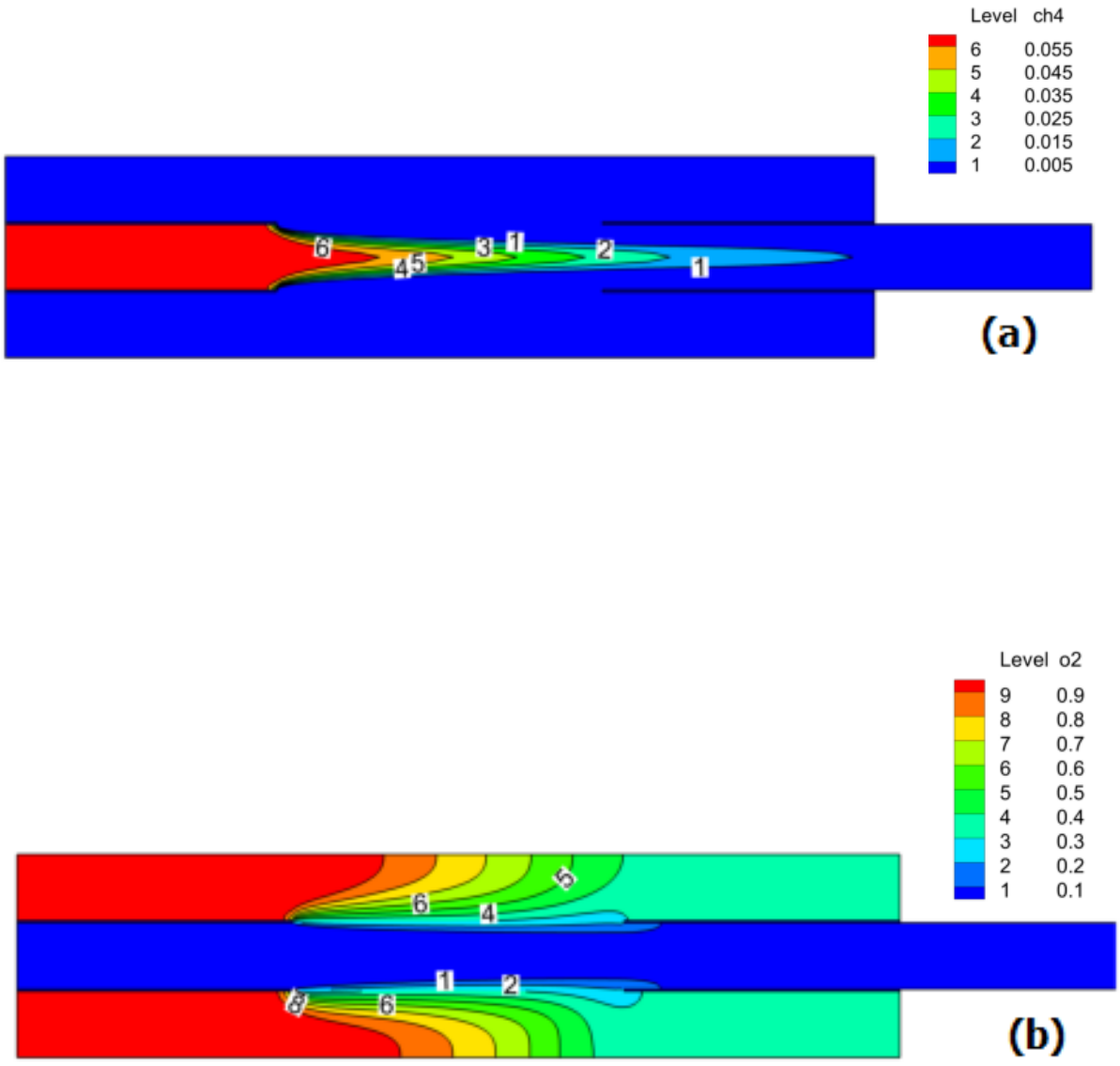

Figure 43: Contours of species mass fraction for OR=0.2 (a) Methane (b) Oxygen

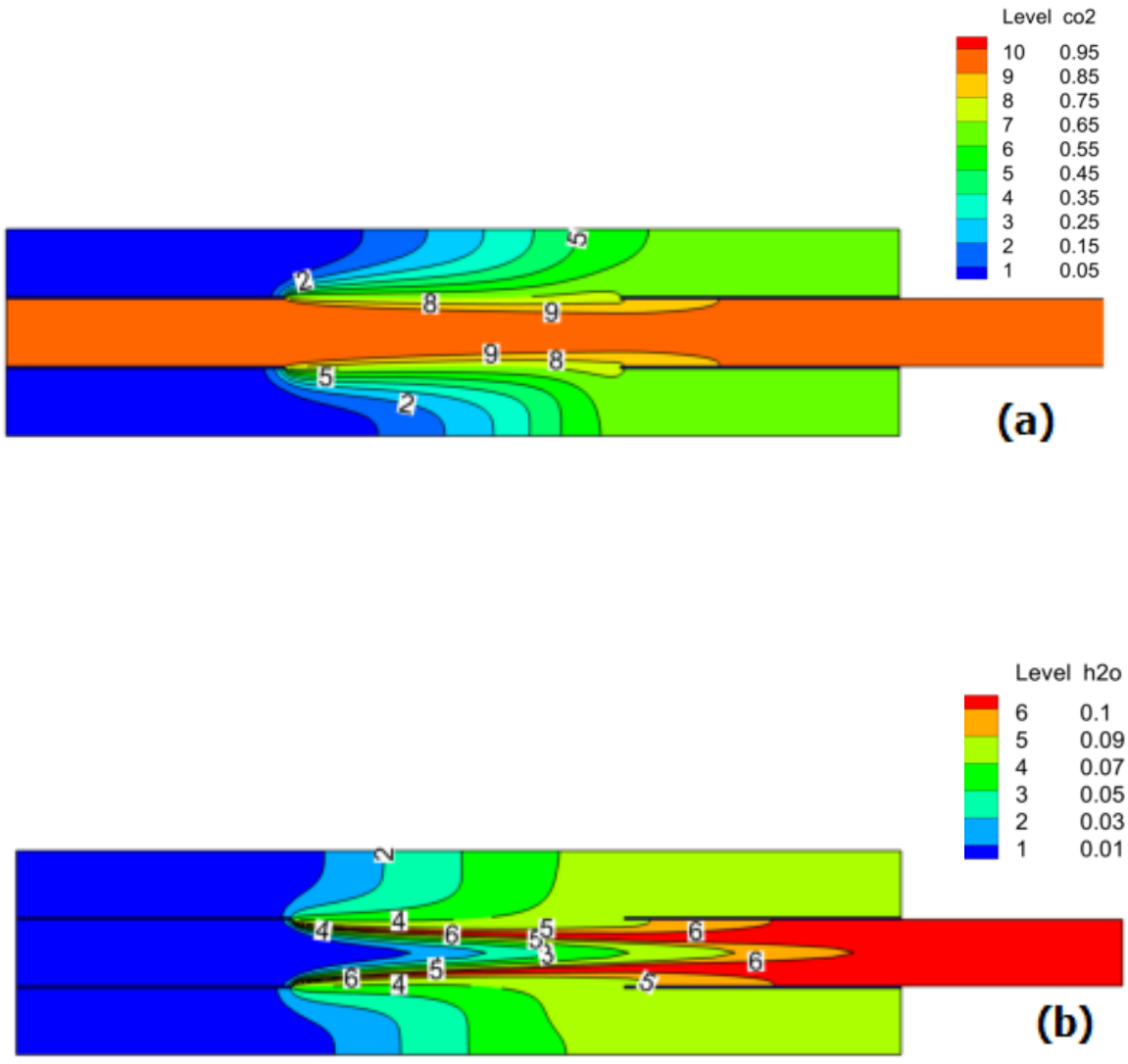

Figure 44: Contours of species mass fraction for OR=0.2 (a) Carbon dioxide (b) Water vapor

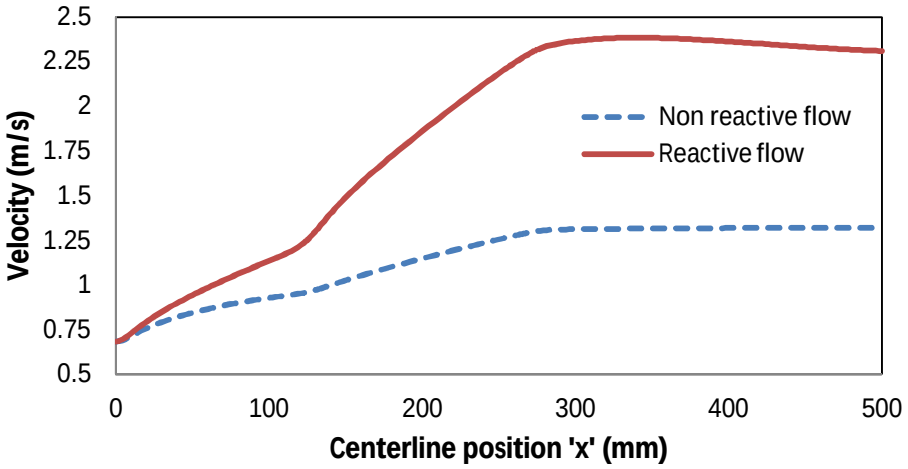

Figure 45: Centerline velocity comparison for reactive and non reactive flow (OR=0.2)

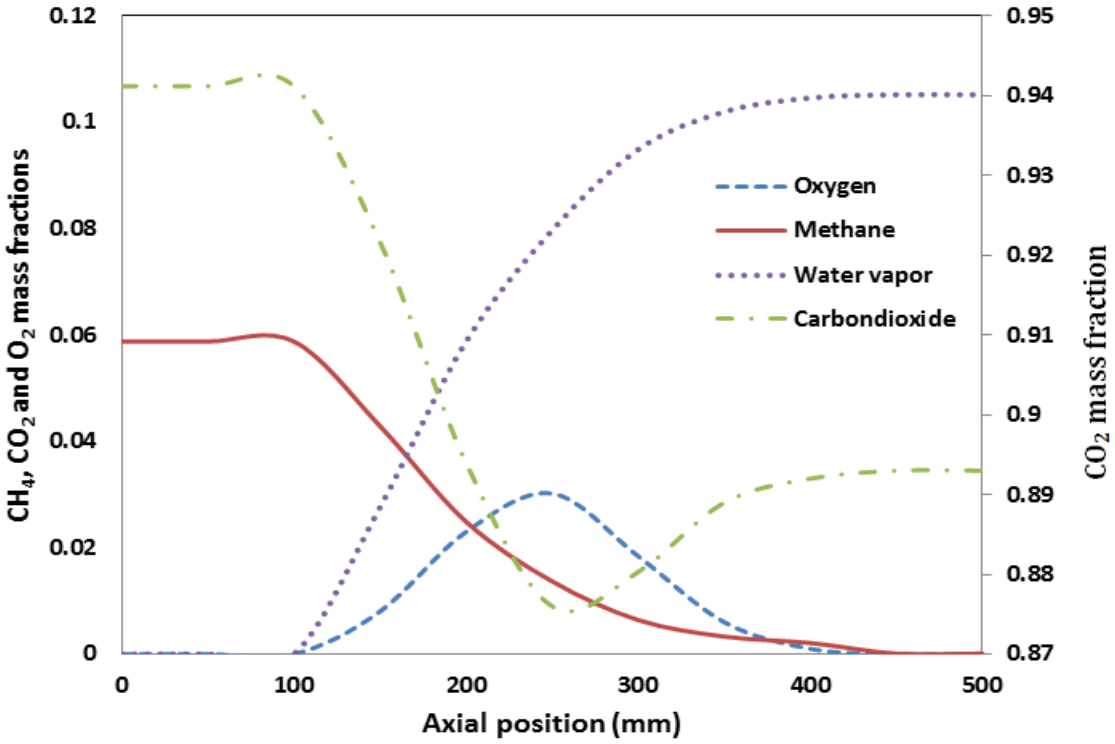

Figure 46: Variation of species mass fraction in the reaction chamber

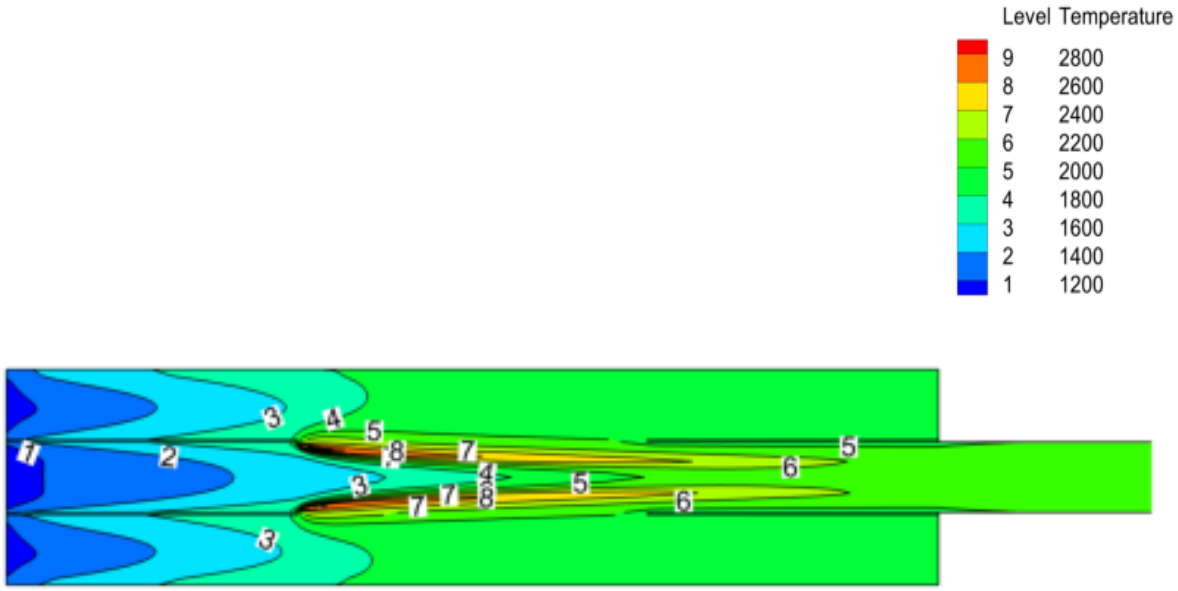

Figure 47: Temperature distribution in 'K' inside the reactor for OR=0.2

The Arhenius reaction rates varies from 0 to 0.728 kgmol/m^3-s as illustrated in Figure 48, where contours are shown only for the values ranging from 0.001 to 0.728 kgmol/m^3-s considering where most of the reaction occurs. The reaction rate gives the number of moles that are converting in to products per unit time. The maximum value is where the combustion starts and it tends to diminish as the reaction completes, the shape of contours are similar to flames as in Figure 47. These contours lie in the region where the oxy-fuel ratio was in the range from 1 to 3 as in Figure 33. So we can predict the combustible region based on non reactive flow either experimental or numerical study. The comparison between the centerline temperature and mass weighted average temperature (calculated at different sections) is shown in Figure 49. The average temperature slightly differs from the centerline temperature at the beginning, but the difference is enlarged as the reaction begins, both lines coincide at the end. This difference in the temperature is due to the fact that combustion starts above and below the centerline and impact of flame is more prominent near the porous plates so the centerline temperature is not the best representative of the energy carried by the flow. In this study all the variations are shown as mass weighted average quantities like temperature, mass fraction etc otherwise stated. After analyzing the combustion having oxidizer ratio OR=0.2, it is evident several factors need to be improved in order to improve the performance of this reactor. These include minimizing the maximum temperature, diffusion of species into top and bottom chamber, temperature of top and bottom chamber, increasing outlet temperature by convection, flame length etc. Parametric study has been carried out to address and optimize these factors.

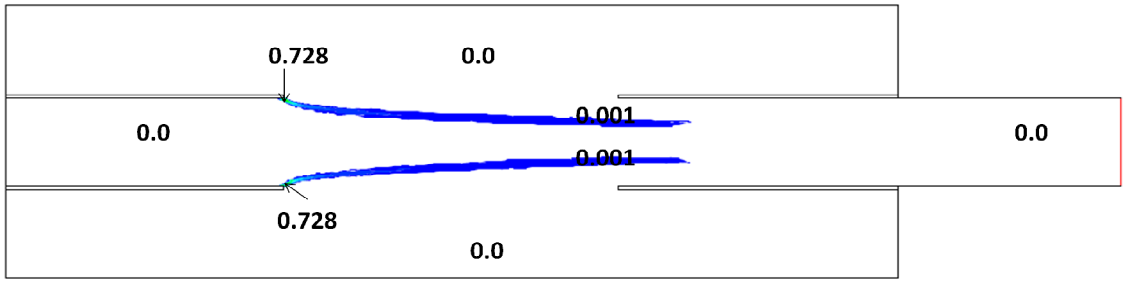

Figure 48: Arhenius reaction rate in kgmol/m^3-s in the reactor

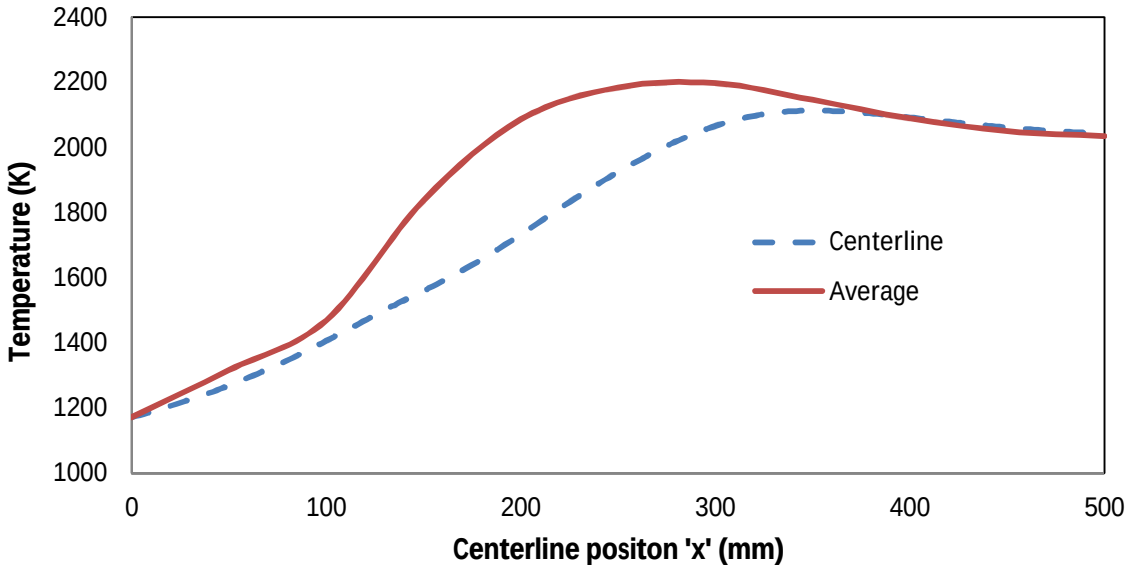

Figure 49: Comparison between sectional average temperature in the reaction chamber and the centerline temperature

5.7.3 Effect of Oxidizer ratio (OR)

The effect of oxidizer ratio (OR) on combustion process has been investigated by varying the ratio starting from 0.2 to 0.4 with the interval of 0.05. The temperature contours are presented in Figure 50. The oxidizer ratio is increased by decreasing the carbon dioxide mass flow rate keeping the stoichiometric ratios. By increasing oxidizer ratio, the flame length decreases, the maximum temperature increases and the outlet temperature decreases as shown in Figure 51. The maximum temperature increases from 2848 K to 3342 K due to the presence of less amount of carrier gas i.e. carbon dioxide. The outlet temperature decreases from 2035 K to 2008 K, because the convection heat transfer decreases and the radiation heat transfer increases due to presence of high temperatures. The axial variation of mass weighted average temperature is shown in Figure 52. It is evident from the figure that the upstream temperature raises due to more radiative heat transfer as the oxidizer ratio increases. Methane depletion rates are compared in Figure 53, where the reaction starts at same position after 100mm and most of the methane is depleted around x=300mm, but as the amount of carrier gas reduces the rate of methane depletion increases. The maximum arhenius reaction rate increases with the increase in oxidizer ratio as shown in Figure 51. The carrier gas is needed in order to limit the maximum temperature but combustion is delayed when using OR=0.21 (molar) as reported in [42], OR=0.27-0.34 (molar) produces better results under oxy-fuel conditions, choosing OR=0.25 (which is equivalent to 0.30 on molar basis) for analyzing the effect of equivalence ratio.

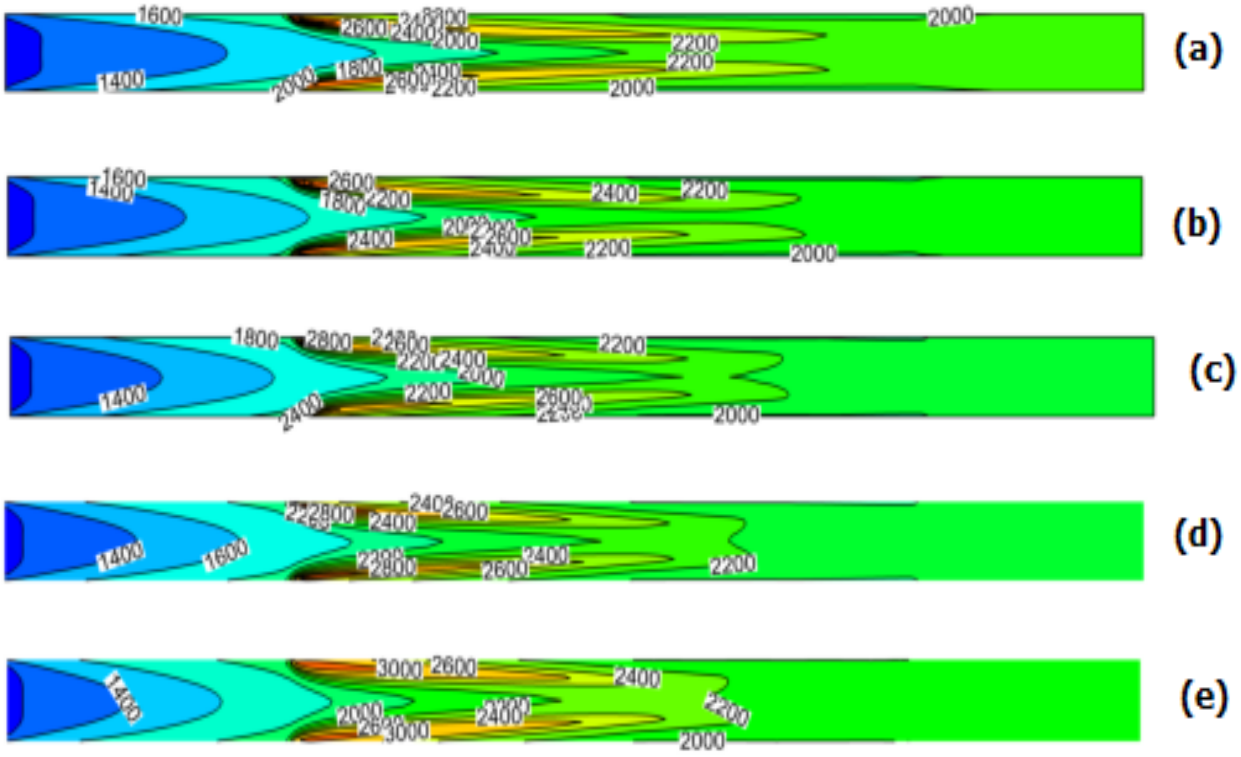

Figure 50: Temperature distribution in 'K' inside reaction chamber for (a) OR=0.20, (b) OR=0.25, (c) OR=0.30, (d) OR=0.35 and (e) OR=0.40

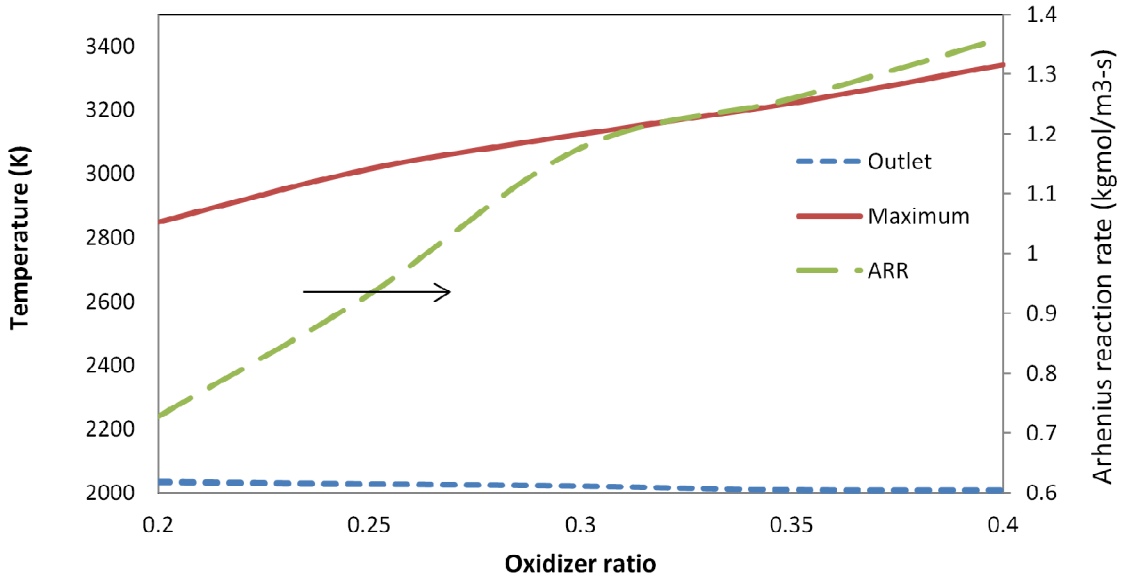

Figure 51: Variation of Arhenius reaction rate, maximum and outlet temperature with oxidizer ratio

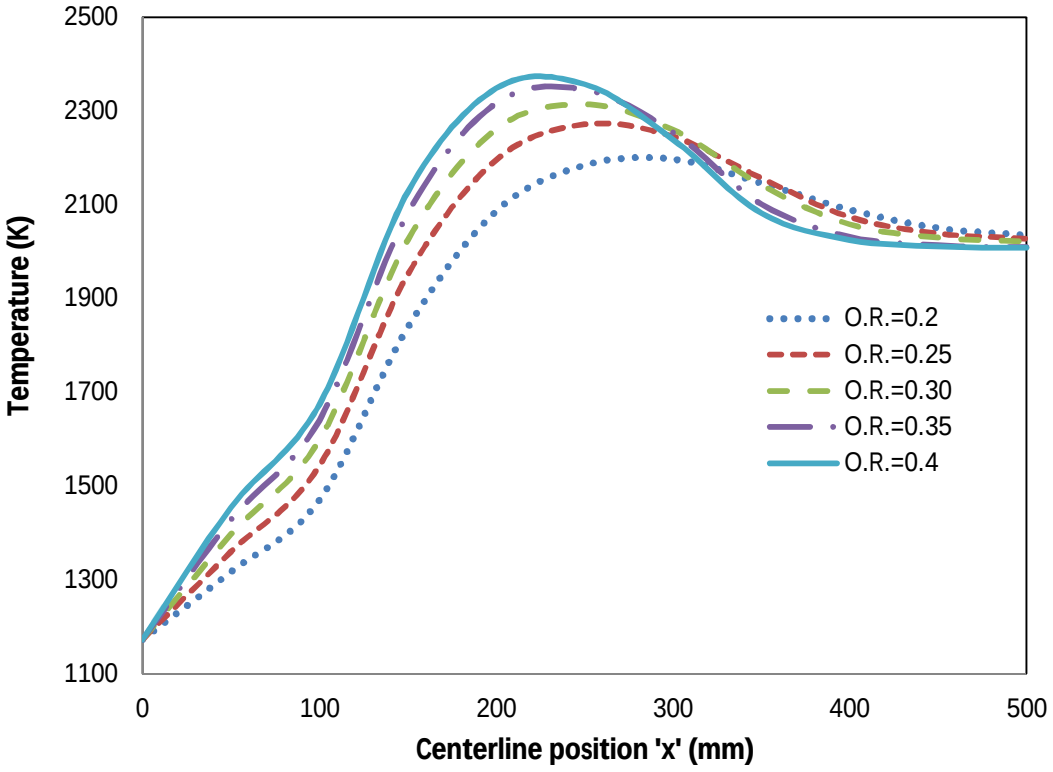

Figure 52: Variation of temperature inside the reaction zone for different oxidizer ratios

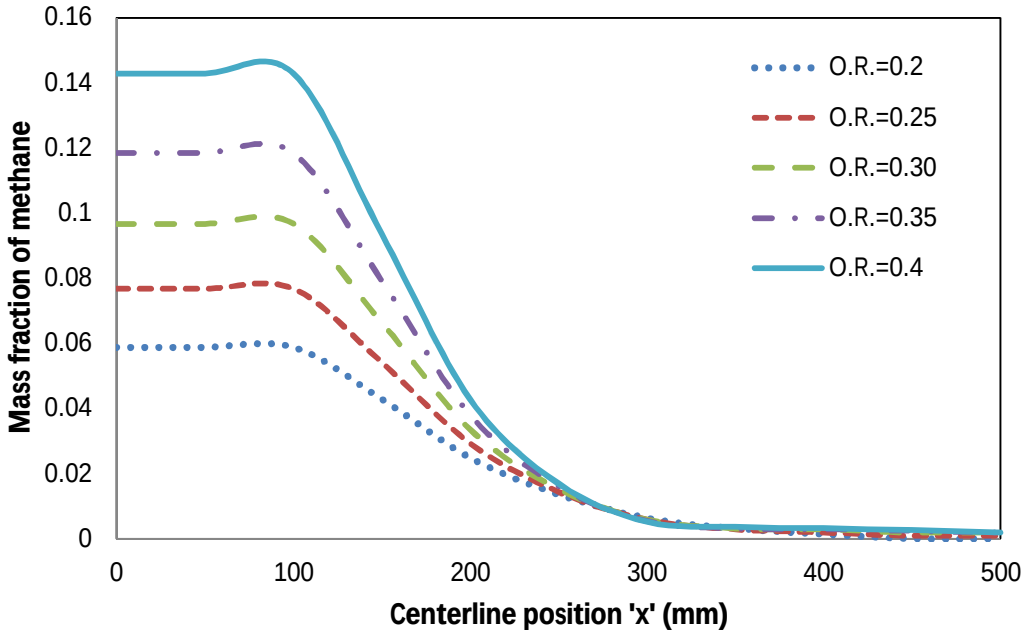

Figure 53: Methane depletion inside the reaction chamber for different oxidizer ratios

5.7.4 Effect of Equivalence ratio (φ)

The effect of equivalence ratio (φ) on combustion process has been investigated by varying the ratio starting from 1 to 0.7 with the interval of 0.1 having fixed OR=0.25. The equivalence ratio is decreased by increasing the oxygen mass flow rate. The temperature contours for different equivalence ratios are presented in Figure 54. As the equivalence ratio decreases, the flame length increases, the flame moves towards the centerline, maximum arhenius reaction rate decreases, the maximum temperature reduces from 3020 K to 2845 K and the outlet temperature increases from 2028 K to 2070 K as shown in Figure 55 and Figure 56. This is due to enhanced convection heat transfer by the induction of more oxygen flow rate. The upstream temperatures are also reduced as the effect of radiation heat transfer reduces due to lower maximum temperatures. The presence of excess oxygen ensures complete combustion that is achieved early for lower equivalence ratio as shown in the methane depletion variation in Figure 57. As the equivalence ratio decreases, the water vapor are directed towards the center so the possibility of diffusion to top and bottom chamber decreases. The diffusion of water vapor to other chamber is an indication of energy loss that raises the temperature of top and bottom chamber that isn't required. Hence decreasing the equivalence ratio or making the mixture lean will effect in better combustion with less energy loss to the surroundings.

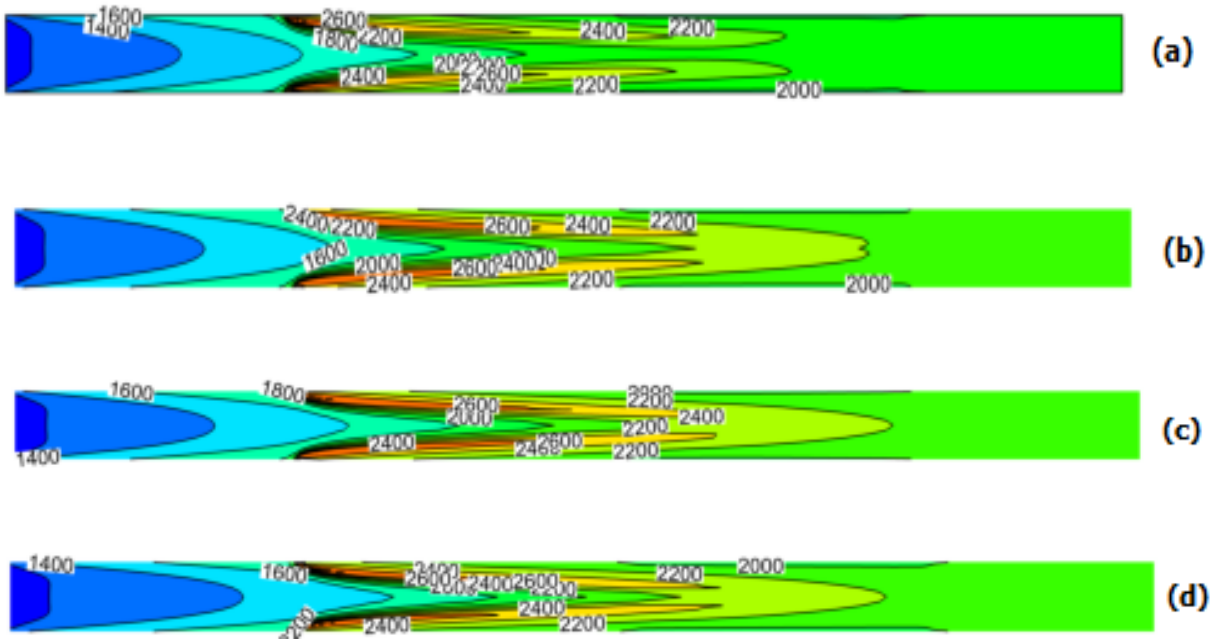

Figure 54: Temperature contours in 'K' for reaction chamber at OR=0.25 with different equivalence ratios (a) φ=1, (b) φ =0.9, (c) φ =0.8 and (d) φ =0.7

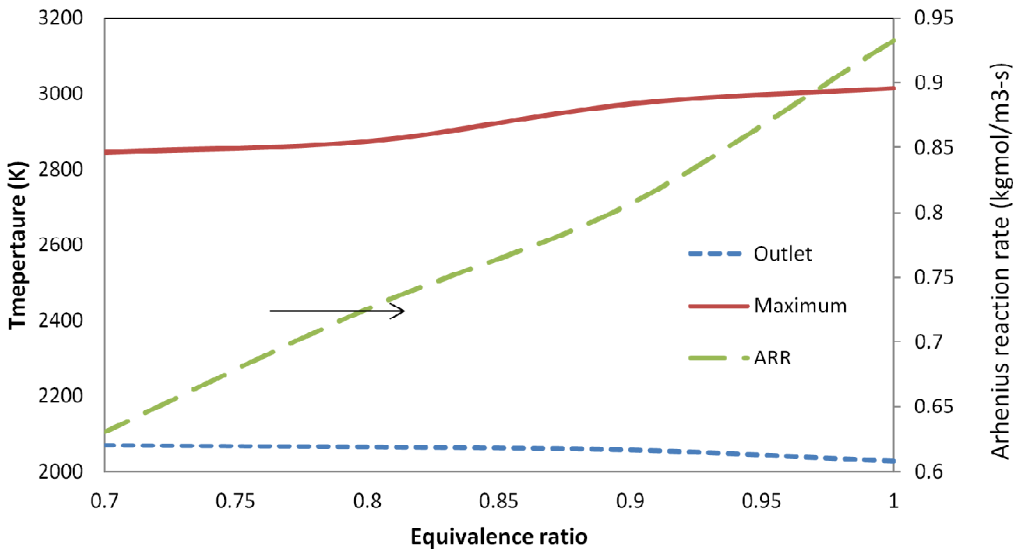

Figure 55: Variation of Arhenius reaction rate, maximum and outlet temperature with equivalence ratio at fixed OR=0.25

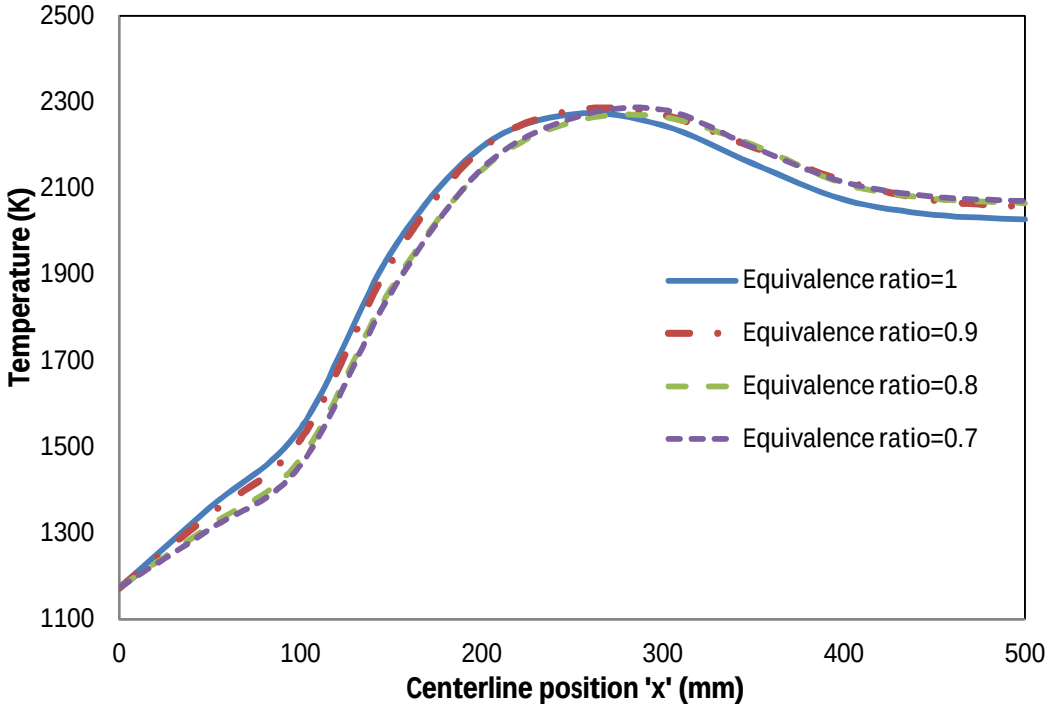

Figure 56: Temperature variation in the reaction chamber for different equivalence ratios

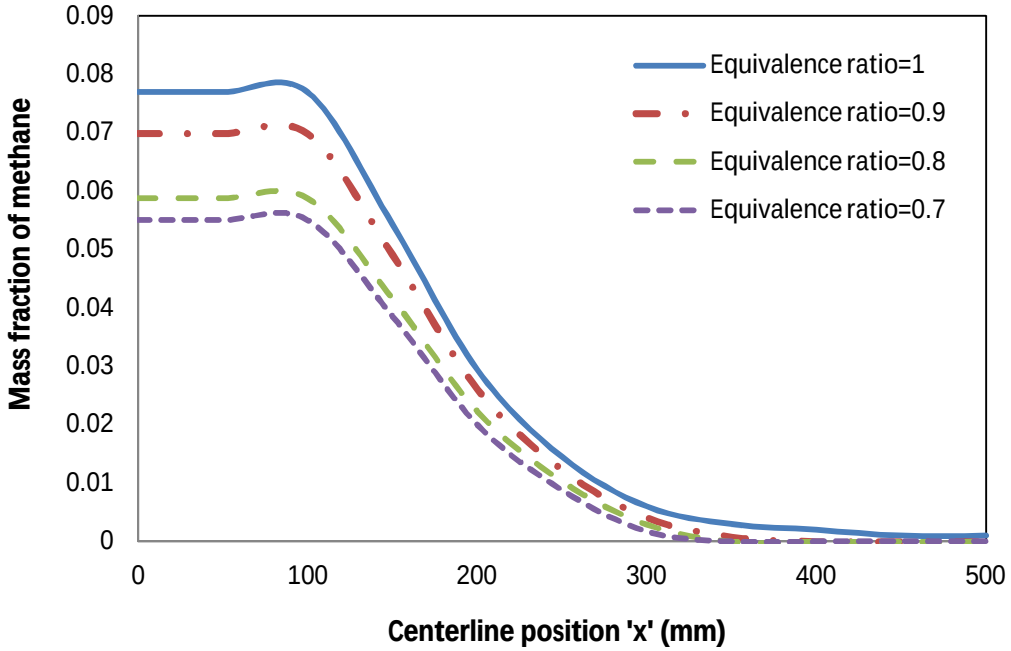

Figure 57: Methane depletion in the reaction chamber for different equivalence ratios

5.7.5 Effect of Permeability

For the fixed mass flow rates having OR=0.25 and φ=0.8, the viscous resistance was varied to investigate effect on combustion process. The values of viscous resistances were taken as 10^{10}, $2.44x10^{13}$ and 10^{15} respectively. The oxygen supply pressure is directly proportional to the viscous resistance of porous plates as shown in Figure 58. The porous plates with high viscous resistance needs high supply pressure that means extra energy is required. The temperature contours for different viscous resistances are shown in Figure 59. Increasing the resistance won't do much benefit as the temperature of the top and bottom chambers and flame shapes are not affected much.

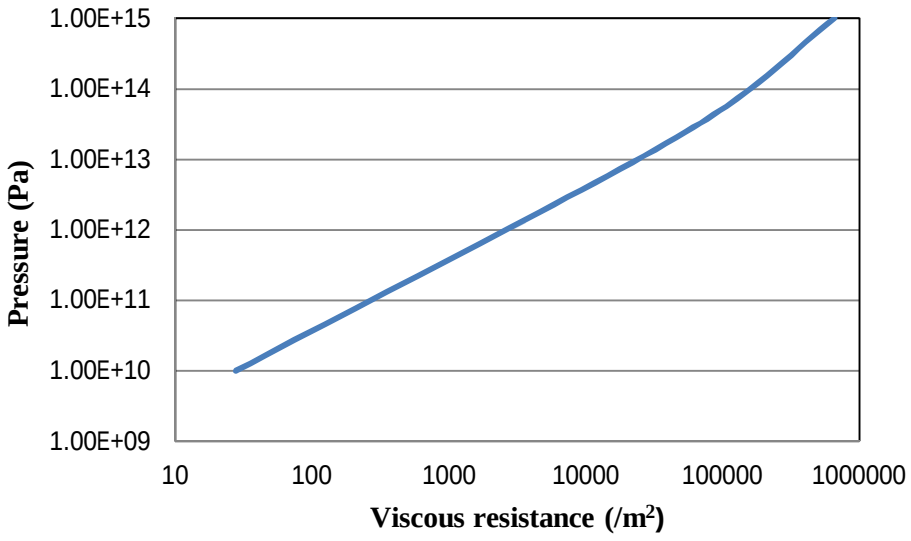

Figure 58: Supply pressure (Pa) Vs Viscous resistance (/m^2)

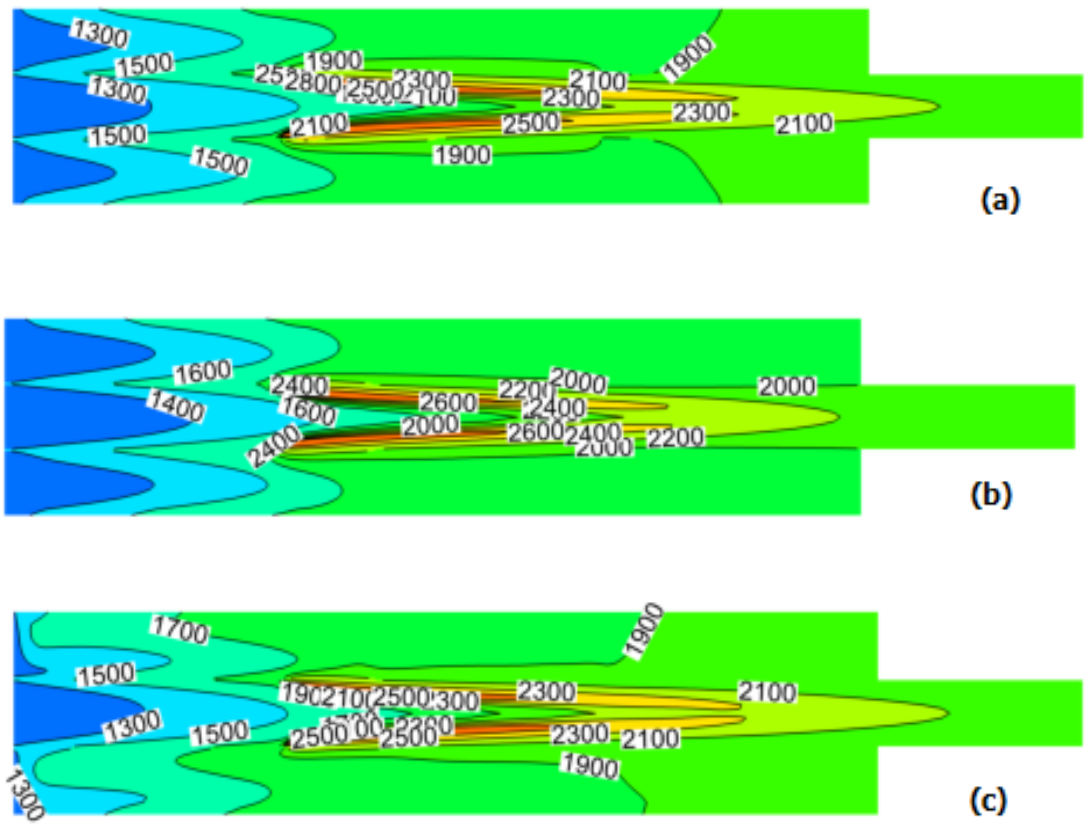

Figure 59: Temperature contours for reactors having different viscous resistances for OR=0.25 and =0.8, (a) 1x10^{10} /m^2 (b) 2.44x10^{13} /m^2 (c) 1x10^{15} /m^2

5.8 Reactive case (two step model)

The results for reactive cases using two step modified reaction model are as follows:

5.8.1 Combustion characteristics

The difference in the one step and two step model is the carbon monoxide formation. The one step model over predicts the temperature due to simplified reactions which neglects the carbon monoxide and its effect like in radiation heat transfer. The contours of both models having OR=0.20 are presented in Figure 60. The mass weighted average temperature profile for both models are presented in Figure 61, in which the temperature rise in one step model is more than the two step model. In two step model, first methane is converted in to carbon monoxide and then into carbon dioxide. The outlet temperature is nearly comparable for both models, when most of the carbon monoxide is converted into carbon dioxide. The CO contours are shown in Figure 62, the maximum mass fraction is around 0.09 in the region of maximum temperature. The incident radiation falling on the upstream flow in two step model is lower than the one step model as shown in Figure 63 due to the difference in temperature profiles in these models. Figure 64 represents the variation of species in terms of mass fractions along the reaction chamber. Methane starts to deplete after x=100mm as the reaction begins, carbon monoxide and water vapor forms as the reaction product, the amount of carbon dioxide increases but the mass fraction decreases as the water vapor are formed. By the end of combustion the species mass fraction will remain constant.

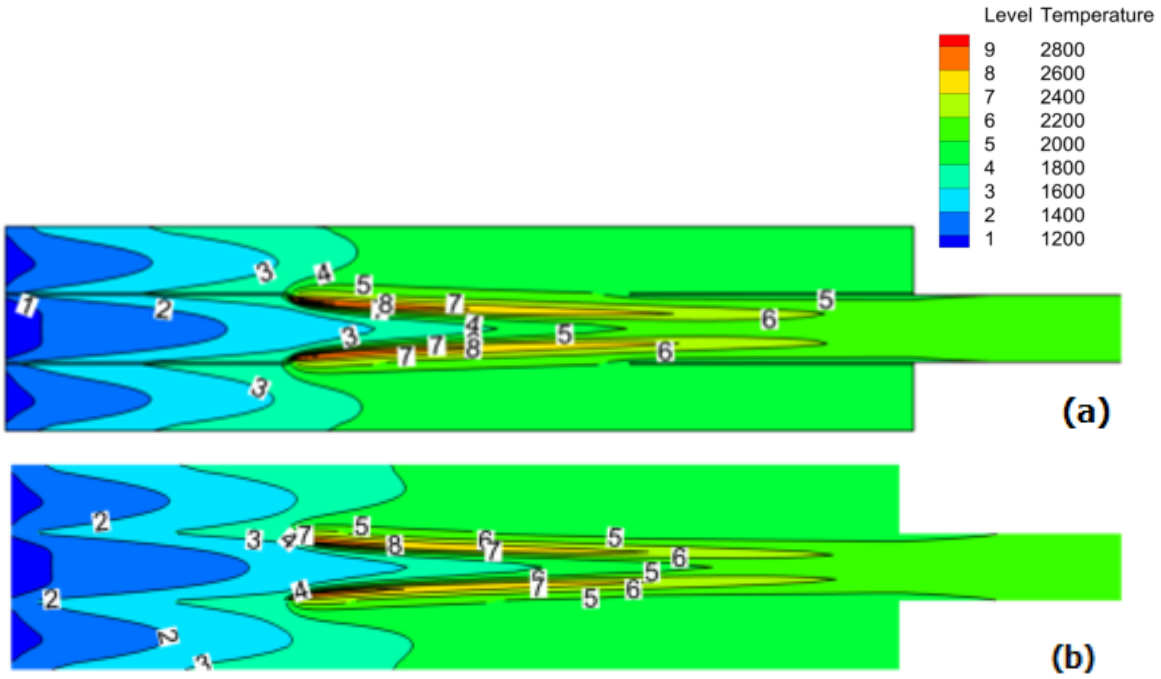

Figure 60: Temperature contours for OR=0.20 (a) one step model and (b) two step model

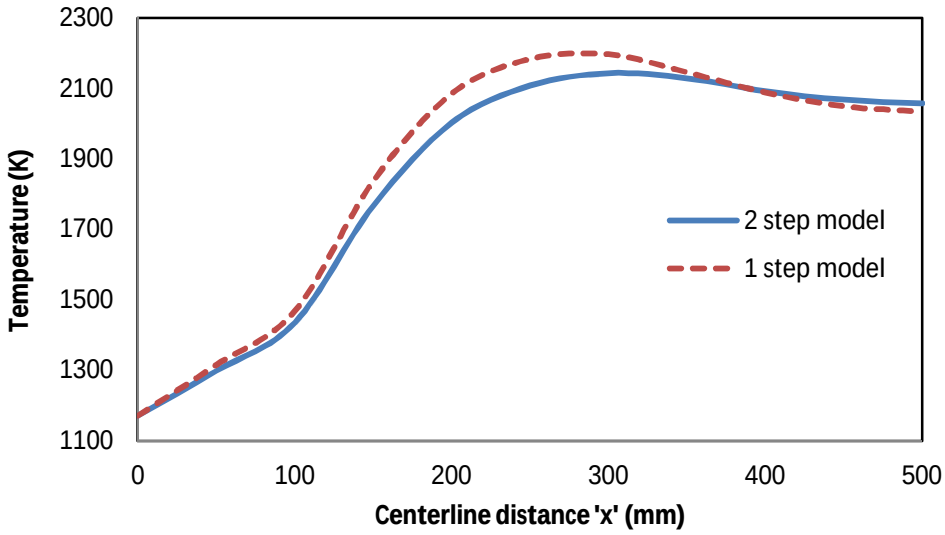

Figure 61: Temperature profiles for OR=0.20 (a) one step model and (b) two step model

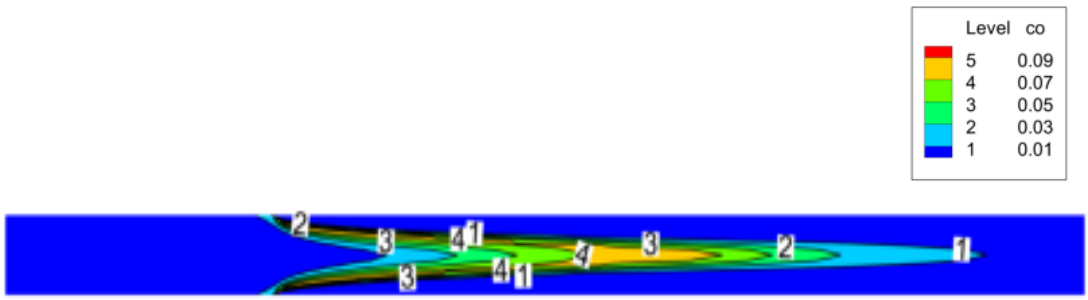

Figure 62: Contours of CO mass fraction for OR=0.20

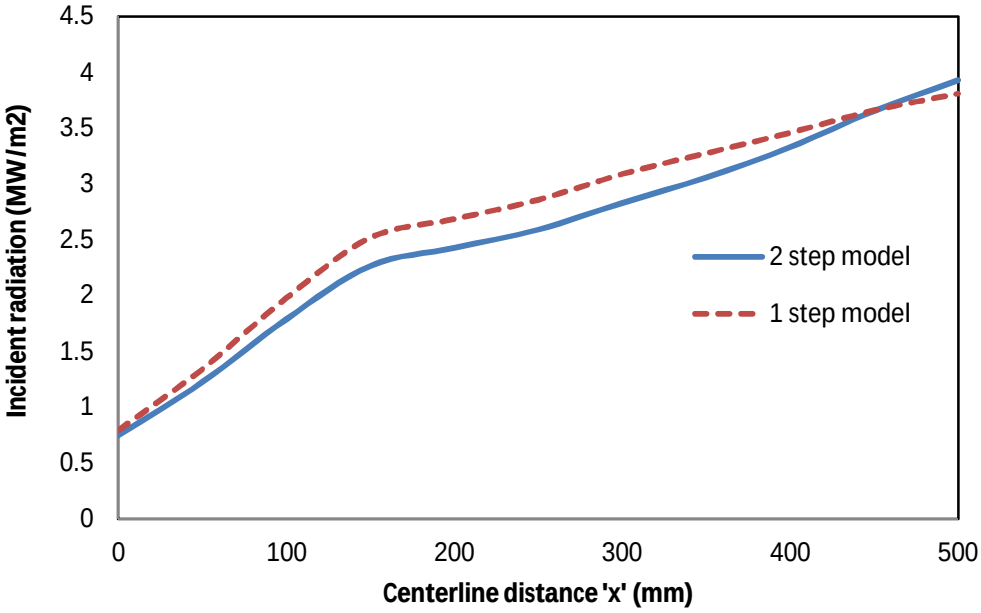

Figure 63: Incident radiation profile for OR=0.20 (a) one step model and (b) two step model

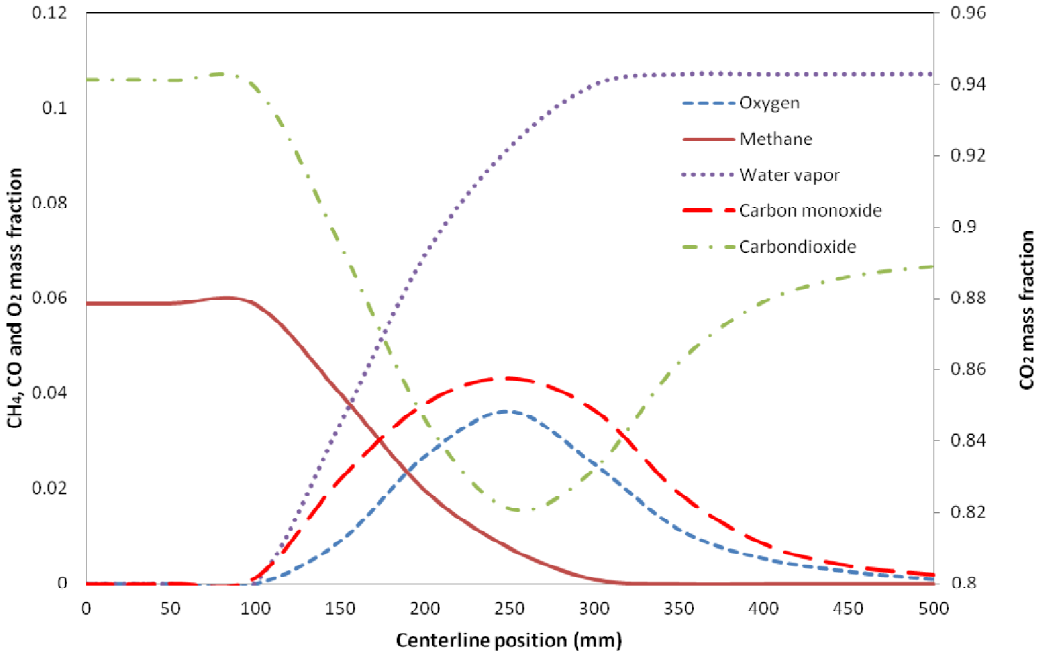

Figure 64: Variation of species mass fraction using two step model for OR=0.20

5.8.2 Effect of oxidizer ratio (OR)

The effect of oxidizer ratio (OR) on combustion process has been investigated by varying the ratio starting from 0.2 to 0.4 with the interval of 0.05 using two step model. By increasing oxidizer ratio, the flame length decreases, the maximum arhenius reaction rates, the maximum temperature increases and the outlet temperature decreases as shown in Figure 65 and Figure 66. The arhenius reaction rates are much lower than the one step model due multi step reactions. The maximum temperature increases from 2724 K to 3158 K due to the presence of less amount of carrier gas i.e. carbon dioxide. The outlet temperature decreases from 2059 K to 2020 K, because the convection heat transfer decreases and the radiation heat transfer increases due to presence of high temperatures. The maximum temperatures are less than the maximum temperatures from one step model. The axial variation of mass weighted average temperature is shown in Figure 67. It is evident from the figure that the upstream temperature raises due to more radiative heat transfer as the oxidizer ratio increases and the sweep flow rate decreases.

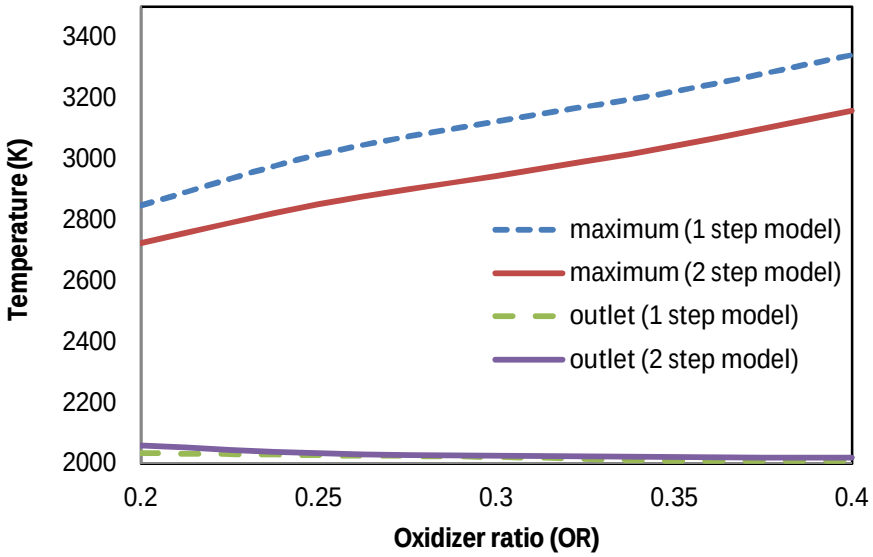

Figure 65: Variation of maximum and outlet temperature with oxidizer ratio

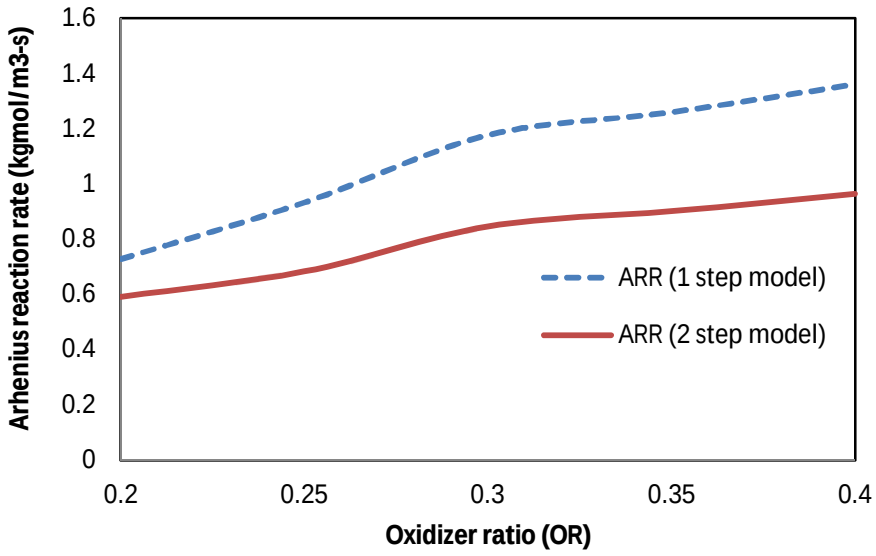

Figure 66: Variation of Arhenius reaction rates with oxidizer ratio

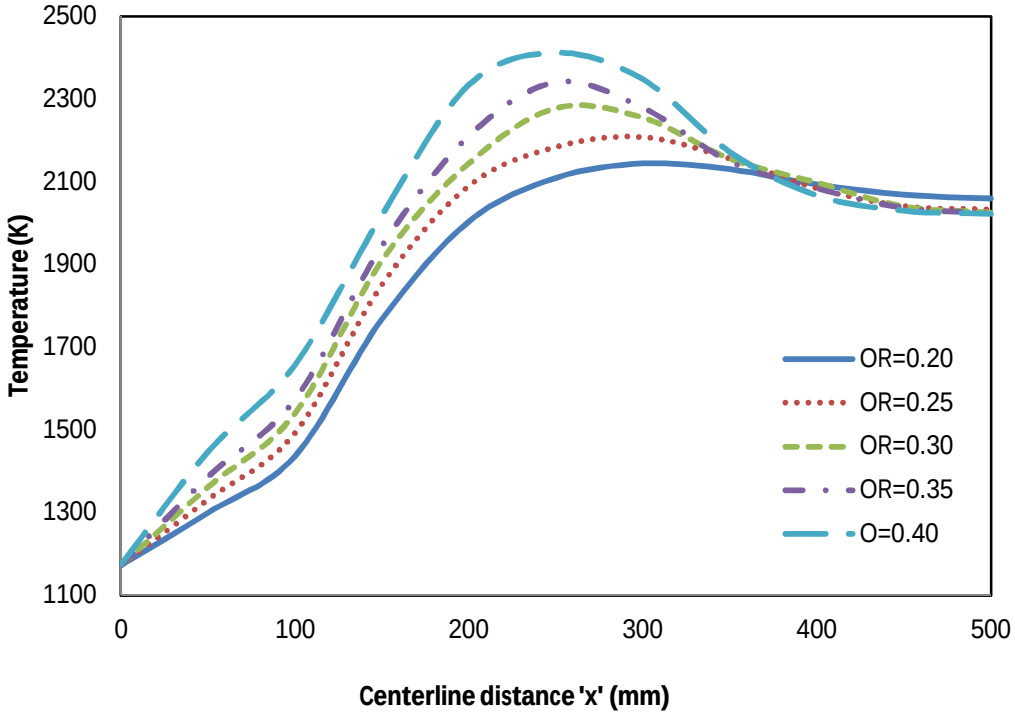

Figure 67: Temperature variation along the reactor for different oxidizer ratios

5.8.3 Effect of equivalence ratio (φ)

The effect of equivalence ratio (φ) on combustion process has been investigated by varying the ratio starting from 1 to 0.7 with the interval of 0.1 having fixed OR=0.25. The equivalence ratio is decreased by increasing the oxygen mass flow rate. As the equivalence ratio decreases, the flame length increases, the flame moves towards the centerline, maximum arhenius reaction rate decreases, the maximum temperature reduces from 2852 K to 2731 K and the outlet temperature increases from 2034 K to 2090 K as shown Figure 68 and Figure 69. This is due to enhanced convection heat transfer by the induction of more oxygen flow rate. The upstream temperatures are also reduced as the effect of radiation heat transfer reduces due to lower maximum temperatures. The maximum temperatures and reaction rates are lower than the one step model.

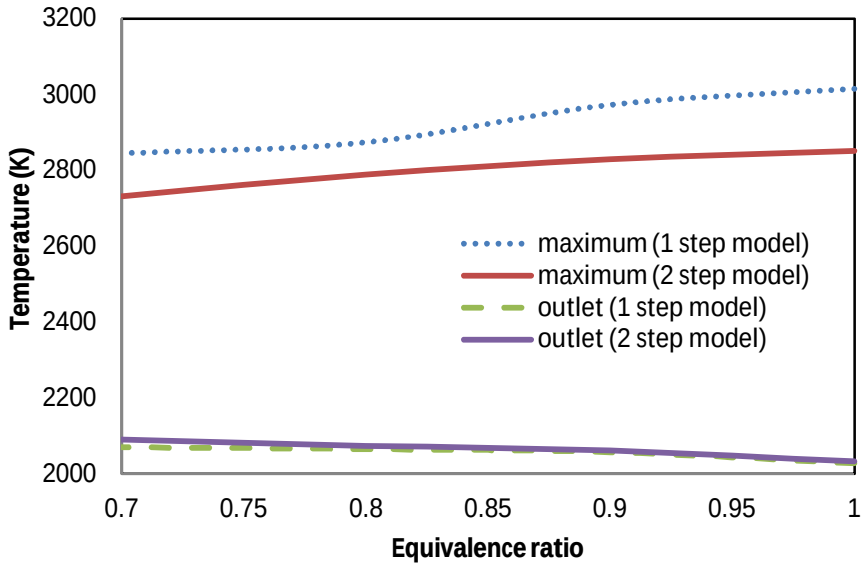

Figure 68: Variation of maximum and outlet temperatures with equivalence ratios

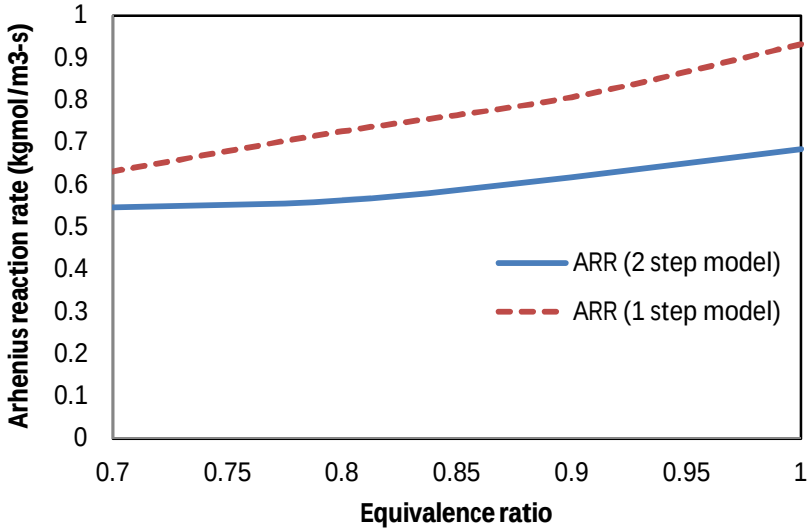

Figure 69: Variation of maximum reaction rate with equivalence ratios

5.8.4 Effect of Reynolds number (Re)

The effect of Reynolds number (Re) on combustion process has been investigated by varying the mass flow rates having OR=0.2 and φ=0.8, the mass flow rate were multiplied by factor 1, 2 and 3 and Reynold number Re= 245, 436 and 600 were achieved by using Eqn. 11 at the exit section respectively. As the Reynold number increases, the outlet temperature increases from 2074 to 2594 K, the maximum temperature rises from 2790 to 3030 K, the flame is directed towards the wall instead of centerline as shown in Figure 70 and Figure 71. The flame is directed towards wall at high Reynolds number is due to the fact that as the Reynolds number increases the combustible region where oxy-fuel ratio is from 1 to 3 moves away from the porous region as shown in Figure 72. The reactors operating at low Reynolds number are suitable as burners, because the high temperature flame will be in the center so it won't affect the walls of reactor much. The reactors operating at high Reynolds number are suitable as heat exchangers, because the high temperature flame will be near the wall so maximum heat transfer is possible. The temperature variations along the reactor are shown in Figure 73. Figure shows that for lower Reynolds number, the temperature rises up to certain limit than decreases due to radiation and mixing of unused oxygen; for higher Reynolds number, the temperature keeps on increasing till end, because the reaction is not complete as shown in Figure 74 by unburned methane.

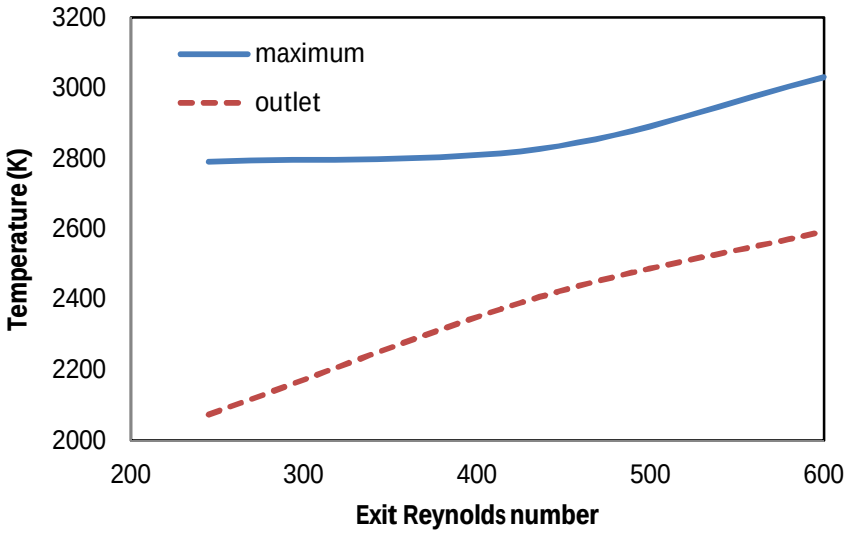

Figure 70: Variations of maximum and outlet temperatures with Reynolds number

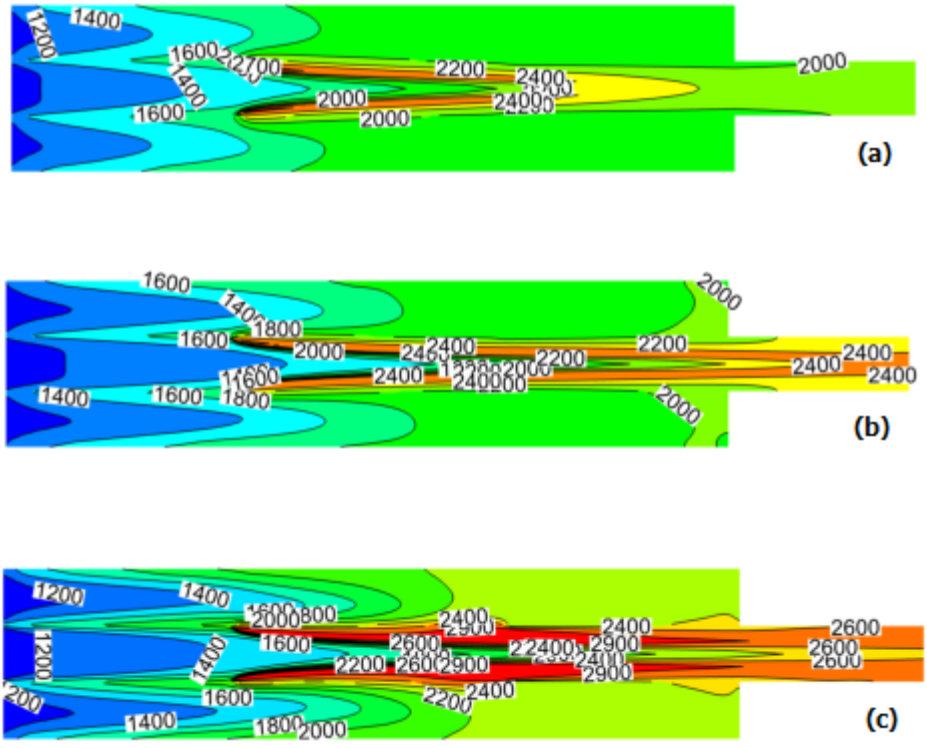

Figure 71: Temperature contours for (a) Re=245, (b) Re=436 and (c) Re=600

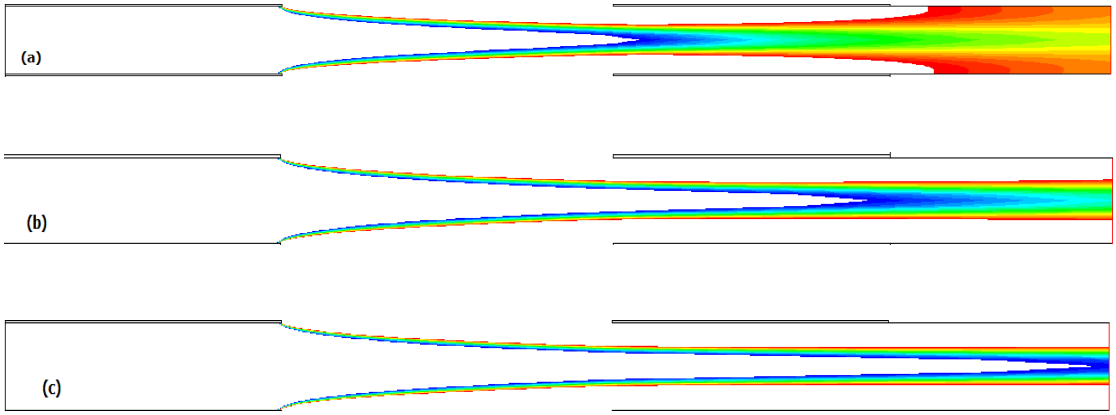

Figure 72: Oxy-fuel ratio for non reactive case ranging from 1 to 3 for different Reynolds number (a) Re=245, (b) Re=436 and (c) Re=600

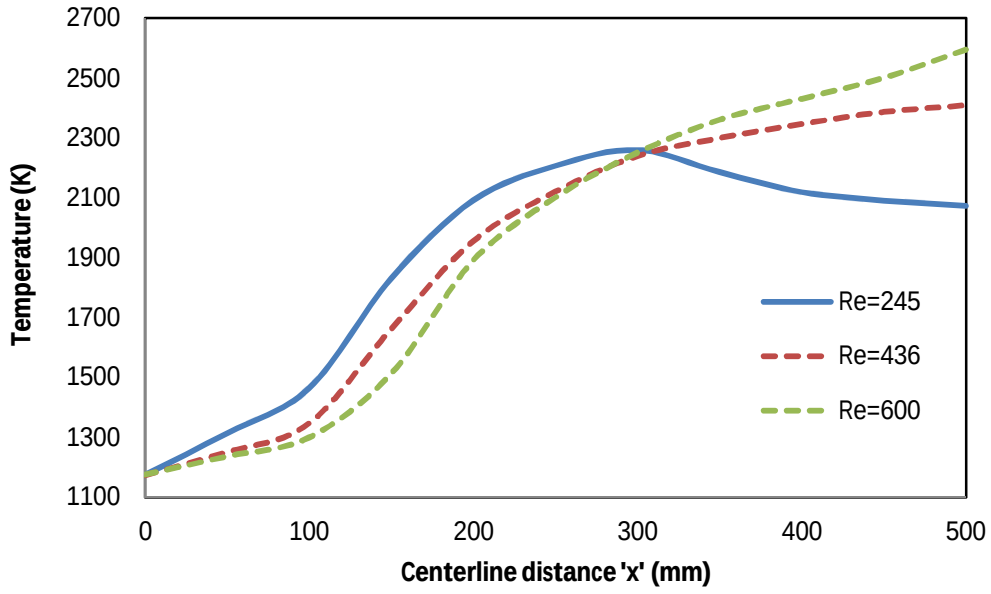

Figure 73: Temperatures variation along the reaction chamber for different Reynolds number

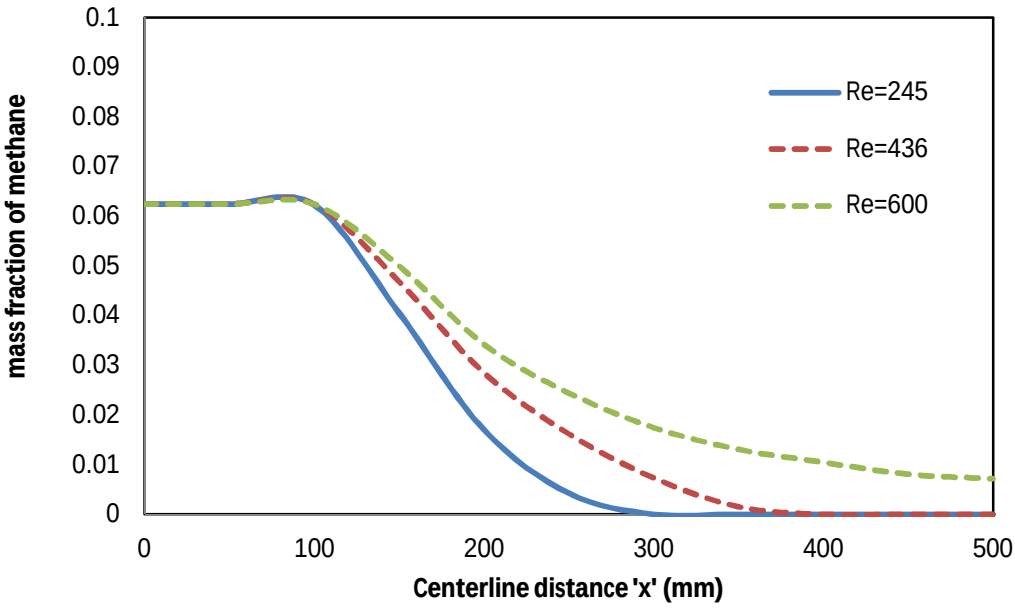

Figure 74: Methane depletion trends for different Reynolds numbers

CHAPTER 6

CONCLUSION AND FUTURE RECOMMENDATIONS

The conclusion is divided in two sections. In the first section the experimental and numerical results are summarized and in the second section, proposed directions have been made for future research.

6.1 Porous plate reactor

An experimental set up has been made comprising of specially designed porous plate reactor in order to investigate combustion characteristics under oxy-fuel combustion conditions. The experiments have been performed for non reactive flows to measure horizontal and vertical species concentration profiles. From these profiles we can predict the combustible zone where the reaction is most likely to happen. A 2D numerical model was developed for the study of reactive and non reactive cases. The experimental data was compared with the numerical predictions which validated the numerical model. The modeling for reactive cases was carried out by using one step and modified two step reactions kinetics model. Detailed parametric study was carried out by varying permeability of porous plates, oxidizer ratios, equivalence ratios and Reynolds number. It was found that the maximum temperature in the reactor increases by increasing oxidizer ratio, equivalence ratio (up to 1) and Reynolds number and the outlet temperature increases by increasing the sweep flow rate, equivalence ratio and Reynolds number. The

one step model over predicts the temperature and reaction rates as compared to two step model. It was found that the reaction zone can be adjusted to desired region within the reaction chamber by varying inlet conditions. The reactor operating at higher Reynolds number pushes the flame towards walls making it a suitable condition to be operated as heat exchanger.

6.2 Future Recommendations

a) Different configurations of the porous plate reactor like vertical and tubular, can be investigated in order to enhance and optimizing the combustion process.

b) Four step model and detailed kinetics model can be implied for accurate results which also help in predicting other species like hydrogen etc.

c) The reactor can also be investigated for different kinds of fuel specially the ones with low calorific values.

NOMENCLATURE

A	:	Pre exponential factor
C_2	:	Viscous resistance
C_p	:	Specific heat capacity in ‘kJ/kg-K’
$D_{i,m}$	:	Diffusion coefficient
d_h	:	Hydraulic diameter (m)
E_a	:	Activation energy
I	:	Total radiation intensity
K	:	Absorption coefficient
k_r	:	Rate of reaction
m	:	Mass flow rate in ‘kg/s’
P	:	Pressure in ‘Pa’
Q_x	:	Flow rate of ‘x’ species in L/min
R	:	Universal gas constant
Re	:	Reynolds Number
r	:	Position vector
T	:	Temperature in ‘K’
U	:	Velocity in ‘m/s’
Y_i	:	Species concentration
z	:	Uncertainty in %age
ΔP	:	Pressure drop (Pa)
Δx	:	Thickness of porous plate (mm)

α	:	Inertial resistance
β	:	temperature exponent
∇	:	Gradient operator
$\boldsymbol{\varphi}$	:	Equivalence ratio
σ_s	:	Scattering coefficient
ρ	:	Density in 'kg/m^3'
μ	:	Viscosity in 'kg/m-s'

REFERENCES

[1] F. Lecomte, P. Broutin, and E. Lebas, *CO2 Capture Technologies to reduce greenhouse gas emissions*. IFP Publications, 2010, pp. 1–10.

[2] IFP-BRGM-ADEME, *CO2 capture and storage in the subsurface*. 2007.

[3] IPCC, "Climate change, Synthesis Report," 2007.

[4] S. Pacala and R. Socolow, "Stabilization wedges: solving the climate problem for the next 50 years with current technologies.," *Science*, vol. 305, no. 5686, pp. 968–72, Aug. 2004.

[5] M. A. Habib, M. Nemitallah, and R. Ben-Mansour, "Recent Development in Oxy-Combustion Technology and Its Applications to Gas Turbine Combustors and ITM Reactors," *Energy & Fuels*, vol. 27, no. 1, pp. 2–19, Jan. 2013.

[6] B. J. P. Buhre, L. K. Elliott, C. D. Sheng, R. P. Gupta, and T. F. Wall, "Oxy-fuel combustion technology for coal-fired power generation," *Prog. Energy Combust. Sci.*, vol. 31, no. 4, pp. 283–307, Jan. 2005.

[7] C. Kunze and H. Spliethoff, "Assessment of oxy-fuel, pre- and post-combustion-based carbon capture for future IGCC plants," *Appl. Energy*, vol. 94, pp. 109–116, Jun. 2012.

[8] C. K. Law, D. L. Zhu, and G. Yu, “Propagation and extinction of stretched premixed flames,” in *Twenty-first Symposium (International) on Combustion/The Combustion Institute*, 1986, vol. i, pp. 1419–1426.

[9] K. Andersson and F. Johnsson, “Flame and radiation characteristics of gas-fired O2/CO2 combustion,” *Fuel*, vol. 86, no. 5–6, pp. 656–668, Mar. 2007.

[10] I. Pfaff and A. Kather, “Comparative thermodynamic analysis and integration issues of CCS steam power plants based on oxy-combustion with cryogenic or membrane based air separation,” *Energy Procedia*, vol. 1, no. 1, pp. 495–502, Feb. 2009.

[11] A. P. Simpson and a. J. Simon, “Second law comparison of oxy-fuel combustion and post-combustion carbon dioxide separation,” *Energy Convers. Manag.*, vol. 48, no. 11, pp. 3034–3045, Nov. 2007.

[12] E. Kakaras, A. Koumanakos, A. Doukelis, D. Giannakopoulos, and I. Vorrias, “Oxyfuel boiler design in a lignite-fired power plant,” *Fuel*, vol. 86. pp. 2144–2150, 2007.

[13] Y. S. Lin, “Microporous and dense inorganic membranes: current status and prospective,” *Sep. Purif. Technol.*, vol. 25, no. 1–3, pp. 39–55, Oct. 2001.

[14] “Clean coal technology.” [Online]. Available: http://www.rmcmi.org/education/clean-coal-technology#.U1i5qvmSy6U.

[15] Q. Merril and E. P. Ted, “2nd International Oxy-fuel Combustion Conference,” in *Integration of ITMs with Oxy combustion Power Generation Systems*, 2011.

[16] A. PA, “Method for predicting performance of an ion transport membrane unit-operation,” 2002.

[17] V. Stein, P. Armstrong, and T. Foster, “New gas turbine integration options for ITM oxygen in gasification applications,” in *Gasification technologies conference*, 2007.

[18] K. Foy and J. McGovern, “Comparison of Ion Transport Membranes,” *FOURTH Annu. Conf. CARBON CAPTURE SEQUESTRATION DOE/NET*, pp. 1–11, 2005.

[19] S. Diethelm, J. Sfeir, and F. Clemens, “Oxygen permeability and stability of L0.4Ca0.6Fe1-xCoxO3-d (x=0,0.25,0.5) membranes,” *J. Power Sources*, vol. 118, no. 270–275, 2003.

[20] H. Wang, Y. Cong, and W. Yang, “Oxygen permeation study in a tubular BSCF oxygen permeable membrane,” *J. Memb. Sci.*, vol. 210, pp. 107–115, 2002.

[21] A. C. Partridge, C. Milestone, C. O. Too, and G. G. Wallace, “Ion Transport Membranes based on conducting Polymers,” *J. Memb. Sci.*, vol. 132, pp. 245–253, 1997.

[22] “US deptarment of energy.” [Online]. Available: http://www.netl.doe.gov/research/coal/energy-systems/gasification/feed-systems/project-de-fc26-98ft40343.

[23] I. International energy agency, “Key World Statistics.,” France, 2007.

[24] “World CO2 emissions.” [Online]. Available: http://commons.wikimedia.org/wiki/File:World-co2-emissions-by-fuel-1990---2035-USDOE-IEA-2011.png.

[25] L. Eide and D. Bailey, “Pre-combustion decarbonisation process,” *Oil gas Sci. Technol.*, vol. 60, no. 3, pp. 475–484, 2004.

[26] D. Singh, E. Croiset, P. . Douglas, and M. . Douglas, “Techno-economic study of CO2 capture from an existing coal-fired power plant: MEA scrubbing vs. O2/CO2 recycle combustion,” *Energy Convers. Manag.*, vol. 44, no. 19, pp. 3073–3091, Nov. 2003.

[27] P. Folger, “Carbon Capture : A Technology Assessment,” 2013.

[28] P. Folger, “Carbon Capture and Sequestration : Research , Development , and Demonstration at the U . S . Department of Energy,” 2014.

[29] E. Rubin, L. Meyer, and H. Conick, “IPCC Special ReportCarbon dioxide Capture and Storage, Technical Summary,” 2005.

[30] M. A. Habib, H. M. Badr, S. F. Ahmed, K. Mezghani, and S. Imashuku, “A review of recent developments in carbon capture utilizing oxy-fuel combustion in conventional and ion transport membrane systems,” no. December 2010, pp. 741–764, 2011.

[31] J.-C. Chen and J.-S. Huang, “Theoretical and experimental study on the emission characteristics of waste plastics incineration by modified O2/RFG combustion technology,” *Fuel*, vol. 86, no. 17–18, pp. 2824–2832, Dec. 2007.

[32] J.-C. Chen, Z.-S. Liu, and J.-S. Huang, “Emission characteristics of coal combustion in different O2/N2, O2/CO2 and O2/RFG atmosphere.,” *J. Hazard. Mater.*, vol. 142, no. 1–2, pp. 266–71, Apr. 2007.

[33] S. Gunasekaran, N. D. Mancini, and a. Mitsos, “Optimal design and operation of membrane-based oxy-combustion power plants,” *Energy*, Apr. 2014.

[34] S. Seepana and S. Jayanti, “Experimental studies of flame extinction in a swirl-stabilized oxy-fuel burner,” *Fuel*, vol. 93, pp. 75–81, Mar. 2012.

[35] C. Yin, L. a. Rosendahl, and S. K. Kær, “Chemistry and radiation in oxy-fuel combustion: A computational fluid dynamics modeling study,” *Fuel*, vol. 90, no. 7, pp. 2519–2529, Jul. 2011.

[36] M. Ditaranto and J. Hals, “Combustion instabilities in sudden expansion oxy–fuel flames,” *Combust. Flame*, vol. 146, no. 3, pp. 493–512, Aug. 2006.

[37] R. J. Harris, W. Horne, and a. Williams, “High intensity oxy□methane combustion in a jet-mixing burner,” *Combust. Flame*, vol. 26, pp. 311–321, Feb. 1976.

[38] N. Nikolopoulos, A. Nikolopoulos, E. Karampinis, P. Grammelis, and E. Kakaras, “Numerical investigation of the oxy-fuel combustion in large scale boilers adopting the ECO-Scrub technology,” *Fuel*, vol. 90, no. 1, pp. 198–214, Jan. 2011.

[39] J. Oh and D. Noh, “Lifted flame behavior of a non-premixed oxy-methane jet in a lab-scale slot burner,” *Fuel*, vol. 103, pp. 862–868, Jan. 2013.

[40] C. Galletti, G. Coraggio, and L. Tognotti, “Numerical investigation of oxy-natural-gas combustion in a semi-industrial furnace: Validation of CFD sub-models,” *Fuel*, vol. 109, pp. 445–460, Jul. 2013.

[41] L. Álvarez, M. Gharebaghi, J. M. Jones, M. Pourkashanian, a. Williams, J. Riaza, C. Pevida, J. J. Pis, and F. Rubiera, “Numerical investigation of NO emissions from an entrained flow reactor under oxy-coal conditions,” *Fuel Process. Technol.*, vol. 93, no. 1, pp. 53–64, Jan. 2012.

[42] P. Heil, D. Toporov, H. Stadler, S. Tschunko, M. Förster, and R. Kneer, “Development of an oxycoal swirl burner operating at low O2 concentrations,” *Fuel*, vol. 88, no. 7, pp. 1269–1274, Jul. 2009.

[43] J. Hong, P. Kirchen, and A. F. Ghoniem, “Numerical simulation of ion transport membrane reactors: Oxygen permeation and transport and fuel conversion,” *J. Memb. Sci.*, vol. 407–408, pp. 71–85, Jul. 2012.

[44] J. Andersen, C. L. Rasmussen, T. Giselsson, and P. Glarborg, “Global Combustion Mechanisms for Use in CFD Modeling under Oxy-Fuel Conditions,” *Energy & Fuels*, vol. 23, pp. 1379–1389, 2009.

[45] J. Bibrzycki and T. Poinsot, “Reduced chemical kinetic mechanisms for methane combustion in O 2 / N 2 and O 2 / CO 2 atmosphere,” *Work. note ECCOMET WN/CFD/10/17, CERFACS*, 2010.

[46] M. Anheden, J. Yan, and G. De Smedt, “Capture par oxy-combustion,” *Oil Gas Sci. Technol. - Rev. IFP*, vol. 60, pp. 485–495, 2005.

[47] L. Chen, S. Z. Yong, and A. F. Ghoneim, “Oxy-fuel combustion of pulverized coal: Characterization, fundamentals, stabilization and CFD modelling,” *Prog. Energy Combust. Sci.*, vol. 38, no. 2, pp. 156–214, 2012.

[48] T. Nozaki, S. Takano, and T. Kiga, “Analysis of the flame formed during oxidation of pulverized coal by an O2-CO2 mixture,” *Energy*, vol. 22, no. 2–3, pp. 199–205, 1997.

[49] N. Kimura, K. Omata, T. Kiga, S. Takano, and S. Shikisima, “The characteristics of pulverized coal combustion in O2/CO2 mixtures for CO2 recovery,” *Energy Convers. Manag.*, vol. 36, no. 6–9, pp. 805–808, 1995.

[50] T. Suda, K. Masuko, J. Sato, A. Yanamoto, and K. Okazaki, “Effect of carbon dioxide on flame propagation of pulverized coal clouds in CO2/O2 combustion,” *Fuel*, vol. 86, no. 12–13, pp. 2008–2015, 2007.

[51] P. Li, B. B. Dally, J. Mi, and F. Wanga, “MILD oxy-combustion of gaseous fuels in a laboratory-scale furnace,” *Combust. Flame*, vol. 160, no. 933–946, 2013.

[52] W. Blasiak, W. H. Yang, K. Narayanan, and J. von Scheele J., “Flameless oxyfuel combustion for fuel consumption and nitrogen oxides emissions reductions and productivity increase,” *Energy Inst.*, vol. 80, no. 1, pp. 3–11, 2007.

[53] N. Krishnamurthy, P. J. Paul, and W. Blasiak, “Studies on low-intensity oxy-fuel burner,” in *Combustion Institute*, 2009, pp. 3139–3146.

[54] H. Liu, R. Zailani, and B. Gibbs, “Comparisons of pulverized coal combustion in air and in mixtures of O/CO,” *Fuel*, vol. 84, no. 7–8, pp. 833–840, May 2005.

[55] A. C.K. Hermsdorf, M. Klostermann, and K. Mieske, “Oxyfuel Process for Hard Coal with CO2 Capture: First results,” in *Fourth Nordic Minisymposium on Carbon Dioxide Capture and Storage, Otaniemi, Espoo (FI),*, 2005.

[56] M. A. Habib, P. Ahmed, R. Ben-Mansour, H. M. Badr, P. Kirchen, and A. F. Ghoniem, “Modeling of a combined ion transport and porous membrane reactor for oxy-combustion,” *J. Memb. Sci.*, vol. 446, pp. 230–243, Nov. 2013.

[57] M. A. Nemitallah, M. A. Habib, and R. Ben Mansour, “Investigations of oxy-fuel combustion and oxygen permeation in an ITM reactor using a two-step oxy-combustion reaction kinetics model,” *J. Memb. Sci.*, vol. 432, pp. 1–12, Apr. 2013.

[58] M. A. Nemitallah and M. A. Habib, “Experimental and numerical investigations of an atmospheric diffusion oxy-combustion flame in a gas turbine model combustor,” *Appl. Energy*, vol. 111, pp. 401–415, Nov. 2013.

[59] H. Abdul Sater and G. Krishnamoorthy, “An Assessment of Radiation Modeling Strategies in Simulations of Laminar to Transitional, Oxy-methane, Diffusion Flames,” *Appl. Therm. Eng.*, vol. 61, pp. 507–518, 2013.

[60] G. Krishnamoorthy, “A new weighted-sum-of-gray-gases model for oxycombustion scenarios,” *Int. J. Energy Res*, 2012.

[61] L. C. Yin, C. R. Johansen, L. A. Rosendahl, and S. K. Kær, “New weighted sum of gray gases model applicable to computational fluid dynamics (CFD) modeling of oxy-fuel combustion: derivation, validation, and implementation,” *Energy & Fuels*, vol. 24, pp. 6275–6282, 2010.

[62] R. Johansson, A. K., B. Leckner, and H. Thunman, “Models for gaseous radiative heat transfer applied to oxy-fuel conditions in boilers,” *Int. J. Heat Mass Transf.*, vol. 53, pp. 220–230, 2010.

[63] T. Kangwanpongpan, F. H. França, R. C. da Silva, P. S. Schneider, and H. J. Krautz, “New correlations for the weighted-sum-of-gray-gases model in oxy-fuel conditions based on HITEMP 2010 database,” *Int. J. Heat Mass Transf.*, vol. 55, pp. 7419–7433, 2012.

[64] C. Yin, “Nongray-gas effects in modeling of large-scale oxy-fuel combustion processes,” *Energy & Fuels*, vol. 26, pp. 3349–3356, 2012.

[65] P. Nakod, G. Krishnamoorthy, M. Sami, and S. Orsino, “A comparative evaluation of gray and non-gray radiation modeling strategies in oxy-coal combustion simulations,” *Appl. Therm. Eng.*, vol. 54, pp. 422–432, 2013.

[66] T. Kangwanpongpan, R. C. da Silva, and H. J. Krautz, “Prediction of oxy-coal combustion through an optimized weighted sum of gray gases model,” *Energy*, pp. 1–8, 2011.

[67] S. Hjartstam, R. Johansson, K. Andersson, and F. Johnsson, “Computational fluid dynamics modeling of oxy-fuel flames: the role of soot and gas radiation,” *Energy & Fuels*, vol. 26, pp. 2786–2797, 2012.

[68] P. Edge, S. R. Gubba, L. MA, R. Porter, M. Pourkashanian, and A. Williams, “LES modelling of air and oxy-fuel pulverised coal combustion-impact on flame properties,” *Proc. Combust. Inst.*, vol. 33, pp. 2709–2716, 2011.

[69] V. Becher, J. P. Bohn, P. Dias, and H. Spliethoff, “Validation of spectral gas radiation models under oxyfuel conditions-part B: natural gas flame experiments,” *Int. jouranl Green house Gas Control*, vol. 5, pp. S66–S75, 2011.

[70] M. A. Habib, R. Ben Mansour, and M. A. Nemit-allah, “Modeling of oxygen permeation through a LSCF ion transport membrane,” *Comput. Fluids*, vol. 76, pp. 1–10, May 2013.

[71] J. Hong, P. Kirchen, and A. F. Ghoniem, “Interactions between oxygen permeation and homogeneous-phase fuel conversion on the sweep side of an ion transport membrane,” *J. Memb. Sci.*, vol. 428, pp. 309–322, Feb. 2013.

[72] L. Kum-Bae and J. R. Howell, “Theoretical and experimental heat and mass transfer in highly porous media,” *Int. J. Heat Mass Transf.*, vol. 34, no. 8, pp. 2123–2132, Aug. 1991.

[73] W. D. Rose, “Optimizing experimental design for coupled porous media flow studies,” *Exp. Therm. Fluid Sci.*, vol. 3, no. 6, pp. 613–622, Nov. 1990.

[74] H. Teng and T. S. Zhao, “An extension of Darcy ’ s law to non-Stokes # ow in porous media,” vol. 55, no. March 1999, pp. 2727–2735, 2000.

[75] Â. F. Miguel, “Contribution to ¯ ow characterisation through porous media,” vol. 43, pp. 2267–2272, 2000.

[76] W. Zhong, G. Tao, X. Li, K. Kawashima, and T. Kagawa, “Determination of flow rate characteristics of porous media using charge method,” *Flow Meas. Instrum.*, vol. 22, no. 3, pp. 201–207, Jun. 2011.

[77] S. Mancin, C. Zilio, A. Cavallini, and L. Rossetto, “Pressure drop during air flow in aluminum foams,” *Int. J. Heat Mass Transf.*, vol. 53, no. 15–16, pp. 3121–3130, Jul. 2010.

[78] S. Mancin, C. Zilio, A. Diani, and L. Rossetto, “Air forced convection through metal foams: Experimental results and modeling,” *Int. J. Heat Mass Transf.*, vol. 62, pp. 112–123, Jul. 2013.

[79] L. Mart, A. Hernández, and P. Prádanos, “Characterisation of three hydrophobic porous membranes used in membrane distillation Modelling and evaluation of their water vapour permeabilities,” vol. 203, pp. 15–27, 2002.

[80] A. B. Shelekhin, A. G. Dixon, and Y. H. Ma, “Adsorption , permeation , and diffusion of gases in microporous membranes . II . Permeation of gases in microporous glass membranes,” vol. 15, pp. 233–244, 1992.

[81] A. B. Shelekhin, A. G. Dixon, and Y. H. Ma, “Adsorption , diffusion and permeation of gases in microporous membranes . III . Application of percolation theory to interpretation of porosity , tortuosity , and surface area in microporous glass membranes,” vol. 83, pp. 181–198, 1993.

[82] M. L. Sawley, P. W. Cleary, and J. Ha, “Modelling of flow in porous media and resin transfer moulding using smoothed particle hydrodynamics,” in *Second International Conference on CFD in the Minerals and Process Industries*, 1999, pp. 473–478.

[83] Bruker, “400-GC Series Brochure,” 2013.

[84] K. US, “Digital Pressure gauges.” [Online]. Available: http://www.kelleramerica.com/digital-pressure-gages/.

[85] J. P. Holman, *Experimental Methods for Engineers*, Eight. McGraw hill, 2012, pp. 60–75.

[86] H. K. Versteeg and W. Malalasekera, *An Introduction to Computational Fluid Dynamics The Finite Volume Method*, Second. 2007, pp. 179–211.

VITAE

Name	:	Furqan Tahir
Nationality	:	Pakistani
Date of Birth	:	03-Feb-1989
Email	:	furqan061@gmail.com g201202820@kfupm.edu.sa
Address	:	B-40, A-1 Complex phase II, Abul Hassan Isphani Road, Gulshan Town, Karachi, Pakistan.
Academic background	:	Master of Science (M.S.) May, 2014 Mechanical Engineering Department King Fahd University of Petroleum & Minerals, Dhahran, Saudi Arabia. Bachelors of Engineering (B.E.) Dec, 2010 Mechanical Engineering Department, NED University of Engineering & Technology, Karachi, Pakistan.